

Combustion Kinetic Studies of Gasolines and Surrogates

Dissertation by

Tamour Javed

In Partial Fulfillment of the Requirements

For the Degree of

Doctor of Philosophy

King Abdullah University of Science and Technology

Thuwal, Kingdom of Saudi Arabia

© 17th November 2016

Tamour Javed

All rights reserved

The dissertation of Tamour Javed is approved by the examination committee.

Committee Chairperson: Prof. William L. Roberts

Committee Member: Prof. Aamir Farooq

Committee Member: Prof. Mani S. Sarathy

Committee Member: Dr. Nabiha Chaumeix

Committee Member: Prof. Omar Knio

ABSTRACT

Combustion Kinetic Studies of Gasolines and Surrogates

Tamour Javed

Future thrusts for gasoline engine development can be broadly summarized into two categories: (i) efficiency improvements in conventional spark ignition engines, and (ii) development of advance compression ignition (ACI) concepts. Efficiency improvements in conventional spark ignition engines requires downsizing (and turbocharging) which may be achieved by using high octane gasolines, whereas, low octane gasolines fuels are anticipated for ACI concepts. The current work provides the essential combustion kinetic data, targeting both thrusts, that is needed to develop high fidelity gasoline surrogate mechanisms and surrogate complexity guidelines.

Ignition delay times of a wide range of certified gasolines and surrogates are reported here. These measurements were performed in shock tubes and rapid compression machines over a wide range of experimental conditions (650 – 1250 K, 10 – 40 bar) relevant to internal combustion engines. Using the measured the data and chemical kinetic analyses, the surrogate complexity requirements for these gasolines in homogeneous environments are specified. For the discussions presented here, gasolines are classified into three categories:

- (i) Low octane gasolines including Saudi Aramco's light naphtha fuel (anti-knock index, $AKI = (RON + MON)/2 = 64$; Sensitivity (S) = $RON - MON = 1$), certified FACE (Fuels for Advanced Combustion Engines) gasoline I and J ($AKI \sim 70$, $S = 0.7$ and 3

respectively), and their Primary Reference Fuels (PRF, mixtures of n-heptane and iso-octane) and multi-component surrogates.

(ii) Mid octane gasolines including FACE A and C (AKI \sim 84, S \sim 0 and 1 respectively) and their PRF surrogates. Laser absorption measurements of intermediate and product species formed during gasoline/surrogate oxidation are also reported.

(iii) A wide range of n-heptane/iso-octane/toluene (TPRF) blends to adequately represent the octane and sensitivity requirements of high octane gasolines including FACE gasoline F and G (AKI \sim 91, S = 5.6 and 11 respectively) and certified Haltermann (AKI \sim 87, S = 7.6) and Coryton (AKI \sim 92, S = 10.9) gasolines.

To assess conditions where shock tubes may not be ideal devices for ignition delay measurements, this work also presents a detailed discussion on shock tube pre-ignition affected ignition data and the ignition regimes in homogeneous environments. The shock tube studies on pre-ignition and associated bulk ignition advance may help engines research community understand and control super-knock events.

ACKNOWLEDGEMENTS

I owe a deep sense of gratitude to Prof. Aamir Farooq for providing me the opportunity to manage the installation, instrumentation, validation and commissioning of two shock tube facilities in his laboratory. His guidance and the opportunities he provided have equipped me to plan and implement research facilities for institutional specific goals. I am also very thankful to Prof. Mani Sarathy for the countless discussions I had with him on research and career development and for always keeping his office doors open for students. I greatly value the time and effort put in by my dissertation examination committee; Prof. Aamir Farooq, Prof. Mani Sarathy, Prof. William Roberts, Prof. Omar Knio and Prof. Nabiha Chaumeix, to provide valuable feedback and critique to my work.

Setting up new research facilities in the middle of the desert can be a challenging task. I must thank several people who provided me all the support I needed to set up the shock tube facilities; Dr. Ettouhami Essebbar, KAUST support staff and service providers, especially NAIZAK team (Mike, Andrew, Raymond, and Tom), without your help these excellent facilities would never have been realized. I would also like to thank Prof. Ron Hanson and Dr. Dave Davidson for allowing me to get trained at Stanford shock tube facilities and Hanson group research students who supervised me during my training (Dr. Matt Campbell, Dr. Ivo Stranic, Dr. Wei Ren, and all others).

KAUST is a fantastic place and provides everything required for an enriching academic life, i.e., excellent research facilities and brilliant people. I have made some friends for life and owe them huge thanks; Usman Majeed, Bilal Janjua, Furrukh Sana, Bilal Sajid, Awad Alquaity, Ahfaz Ahmed, Muneeb Khurshid, Shahid Rasul, and all others, for their sincere friendship and ever so interesting discussions over lunch and tea on

science, politics, sports and life.

I have been fortunate to be surrounded by amazing people in my research group and at the CCRC; I would like to thank Dr. Binod Giri, Dr. Utsav KC, Dr. Jihad Badra, Ehson Nasir, Fathi Khalid, Mohammed Al-Abbad, Miguel Labastida, and all others, for your support and discussions on research and life.

I would like to thank my family for their continuous support throughout my Doctoral journey. My mother Naila Javed and father Dr. Javed Iqbal have always encouraged me to excel in studies and research. My siblings, Dr. Nida Javed, Fatima Javed, Bilal Javed and Umar Iqbal for being always there for me and for all the happy moments that we have had together. Finally, and most importantly, I would like to thank my wife, Sara, and my son, Mahd, for bringing so much happiness and love into my life.

*I would like to dedicate this work to my grandfather, **Ahmed Ali**, who recently left us on an eternal journey. Your memories will stay with us for life, and we will always try to emulate the character you stood for. May your soul rest in peace.*

Tamour Javed

17th November, 2016

TABLE OF CONTENTS

ABSTRACT.....	3
ACKNOWLEDGEMENTS	5
Chapter 1 : INTRODUCTION.....	16
1.1 Background and motivation	16
1.2 Overview of the dissertation	21
Chapter 2 : CHEMICAL KINETICS AND LASER SENSORS LABORATORY.....	25
2.1 Shock tube facilities and ignition measurements	25
2.1.1 Test time in shock tubes.....	31
2.1.2 Uncertainty in shock tube ignition delay time measurements	34
2.1.3 Reflected shock bifurcation	37
2.2 Rapid compression machine facility and ignition measurements	40
2.2.1 Uncertainty in RCM ignition delay time measurements.....	42
2.3 Lasers diagnostics	43
Chapter 3 : IGNITION STUDIES OF LOW OCTANE GASOLINES AND SURROGATES	45
3.1 Introduction	45
3.2 Methodologies	49
3.2.1 Light naphtha fuel characterization and surrogate formulation	49
3.2.2 FACE gasoline I and J fuel characterization and surrogate formulation	51
3.3 Results and discussion.....	54
3.3.1 Ignition delay times of light naphtha and surrogates	54
3.3.2 Ignition delay times of FACE gasoline I and J and surrogates.....	57
3.3.3 Chemical kinetic analyses for light naphtha and surrogates.....	61
3.3.4 Chemical kinetics analysis for FACE I and J and surrogates	66
Chapter 4 : SPECIATION AND IGNITION STUDIES OF MID OCTANE GASOLINES AND SURROGATES	72
4.1 Introduction	72
4.2 Methodology	76
4.2.1 Ignition delay measurements	76

4.2.2	Laser absorption measurements	76
4.2.3	Calculation of temperature time-history	77
4.2.4	Validation of laser diagnostics	78
4.3	Results and discussion	80
4.3.1	Ignition delay times of FACE gasolines and PRF surrogate	80
4.3.2	Species time-histories of FACE gasolines and PRF surrogate	83
Chapter 5 : IGNITION STUDIES OF HIGH OCTANE GASOLINES AND SURROGATES		90
5.1	Introduction	90
5.2	Methods	93
5.2.1	TPRF Surrogate Formulation	93
5.2.2	Experimental Details	95
5.3	Results and Discussion	95
5.3.1	Effect of Pressure	96
5.3.2	Effect of Equivalence Ratio	100
5.3.3	Effect of Octane Number	104
5.4	Chemical Kinetic Analyses	107
5.5	Comparisons with certified high octane gasolines	112
Chapter 6 : SHOCK TUBE IGNITION DELAY DATA AFFECTED BY LOCALIZED IGNITION PHENOMENA		116
6.1	Introduction	116
6.2	Experimental Details	120
6.3	Ignition Delay Times of n-Heptane and n-Hexane	120
6.4	Chemical Kinetic Mechanisms of n-Alkanes	125
6.5	Pre-Ignition Heat Release	127
6.6	CFD Simulations of Pre-Ignition	130
6.6.1	Numerical Setup	130
6.6.2	CFD Modeling Results	133
6.6.3	Ignition Regimes	137
Chapter 7 : SUMMARY AND FUTURE WORK		146
7.1	Summary of results	146

7.1.1	Ignition studies of Low Octane Gasolines and Surrogates	146
7.1.2	Speciation and Ignition studies of Mid Octane Gasolines and Surrogates	147
7.1.3	Ignition studies of High Octane Gasolines and Surrogates	147
7.1.4	Shock tube ignition delay data affected by localized ignition phenomena	148
7.2	Future work	150
7.2.1	Surrogate complexity guidelines for homogeneous environments	150
7.2.2	Surrogate complexity requirements for various engine modes	151
7.2.3	Understanding the mechanisms of pre-ignition initiated super-knock using shock tubes and rapid compression machines	153
APPENDIX A		155
APPENDIX B		165
	Example high pressure shock tube ignition measurements pressure traces	165
REFERENCES		169

LIST OF FIGURES

Figure 2-1: Shock tube configuration for ignition delay time measurements.	29
Figure 2-2: Representative shock tube pressure and OH* emission traces during ignition delay experiment.....	30
Figure 2-3: Test times measured in the LPST, for each case driver and driven section of 9.1 m length were used. (a) Helium as driver gas, $T_5 = 613$ K, $P_5 = 2.4$ bar, Driven gas is Argon, (b) Helium/Nitrogen (17% vol Helium) as tailored driver gas, $T_5 = 593$ K, $P_5 = 1.6$ bar, Driven gas is Argon, (c) Helium/Nitrogen (17% vol Helium) as tailored driver gas, $T_5 = 608$ K, $P_5 = 1.6$ bar, Driven gas is Argon with 5% buffer Helium gas(d) Helium/Carbon dioxide (35% vol Helium) as tailored driver gas, $T_5 = 518$ K, $P_5 = 2.3$ bar, Driven gas is Argon with 2.6% buffer Helium gas.....	33
Figure 2-4: Test time as a function of temperature behind the reflected shock wave in the LPST. Driver and driven sections length is 9.1 m. Experimental measurements are included in the figure. The symbols are the measurements and the line is the simulation using KASIMIR [46] software.	34
Figure 2-5: Measured pressure profile showing weak shock bifurcation effects. Mixture: 2% n-heptane, 44% O ₂ , Ar. $T_5 = 1124$ K, $P_5 = 1.6$ bar.....	40
Figure 2-6: Representative RCM pressure trace during ignition delay experiment.	42
Figure 3-1: Measured and simulated ignition delay times for: (a) light naphtha at $\phi = 0.5$, (b) light naphtha at $\phi = 1$, (c) light naphtha at $\phi = 2$, and (d) light naphtha, LN-KAUST and PRF 64.5 surrogates at $\phi = 2$. Solid symbols: shock tube data, open symbols: RCM data. Solid lines: LN-KAUST surrogate simulations, dotted lines: PRF 64.5 simulations.	56
Figure 3-2: Ignition delay times of PRF 70, FACE I and FACE J at 20 and 40 bar for equivalence ratios of (a) 1 and (b) 0.5.	58
Figure 3-3: Comparison of experiments (scatter) and simulations (lines) for equivalence ratio 1 at (a) 20 bar and (b) 40 bar. Simulations done using FACE gasoline mechanism [30]......	61
Figure 3-4: Comparison of experiments (scatter) and simulations (lines) for equivalence ratio 0.5 at (a) 20 bar and (b) 40 bar. Simulations done using FACE gasoline mechanism [30]......	61
Figure 3-5: Simulated constant volume temperature, OH and HO ₂ profiles during the oxidation of PRF 64.5 and LN-KAUST surrogates. Initial conditions: $T = 650$ K, $P = 20$ bar, $\phi = 2$. FACE gasoline mechanism is used for simulations. The arrows are drawn at $2/3 \tau_{ign}$	63
Figure 3-6: Rate of production (ROP) analysis of OH (a, c) and HO ₂ (b, d). Upper panel: LN-KAUST surrogate, Lower panel: PRF 64.5 surrogate. $T = 650$ K, $P = 20$ bar, $\phi = 2$. FACE gasoline mechanism is used. ROP analysis was performed at $2/3 \tau_{ign}$	65
Figure 3-7: ROP OH analysis at for various fuel/air mixtures at an equivalence ration of 1.	

T = 700 K, P = 20 bar.	69
Figure 3-8: Experimentally measured low temperature ignition delay data for a wide range of fuels at 20 bar and $\phi = 1$. FACE A, FACE C and PRF 84 data taken from [29], TPRF 70 – 97.5 data taken from [69], FACE I, FACE J and PRF 70 (current study), and FACE F and G data taken from [30].	70
Figure 4-1: Simulated profiles of major species formed during the oxidation of PRF 84. Mixture: 0.2% PRF84/O ₂ /Ar ($\Phi = 1$), T = 1500 K , P = 2 atm. Constant internal energy and volume (constant UV) simulations performed in Chemkin-Pro [97] using Mehl et al. mechanism [79].	75
Figure 4-2: Comparison of modeled (a) temperature and (b) pressure using various gasdynamic models (UV = constant internal energy and volume, UMP = constant internal energy with measured pressure) during the oxidation of 0.2% n-heptane/ O ₂ /Ar ($\Phi = 1$), T = 1440 K , P = 1.94 atm. Temperature output using ChemShock [98] code is also shown. Simulations performed using Mehl et al. [79] mechanism.	79
Figure 4-3: Comparison of model prediction with experimentally measured species profiles for 0.2% n-heptane/O ₂ /Ar ($\Phi = 1$), T = 1440 K , P = 1.94 atm; solid lines: experimental profiles, dashed lines: Constant UV simulations using Mehl et al. [79] mechanism.	80
Figure 4-4: Ignition delay times during the oxidation of stoichiometric mixtures with 0.2% fuel (iso-octane, PRF 84, FACE A, FACE C, n-heptane) / O ₂ / Ar, P \approx 2 atm; Scatter: Experimental, Dashed lines: Mehl et al. [79] mechanism. Dotted line: Bieleveld et al. mechanism [102].	81
Figure 4-5: Ignition delay times during the oxidation of 0.4% fuel (iso-octane, PRF 84, FACE A, FACE C, n-heptane) / O ₂ / Ar, P = 10 atm at $\phi = 0.5$ and 1. Data obtained in KAUST low pressure shock tube and presented in [29].	83
Figure 4-6: Ignition delay times during the oxidation of stoichiometric fuel / air mixtures (iso-octane, PRF 84, FACE A, FACE C) / at (a) 20 atm and (b) 40 atm. Data taken from [29].	83
Figure 4-7: Measured species profiles during the oxidation of 0.2% fuel, $\Phi = 1$, P \approx 2 atm; Reflected-shock temperatures are PRF 84: 1459 K; FACE A: 1455 K; FACE C: 1443 K. Note that the CO ₂ data are not available at early times due to the 100 ppm detection limit of the CO ₂ diagnostic used here.	85
Figure 4-8: Comparison of multi-species measurements with kinetic simulations during the oxidation of 0.2% PRF84/O ₂ /Ar ($\Phi = 1$), T = 1526 K , P = 2 atm. Solid lines: Measurements, Dashed lines: Mehl et al. [79] simulations, Dotted lines: Bieleveld et al. [102] simulations.	86
Figure 4-9: Comparison of measured profiles with kinetic simulations during the oxidation of 0.2% PRF84/O ₂ /Ar ($\Phi = 1$), Solid lines: Measurements, Dashed lines: Mehl et al. [79] simulations.	87
Figure 4-10: Hydroxyl sensitivity at two instants: 15% and 75% of the predicted ignition delay time. 0.2% PRF84/O ₂ /Ar ($\Phi = 1$), T = 1430 K, P = 2 atm.	88
Figure 5-1: Effect of pressure (10, 20, 40 bar), at $\phi = 1$, on the ignition delay times of (a)	

TPRF 70, (b) TPRF 80, (c) TPRF 91, (d) TPRF 97.5. Scatter: solid symbols – HPST data, open symbols – RCM data. Lines: solid lines – shock tube simulations, dashed lines – RCM simulations. LLNL mech [79] is used for simulations. 98

Figure 5-2: Effect of pressure (10, 20, 40 bar), at $\phi = 0.5$, on the ignition delay times of (a) TPRF 70, (b) TPRF 80, (c) TPRF 91, (d) TPRF 97.5. Scatter: solid symbols – HPST data, open symbols – RCM data. Lines: solid lines – shock tube simulations, dashed lines – RCM simulations. LLNL mech [79] is used for simulations. 99

Figure 5-3: Effect of equivalence ratio ($\phi = 0.5$ and 1.0), at 10 bar, on the ignition delay times of (a) TPRF 70, (b) TPRF 80, (c) TPRF 91, (d) TPRF 97.5. Scatter: open symbols – RCM data. Lines: dashed lines – RCM simulations. LLNL mech [79] is used for simulations. Ignition delay times were not measured in the shock tube for 10 bar. 102

Figure 5-4: Effect of equivalence ratio ($\phi = 0.5$ and 1.0), at 20 bar, on the ignition delay times of (a) TPRF 70, (b) TPRF 80, (c) TPRF 91, (d) TPRF 97.5. Scatter: solid symbols – HPST data, open symbols – RCM data. Lines: solid lines – shock tube simulations, dashed lines – RCM simulations. LLNL mech [79] is used for simulations. 103

Figure 5-5: Effect of equivalence ratio ($\phi = 0.5$ and 1.0), at 40 bar, on the ignition delay times of (a) TPRF 70, (b) TPRF 80, (c) TPRF 91, (d) TPRF 97.5. Scatter: solid symbols – HPST data, open symbols – RCM data. Lines: solid lines – shock tube simulations, dashed lines – RCM simulations. LLNL mech [79] is used for simulations. 104

Figure 5-6: Effect of RON (97.5, 91, 80, 70), at $\phi = 1$, on the ignition delay times of TPRF 97.5 (■), TPRF 91 (●), TPRF 80 (▲), TPRF 70 (▼) at (a) 10 bar, (b) 20 bar and (c) 40 bar. Scatter: solid symbols – HPST data, open symbols – RCM data. Lines: solid lines – shock tube simulations, dashed lines – RCM simulations. LLNL mech [79] is used for simulations. 106

Figure 5-7: Effect of RON (97.5, 91, 80, 70), at $\phi = 0.5$, on the ignition delay times of TPRF 97.5 (■), TPRF 91 (●), TPRF 80 (▲), TPRF 70 (▼) at (a) 10 bar, (b) 20 bar and (c) 40 bar. Scatter: solid symbols – HPST data, open symbols – RCM data. Lines: solid lines – shock tube simulations, dashed lines – RCM simulations. LLNL mech [79] is used for simulations. 107

Figure 5-8: ROP analyses of $\dot{O}H$ radical at $T = 700$ K, $p = 20$ bar, $\phi = 1$; (a) TPRF 70/air, (b) TPRF 80/air, (c) TPRF 91/air, and (d) TPRF 97.5/air mixtures. LLNL mech [79] is used for ROP analyses. The ROP analyses are conducted at a time corresponding to two-thirds of the exponential growth of $\dot{O}H$ radical concentration. 110

Figure 5-9: ROP analysis of $\dot{H}O_2$ radical at $T = 825$ K, $p = 20$ bar, $\phi = 1$ for TPRF 97.5/air (magenta bars), TPRF 91/air (blue bars), TPRF 80/air (red bars), and TPRF 70/air (black bars) mixtures. LLNL mech [79] is used for ROP analysis. The ROP analyses are conducted at the time corresponding to two-thirds of the exponential growth of $\dot{H}O_2$ radical concentration. 111

Figure 5-10: Comparison of RON and Sensitivity of TPRFs and commercial gasolines 113

Figure 5-11: Comparison of ignition delay times of TPRF 91 and 97.5 with FACE F and G and Coryton and Haltermann gasolines at stoichiometric conditions and at (a) 20 bar and

(b) 40 bar. Data for FACE F and G is taken from [30] and for Haltermann and Coryton gasolines from [118].	114
Figure 6-1: Comparison of measured ignition delay data (symbols) with predictions using the Mehl et al. [79] mechanism. Solid lines: constant volume simulations. Dashed lines: simulations with 3% dP_5/dt correction. Mixtures: 2% n-heptane / 44% O_2/Ar ($\Phi = 0.5$) and 5% n-hexane / 44% O_2/Ar ($\Phi = 1$)	122
Figure 6-2: Ignition delay results for various n-heptane mixture compositions. Experimental: ■ 2 % n-heptane/44 % O_2/Ar ($\Phi = 0.5$), ◆ 2 % n-heptane/22 % O_2/Ar ($\Phi = 1$), ★ 1 % n-heptane/11 % O_2/Ar ($\Phi = 1$). Lines: Constant UV simulations with Mehl et al. [79] mechanism.....	123
Figure 6-3: Ignition delay validation using stoichiometric n-heptane mixtures: (a) KAUST 12 bar (present study), Sheen et al. [138] 12 atm, Ciezki et al. [104] 13.5 bar, Silke et al. [101] 10 atm, and Gauthier et al. [23] 20 atm data normalized to 12 bar. (b) In addition to data plotted in (a), Minetti et al. [105] 4 atm, Shen et al. [138] 50 atm, Ciezki et al. [104] 41 atm, and Gauthier et al. [23] 55 atm data are plotted. Lines in (a) and (b) represent constant UV simulations at 4 (red line), 12 (black line) and 50 (blue line) bar using Mehl et al. [79] mechanism.....	125
Figure 6-4: Ignition delay simulations using various mechanisms for 2 % n-heptane/44 % O_2/Ar ($\Phi = 0.5$).	126
Figure 6-5: Various types of pressure profiles (energy release patterns) observed during shock tube ignition delay measurements: (a) strong ignition (b) pre-ignition energy release (c) combination of pre-ignition and two-stage behavior, and (d) near-homogeneous energy release. (a–c) are for 2% n-heptane/ 44% O_2/Ar and (d) is for 5% n-hexane / 47.5% O_2/Ar	130
Figure 6-6: Two-dimensional (2D) cut-plane of the numerical domain showing the grid refinement in the area of interest.	132
Figure 6-7: Comparison of the ignition delay times from experimental measurements (solid squares), constant-UV calculations using CHEMKIN (solid blue line), CONVERGE-UV calculations (solid black line), and CONVERGE pre-ignition simulations with 2D 50 cm domain length (dashed lines), 2D 1m domain length (open triangles) and 3D 5 cm domain length (dotted lines). The pre-ignition source is active from 2 – 6 ms with 25 mJ total energy. Reactive mixture is 2% n-heptane / 44% O_2/Ar , and pressure at 1.5 atm.....	134
Figure 6-8: Parametric study on the magnitude of pre-ignition energy source. Reactive mixture is 2% n-heptane / 44% O_2/Ar , and pressure at 1.5 atm.....	135
Figure 6-9: Parametric study on the pre-ignition source (a) source diameter 0.5 mm (b) source diameter 1 mm (c) source diameter 2 mm, and (d) comparison of various energy source diameters for 2 – 6 ms duration. For each source size, source initiation and duration times are parameterized. Square symbols represent measurements. Reactive mixture is 2% n-heptane / 44% O_2/Ar . Pressure ~ 1.5 atm.	137
Figure 6-10: Simulated pressure-time histories at initial temperatures of (a) 900 K, (b) 800 K and (c) 600 K. Black lines: homogeneous ignition results. Blue lines: 3D pre-ignition simulation results. Mixture: 2% n-heptane/44% O_2/Ar . P = 1.5 atm. Simulations performed	

using 3D 5 cm domain length.	139
Figure 6-11: Simulated pressure and maximum temperature profiles at initial temperatures of (a) 900 K and (b) 800 K. Pre-ignition source (2 mm size and 2 – 6 ms timing). Mixture: 2% n-heptane / 44% O ₂ / Ar. P = 1.5 atm. Simulations performed using 3D 5 cm domain length.....	142
Figure 6-12: Flame speed calculated in CHEMKIN-Pro (solid line) and the front speed calculated from the CONVERGE [146] CFD simulations (dashed line).	142
Figure 6-13: Simulated pressure and maximum temperature profiles at initial temperatures of (a) 900 K and (b) 800 K. Pre-ignition source (2 mm size and 2 – 6 ms timing). Mixture: 2% n-heptane / 44% O ₂ / Ar. P = 1.5 atm. Simulations performed using 2D 50 cm domain length.....	144
Figure 6-14: Simulated pressure and maximum temperature profiles at initial temperature of 600 K. Pre-ignition source (2 mm size and 2 – 6 ms timing). Mixture: 2% n-heptane / 44% O ₂ / Ar. P = 1.5 atm. Simulations performed using 3D 5 cm domain length.	145

LIST OF TABLES

Table 2-1: Various parameters effecting shock tube ignition measurements	36
Table 3-1: Properties of light naphtha and its surrogates. Hydrocarbon types are given in mol%	50
Table 3-2: Properties of FACE gasoline I and J and multi-component and Primary Reference Fuel (PRF) surrogates. Hydrocarbon types are given in mol%	53
Table 3-3: Composition of the multi-component and PRF surrogates. Note that compositions are listed as mole fractions here.	53
Table 4-1: Properties of FACE gasoline fuels and PRF surrogate. The hydrocarbon types for FACE A and C were determined by Detailed Hydrocarbon Analysis (DHA) technique.	74
Table 5-1: TPRF surrogates investigated in this work. See Table A4 in Appendix for compositions in mole fractions.	95
Table 5-2: Comparison of TPRF surrogates with certified gasolines. Hydrocarbon classes are presented as mol %.	113
Table 6-1: Details of the various pre-ignition energy sources used in the CFD simulations.	136
Table 7-1: Test fuels for evaluating surrogate complexity requirements for various engine modes	152
Table 7-2: Various fuels/surrogates evaluation in different engine operating modes	153

Chapter 1: INTRODUCTION

1.1 Background and motivation

Energy is considered to be the driving force and lifeline of modern economies. World GDP is expected to double by 2035 [1] and will be accompanied by about 34% increase in energy demand. Although the share of renewables in the energy mix is always growing, fossil fuels will remain the dominant source of energy accounting for around 80% of energy supply in 2035 [1]. Growth in liquid fuels will be predominantly driven by the transportation sector (~ 70% [1]). This increase in energy demand will result in about 20% increase in carbon emissions through 2035 [1] for base case scenarios. The transportation sector accounts for nearly half of global oil consumption and about 23 % of global CO₂ emissions [2, 3]. Post COP 21 (Paris 2015) world demands stringent restrictions on emissions and associated environmental impact. Thus improvements in the transportation sector are necessary to reduce its environmental footprint.

Commercial transportation grade gasoline is the most widely used light duty transportation fuel and is a complex mixture of hundreds of hydrocarbons including linear and branched paraffins, naphthenes, olefins, and aromatics [4]. US Department of Energy has recently launched a program for targeted co-optimization of fuels and engines (OPTIMA program) [5] for sustainable transportation. This program has two major thrusts for gasoline engines development: (i) to design optimal fuel/engine combinations for efficiency increase in conventional spark ignition gasoline engines, and (ii) to develop the advanced compression ignition engine concepts that can achieve much higher efficiencies

compared to conventional gasoline engines and will also significantly improve the environmental footprint.

The co-optimization of fuel/engine systems requires in-depth knowledge of the combustion kinetics behavior of fuel. Higher efficiency spark ignition engine modes are often limited by the knocking of end-gas, knocking is fundamentally related to fuels auto-ignition (combustion kinetics) characteristics. Moreover, futuristic compression ignition (CI) engine technologies such as homogeneous charge compression ignition (HCCI), dual-fuel reactivity controlled compression ignition (RCCI), partially premixed compression ignition (PPCI) and other variants have the potential to increase the efficiency of traditional engines [6], and auto-ignition of fuel is one of the primary combustion phasing control mechanisms in CI technologies. Thus, accurate chemical kinetics representation of fuels auto-ignition is key if such systems are to be successfully modeled.

Ignition delay time measurements have been widely used in the past for chemical kinetics mechanisms development [7-12]. Almost all the chemical kinetics mechanisms are validated against shock tubes (ST) and rapid compression machines (RCM) ignition delay data. Ignition delay time measurements are one of the simplest yet most illustrative chemical kinetics target. Detailed mechanisms typically comprise of several hundred species and several thousand reaction pathways. The complexity of these mechanisms increases with increasing carbon chain length. When fuel is subjected to high temperature and pressure conditions, it will go through several chemical processes towards ignition/heat release. Ignition delay time can be thought of as the overall global effect of all the chemical processes and hence it is a measure of the overall global reactivity of the fuel. Therefore validating chemical kinetic mechanisms against ignition delay data can shed valuable

insights on the overall global performance of mechanisms.

Due to complex composition of gasolines and other commercial fuels, it is not feasible to study all the components present in them both experimentally as well from modeling perspective. To get around this difficulty, surrogate mixtures of few components are employed to emulate the target properties of the real fuel. Primary reference fuels (PRF), n-heptane and iso-octane, are commonly used as surrogates for gasoline spark-ignition (SI) engines. A standard scale for rating the ignition properties of gasoline fuels is the research octane number (RON) and the motor octane number (MON) based on PRF blends of n-heptane and iso-octane. Various experimental and chemical kinetics mechanism development studies can be found in the literature on n-heptane and iso-octane [7-10, 13-16].

Fieweger et al. [15] measured the ignition delay times of stoichiometric PRF 90,80 and 60 (where PRF_{xx} refers to xx % age by volume of iso-octane in a mixture of iso-octane and n-heptane) near 40 bar. Callahan et al. [18] measured the ignition delay times of PRF100, 95 and 90 in a RCM and developed a semi-detailed kinetics scheme. Tanaka et al. [17] measured the ignition delay times of various PRF mixtures and found out that the ignition delay depends only on the molar ratio of n-heptane to oxygen and not on iso-octane. Hartmann et al. [18] measured the ignition delay times of PRF0, 80 and 100 behind reflected shock waves near 40 bar and covered a temperature range of 650 – 1200 K. Notable research groups who developed predictive capabilities for PRF blends are LLNL [19], Milano [20] and Nancy [21].

Chemical kinetics primarily controls the low-temperature combustion in engines. In HCCI combustion, for example, the heat released is strongly dependent on the pressure and

temperature evolution in the cylinder which in turn is dependent on chemical kinetics [22]. In SI engines auto-ignition is undesirable as it results in knock, whereas in HCCI engines it is essential for heat release mechanism. The kinetics of the fuel is influenced by its compositional make-up. Hence PRF blends can only be used for high paraffinic content gasoline. Typical commercial gasolines have a significant proportion of aromatic content present in them. Hence a simple binary PRF surrogate, in whom aromatics by definition are completely absent, will not be able to match all the target properties of the real gasoline.

For the reasons stated above, ignition delay studies on more complex surrogates may be found in the literature. Gauthier et al. [23] studied the auto-ignition characteristics of n-heptane/air, gasoline/air, and ternary surrogate/air (63% iso-octane/20% toluene/17% n - heptane by liquid volume) mixtures in low-temperature high-pressure HCCI like conditions behind the reflected shock waves. They showed that the ternary surrogate could well capture the auto-ignition behavior of certified RD387 gasoline. Chaos et al. [24] also proposed the use of ternary (iso-octane/n-heptane/toluene) surrogate and also developed an optimized kinetics mechanism. Vanhove et al. [25] used a isooctane/1-hexene/toluene ternary surrogate. They interestingly preferred 1-hexene for low-temperature chemistry over n-heptane. Naik et al. [26] developed a chemical kinetics mechanism using five component surrogate representing various compositional classes present in real gasoline. They used iso-octane, n-heptane, 1-pentene, toluene, and methyl-cyclohexane to represent paraffins, olefins, aromatics, and cycloalkanes content of the gasoline. Kukkadapu et al. [27] studied RD387 gasoline and showed good agreement with [23]. Kukkadapu et al. [28] found out a better agreement of a four component (iso-octane, n-heptane, toluene and 2-pentene) surrogate with ignition delay times of RD387.

At KAUST, we have contributed significantly towards the combustion kinetics development of gasolines of varying compositions and octane numbers and also surrogate formulation for these gasolines [29-31]. Sarathy et al. [29] studied the ignition delay times of FACE (Fuels for Advanced Combustion Engines) gasolines A and C using shock tubes and rapid compression machines and also developed surrogates for simulations for these gasolines based on detailed hydrocarbon analysis (DHA). Both FACE gasolines A and C exhibited similar octane numbers (RON and MON \sim 84) but were of different compositions (albeit both gasolines were $>$ 90% mol paraffinic). They have shown that the two gasolines of similar octane ratings exhibit comparable ignition delay times at all experimental conditions and a PRF surrogate adequately captures the ignition requirements of these gasolines (with some discrepancies at low temperatures). Sarathy et al. [30] studied the ignition behavior and surrogate formulation of FACE gasolines F (RON = 94.4, MON = 88.8) and G (RON = 96.8, MON = 85.8) with similar antiknock index (AKI = (RON+MON)/2 \sim 91.5) but varying sensitivities ($S = \text{RON} - \text{MON}$) and compositions. They have shown that at high temperatures ($T > 900$ K) both the gasolines were equally reactive. At low temperatures ($T < 750$ K) the fuel with lower RON (FACE F) was slightly more reactive compared to high RON (FACE G) fuel and fuel with low sensitivity (FACE F) showed greater NTC behavior. Finally the fuel with lower MON (FACE G) was more reactive in 800 – 900 K temperature range. Based on DHA analysis, multi-component surrogates were developed for FACE F and G and it was shown that for a highly sensitive fuel like FACE G, a multi-component surrogate best captures the ignition requirements.

The current work aims to continue the efforts in developing chemical kinetics for the gasolines and surrogates. Ignition delay times of a wide range of gasolines and their

surrogates, with varying octane numbers (RON and MON) and compositions, are reported in this work. These data were obtained in the shock tubes and rapid compression machines. For the discussions presented here, gasolines are classified into three categories: (i) low octane gasolines including Saudi Aramco's light naphtha fuel (anti-knock index, AKI = $(\text{RON} + \text{MON})/2 = 64$; Sensitivity (S) = $\text{RON} - \text{MON} = 1$) and certified FACE (Fuels for Advanced Combustion Engines) gasoline I and J (AKI ~ 70 , $S = 0.7$ and 3 respectively) and their Primary Reference Fuels (PRF, mixtures of n-heptane and iso-octane) and multi-component surrogates, (ii) mid octane gasolines including FACE A and C (AKI ~ 84 , $S \sim 0$ and 1 respectively) and their PRF surrogate, and (iii) wide range of n-heptane/iso-octane/toluene (TPRF) blends to adequately represent the octane and sensitivity requirements of high octane gasolines including FACE gasoline F and G (AKI ~ 91 , $S = 5.6$ and 11 respectively) and certified Haltermann (AKI ~ 87 , $S = 7.6$) and Coryton (AKI ~ 92 , $S = 10.9$) gasolines. Moreover, laser absorption measurements of intermediate and product species formed during gasoline / surrogate oxidation are also reported here. One of the concerns in designing high efficiency downsized turbocharged engines is the occurrence of so-called "super-knock" phenomena which is initiated by pre-ignition flame initiation; this work also presents a detailed discussion on shock tube pre-ignition affected ignition data and the ignition regimes in homogeneous environments. This work provides a wealth of combustion kinetic data that is required to develop high fidelity gasoline surrogates mechanisms and surrogate formulation guidelines for gasoline fuels.

1.2 Overview of the dissertation

Chapter 2 provides a general introduction to the Chemical Kinetics and Laser Sensors Laboratory at KAUST. This laboratory features two shock tube facilities, a rapid

compression machine and a wide range of laser sensors. A brief overview of experimental methods utilized in this work, the ignition delay measurements and simulations and laser sensors, are also presented in this chapter. The author would like to acknowledge the help and support of Dr. Ettouhami Essebbar during the laboratory development phase.

Chapter 3 presents the ignition measurements of a lightweight highly paraffinic low octane fuel, light naphtha (anti-knock index, $AKI = (RON + MON)/2 = 64$; Sensitivity (S) = $RON - MON = 1$), and two low octane full boiling range FACE gasolines, FACE I and J ($AKI \sim 70$, $S = 0.7$ and 3 respectively), using the shock tube and rapid compression machine. Multi-component surrogates for these fuels, formulated using an in-house developed methodology, are also presented. Experiments and simulations of a Primary Reference Fuel (PRF) surrogate, matching the AKI of these fuels, and simulations of multi-component surrogate are also reported. Furthermore, chemical kinetic analyses are used to explain the various trends in the ignition data. It is shown that for highly paraffinic fuels, a PRF surrogate satisfactorily matches the ignition requirements, with some discrepancies at low temperatures for lightweight fuels. The author would like to acknowledge the expertise provided by Ph.D. student Ahfaz Ahmed for the multi-component surrogate formulation.

Chapter 4 discusses high-temperature laser absorption based species time histories and ignition delay times measured during the oxidation of two highly paraffinic mid-octane FACE A and C gasolines ($AKI \sim 84$, $S \sim 0$ and 1 respectively). PRF speciation and ignition data are also compared with the trends found for these gasolines. It is shown that the two highly paraffinic gasolines have not only same global reactivity (ignition delay times) but also key reaction progress and completion species (OH , H_2O , CO , CO_2) evolve quite similarly during their oxidation. It is also shown that a PRF surrogate satisfactorily captures

the kinetics (speciation, ignition delay times) trends of gasolines. Finally, a wide range of data for these gasolines, from the literature, covering practical thermodynamic conditions is used to exhibit same trends like those found at high-temperatures. The expertise provided by Dr. Ettouhami Essebbar and Ph.D. student Ehson Nasir in setting up lasers sensors are acknowledged by the author.

Chapter 5 presents detailed ignition delay measurements of ternary blends of toluene/*n*-heptane/iso-octane (TPRFs). Commercial high octane gasolines have high non-paraffinic content (Sensitivity = RON – MON > 7). TPRFs surrogates are used to represent the sensitivity requirements of commercial high octane gasolines adequately. A wide range of TPRF ignition data are collected using shock tube and rapid compression machine. The data are analyzed based on its pressure, equivalence ratio and octane dependence. Chemical kinetics analysis is used to explain experimental trends. The data are also compared with ignition delay data of certified high octane gasolines. The author would like to acknowledge Ph.D. student Mohammed Al-Abbad for support during high pressure shock tube measurements and Dr. Changyoul Lee (NUIG) for gathering low temperature TPRFs ignition data and for sharing Coryton and Haltermann gasolines ignition data.

Chapter 6 presents the shock tube pre-ignition affected ignition data. Low temperature and long ignition delay times shock tube data suffer from various non-idealities, pre-ignition flame kernel initiation and propagation resulting in bulk ignition advance are discussed in detail here. Using experiments and CFD analysis, various ignition regimes are discussed. Pre-ignition leading to super-knock is very relevant subject for engine research community, and shock tubes can significantly contribute to understanding and mitigating such events in engines. The author would like to acknowledge the expertise

provided by Ph.D. student Mohammed Jaasim Mubarak Ali and Dr. Jihad Badra in setting up the CONVERGE CFD simulations.

Chapter 7 presents a detailed summary of the findings of this work and gives an account of future research directions.

Chapter 2: CHEMICAL KINETICS AND LASER SENSORS

LABORATORY

In this chapter, a brief overview of chemical kinetics and laser sensors laboratory at the King Abdullah University of Science and Technology (KAUST) is presented. This laboratory features two shock tube facilities and a rapid compression machine. A wide range of lasers sensors for combustion, environmental and medical research are also featured in this laboratory. Combined these facilities can cover the operating conditions of a wide range of practical energy conversion systems and can be used to provide ignition, speciation, reaction rate and pollutants data.

2.1 Shock tube facilities and ignition measurements

The use of shock tubes for studying combustion processes has fascinated scientists for more than 100 years. French physicists, Mallard, Le Chatelier, Berthelot and Vieille had discovered the formation of deflagration to detonation transition during the combustion process inside hollow tubes way back in 1881 [32]. These discoveries led Paul Vieille [33] to the construction of first shock tube in 1899. The shock tube presents a very simple way of step-raising the temperature and pressure of test gas specimen. Since the invention of shock tube in 1899, its use was only limited in studies related to combustion chemistry till the 1950s. The main reasons [34] for the dormancy of shock tube during this period was the unavailability of fast measuring equipment, lack of computer power to solve complex chemical kinetic mechanisms and simply the fact that researchers were unaware of the potential that shock tube presents for studying combustion chemistry. With current fast measuring equipment and computing power in place, shock tube based combustion

chemistry studies are well established now [34-38], so much so that it is one of the most reliable techniques for studying high temperature and pressure combustion processes.

Essentially shock tube is a long cylindrical tube separated into high and low-pressure regions, referred as the driver and driven sections respectively, by using polycarbonate or metallic diaphragms. The test gas is introduced into the driven section, the test gas pressure in driven section (P_1) is usually low ranging from 10s of Torr to few hundred Torr. The driver section is then filled in by driver gas (Helium, Nitrogen or other inert gases are usually used as driver gases) to very high pressures which eventually bursts the diaphragm (P_4). The sudden release of this high pressure into the low pressure driven region creates a shock wave which travels down the driven section and compresses the test gas behind it hence raising its temperature and pressure (T_2, P_2). At the same time, the expansion wave travels down the length of driver section. The incident shock is supersonic and usually travels down the driven section at few Mach numbers depending primarily upon the ratio of P_4 to P_1 . The incident shock gets reflected from the driven section endwall and further compresses the test gas (T_5, P_5) and also stagnates the flow. Due to the stagnation of the flow behind the reflected shock wave, the particle time experienced by the gas molecules and the lab times are the same, and hence, chemical kinetic studies are well suited behind reflected shock wave where compressed gas temperature and pressure (T_5, P_5) can be calculated using measured incident shock speeds from 1-D shock jump relations. After certain time elapse, referred to as the test time, the reflected expansion fan interacts with the stagnated high temperature and pressure observation location hence significantly reducing uniform temperature and pressure conditions and thus ending the test time.

The chemical kinetics and laser sensors laboratory features two shock tube facilities,

a low-pressure shock tube (LPST) facility which can operate up to a peak pressure of 60 bar, and a high-pressure shock tube (HPST) facility which is certified for operation till 300 bar.

The LPST is constructed from stainless steel with the internal surface honed and electro-polished. The inner diameter of the shock tube is 14.2 cm and the driven section is 9.1 m long. The driver section is modular in design with the maximum length being 9.1 m. High purity is ensured by employing turbomolecular vacuum pump to achieve an ultimate pressure of about 1×10^{-6} mbar by overnight pumping. Thirty minutes of pumping usually achieves vacuum level of 1×10^{-5} mbar with a leak rate of $< 1 \times 10^{-6}$ mbar/min. The driver and driven sections are separated by a polycarbonate diaphragm, which is ruptured by a cross-shaped cutter blade configuration when the driver section is pressurized with the driver gas. The rupturing diaphragm pressure P_4 can be varied by changing the diaphragm thickness and the cutter blade position. The incident shock speed is measured by recording the time interval between five PCB 113B26 piezoelectric pressure transducers (PZTs) that are located axially along the last 1.3 m of the driven section. Linear extrapolation of measured incident shock speed is used to determine the end-wall shock speed. Shock attenuation rates are usually less than 0.8%/m, and the error in the calculated end-wall shock speed between 0.01 – 0.2%. One-dimensional shock-jump equations are used to calculate the conditions (T_5 , P_5) behind reflected shock waves with errors of less than 1%.

The HPST at KAUST is also constructed from stainless steel with an inner diameter of 10 cm. The driven section is 6.6 m long, and the driver section has a modular design to vary its length from 2.2 m to a maximum of 6.6 m. The mid-section of the tube houses two pre-scored aluminum diaphragms in a double-diaphragm arrangement which allows better

control of the post-reflected shock conditions compared to single diaphragm arrangement, and hence provides excellent control over reflected shock thermodynamic conditions. The driven section of the shock tube can be pumped down to very low pressures using turbo-pumping to achieve high-purity conditions. Incident shock speed is measured by six equispaced pressure sensors placed axially along the last 3.7 m from the driven section end-wall. Thermodynamic conditions behind the reflected shock are calculated using standard shock jump relations; estimated uncertainties in pressure and temperature are less than 1% and 1.8% respectively.

The driven and diaphragm sections of both facilities are heated using custom built heating jackets to accommodate fuels with low vapor pressures. Also, the mixing tanks which are magnetically stirred to ensure homogeneity of the mixtures, and the mixing manifold are heated using customized heating jackets and heating tapes respectively. Typically, for the gasolines and surrogates experiments presented in this work, the shock tube and the mixing setup was heated to a maximum temperature of 100 °C. The temperature homogeneity, especially across the shock tube driven section, is ensured using separate temperature controllers for small sections (around 1.5 m); the temperature uniformity is also monitored during experiments using thermocouples, and any temperature gradients found across the shock tube driven section are compensated by adjusting the respective temperature controllers.

Shock tubes are routinely used for ignition delay measurements, and interpretation of these data is listed in detail in ref [39, 40]. In this work, two types of ignition delay data are reported. In the HPST, a molar ratio of 3.76:1 of N₂:O₂ is used to make the so-called “Fuel / air” mixtures are carried out. For such mixtures, there’s only one way to make the

mixture for a given stoichiometric value. In the LPST, typically the so-called “Argon diluted” mixtures, with high dilution levels (~ 90 % dilution), are utilized. In these diluted experiments, it is necessary to specify both the fuel percentage utilized and also the stoichiometry to properly constrain the mixtures. However, in both cases, the method to obtain ignition delay times remain same. The time zero for ignition delay measurements is defined using pressure sensors located near the endwall of driven section (2 cm for LPST and 1 cm for HPST). The onset of ignition is determined by sidewall pressure spike and by side and end wall OH* chemiluminescence, associated with $A^2\Sigma^+ \rightarrow X^2\Pi$ transition near 306 nm, detected with a lens/slit setup, a modified Thorlab PDA36A detector and a narrow bandpass filter (centered at 306nm with FWHM < 10nm). A typical shock tube experimental setup (in this case for LPST) is shown in Figure 2-1 and a typical shock tube ignition delay pressure and OH* chemiluminescence measurement (in this case for HPST), showing the definition of ignition delay time, is shown in Figure 2-2.

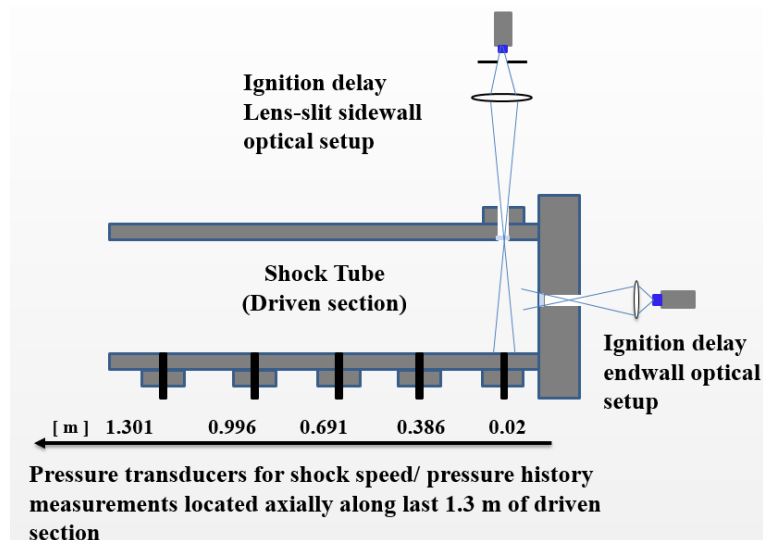


Figure 2-1: Shock tube configuration for ignition delay time measurements.

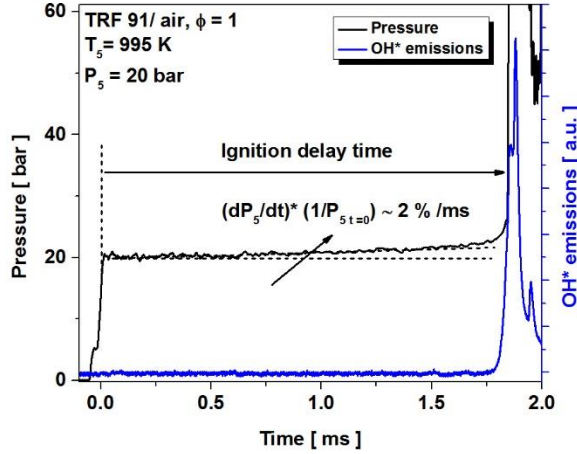


Figure 2-2: Representative shock tube pressure and OH* emission traces during ignition delay experiment.

The pressure behind the reflected shock wave gradually increases due to the interaction of the reflected shock wave with boundary layers [41]. This pressure increase and accompanying temperature increase can be neglected for high-temperature ignition experiments where ignition delay times are less than 2 – 3 ms. However, these pressure/temperature changes become significant when measuring relatively long ignition delay times. This effect is referred to as dP_5/dt and is facility-dependent with reported values in the literature ranging 1 – 10 %/ms. Shock tubes with smaller diameters have larger dP_5/dt . To account for this effect, the measured pressure variation over time is converted to volume variation using the isentropic relation and is included in the Chemkin simulations [39, 42, 43]. For the experiments reported here, dP_5/dt was found to vary between 1.5 to 3 %/ms. Assuming the worst case scenario, $3 \text{ \% /ms} \frac{dP_5}{dt} * \left(\frac{1}{P_{5t=0}}\right)$ is imposed on the constant volume reactor simulations, henceforth referred as “shock tube simulations”. The estimated uncertainty in the shock tube ignition delay measurements is $\pm 20\%$. The pressure time histories during the HPST ignition delay measurements of a wide

range of selected fuels, at high, intermediate and low temperatures, are shown in APPENDIX B.

Low-temperature long ignition delay times ($> 4 - 5$ ms) shock tube ignition data should be used with extreme caution. Such data are susceptible to pre-ignition and eventual flame kernel formation and propagation resulting in artificially shortening ignition delay times (see section 5.3.1 and Chapter 6 for detailed discussions on pre-ignition affected shock tube ignition data).

2.1.1 Test time in shock tubes

The high and low pressure shock tubes at KAUST typically use Helium as the driver gas for high-temperature ignition delay measurements. For low-temperature ignition delay measurements, however, driver gas tailoring [44, 45] is utilized to achieve long test times required for these measurements. The driver gas tailoring is achieved in real time by mixing Helium and Nitrogen (or other inert gases) gas streams from two separate mass flow controllers. The driver gas tailoring theory [44, 45] only provides general guidelines, and experimental corrections are usually required to avoid the creation of expansion or compression waves from the interaction of reflected shock wave and the contact surface (the interface between driver and driven gases). In the present work, non-reactive shock experiments (obtained by replacing O_2 with N_2 in the fuel mixture) are conducted to analyze and minimize contact surface non-idealities.

Figure 2-3 shows the measured test times in the LPST. Firstly, Figure 2-3 (a) shows the available test times (time between the arrival of reflected shock wave at the observation location and the head expansion wave), in the cases where Helium is used as the driver gas, are around 10 ms at reflected shock temperatures of around 600 K. Next, in an attempt to

increase the available test times, Helium/Nitrogen tailored gas is used. It can be seen from Figure 2-3 (b) that although the tailored driver gas significantly delays the arrival of head expansion wave at the observation location, there are some expansion waves (“under-tailored”) that are also sent into to the test by the interaction of reflected shock wave and the contact surface due to imperfect tailoring. Hence, where possible, such cases were avoided during the experiments. As mentioned before, the driver gas tailoring theories only provide mere guidelines and experimental corrections are usually required to address the non-idealities. Hong et al. [45] suggested the use of “buffer gas” to overcome these non-idealities related to imperfect driver gas tailoring. The buffer-gas, typically Helium, is a thin layer of gas introduced in the driven section close to the diaphragm location (far away from observation location, around 9.1 m away from driven endwall). This layer reduces the so called “shock-impedance” [45] by reducing the molecular weight of the driver gases at the start of contact surface. Here we utilized 5% Helium buffer gas in the driven section. The result of tailored driver gas with a thin layer of buffer gas in the driven section is shown in Figure 2-3 (c) where pressure trace shows negligible contact surface interaction with the test section resulting in a test time of around 43 ms (a factor of 4 increase in test time compared to Helium driver gas case Figure 2-3 (a)). Figure 2-3 (d) shows a similar test time increase (test time ~ 51 ms) using Helium/Carbon dioxide tailoring, note that a 2.6 % Helium buffer gas was used in this case to reduce contact surface reflected shock interaction.

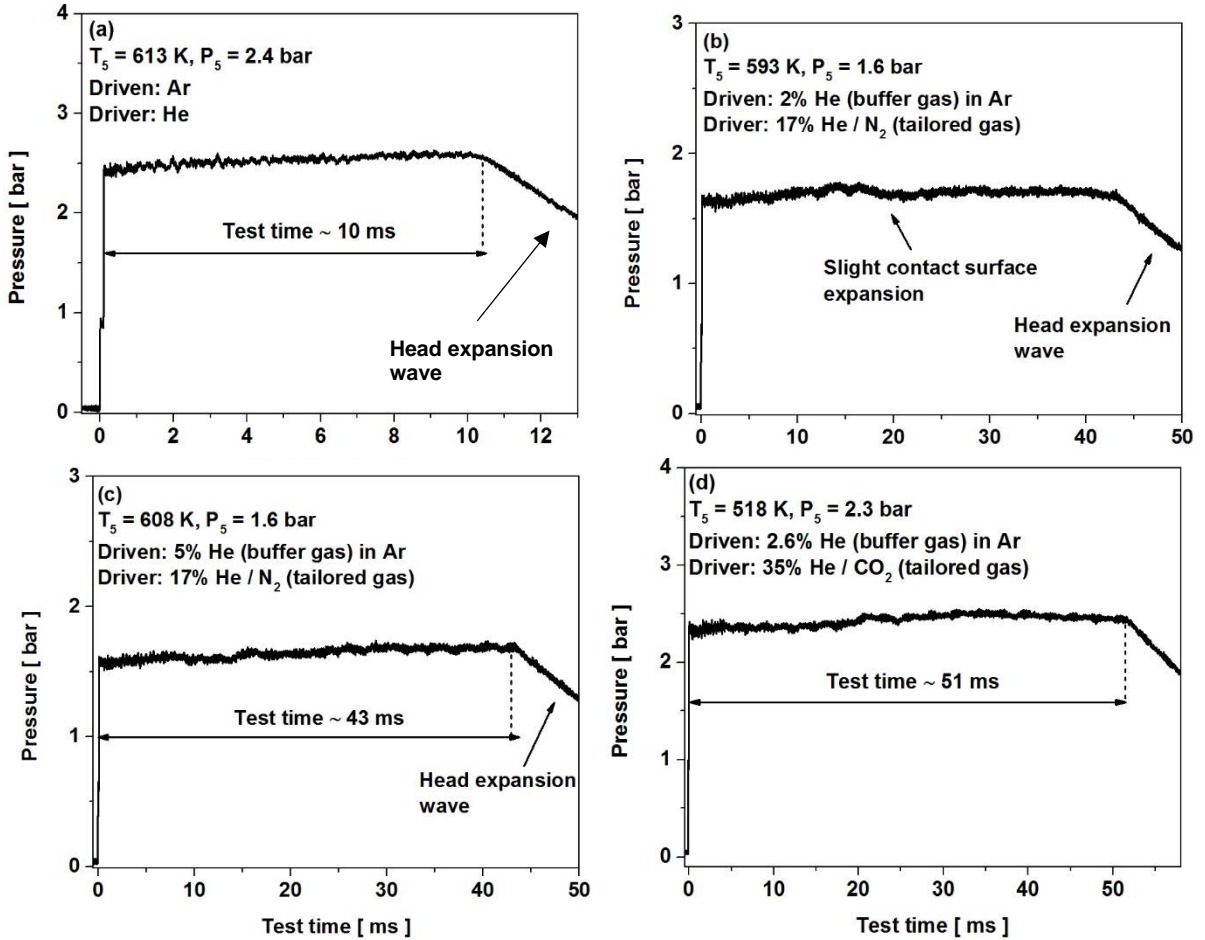


Figure 2-3: Test times measured in the LPST, for each case driver and driven section of 9.1 m length were used. (a) Helium as driver gas, $T_5 = 613 \text{ K}$, $P_5 = 2.4 \text{ bar}$, Driven gas is Argon, (b) Helium/Nitrogen (17% vol Helium) as tailored driver gas, $T_5 = 593 \text{ K}$, $P_5 = 1.6 \text{ bar}$, Driven gas is Argon, (c) Helium/Nitrogen (17% vol Helium) as tailored driver gas, $T_5 = 608 \text{ K}$, $P_5 = 1.6 \text{ bar}$, Driven gas is Argon with 5% buffer Helium gas (d) Helium/Carbon dioxide (35% vol Helium) as tailored driver gas, $T_5 = 518 \text{ K}$, $P_5 = 2.3 \text{ bar}$, Driven gas is Argon with 2.6% buffer Helium gas

Figure 2-4 shows the test time in the LPST as a function of reflected shock temperature (T_5). It can be seen from the figure that when Helium is used as the driver gas, test times at the lowest temperature are around 10 ms for Argon diluted driven gas and around 7 ms for Fuel / air driven mixtures. However, using tailoring, the Argon diluted driven mixtures test times increases to as long as 50 ms and that for Fuel / air mixtures to

around 30 ms. Results from KASIMIR [46] simulations are also shown in the figure, and the agreement between ideal theory and experimental results is rather good (within 13 %). The increased test times presented in Figure 2-4 are for the LPST; HPST has a shorter driver and driven sections and so the maximum test times achievable with current configuration is around 10 – 15 ms.

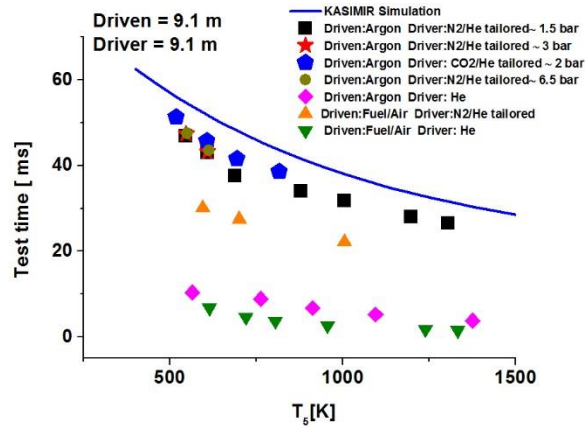


Figure 2-4: Test time as a function of temperature behind the reflected shock wave in the LPST. Driver and driven sections length is 9.1 m. Experimental measurements are included in the figure. The symbols are the measurements and the line is the simulation using KASIMIR [46] software.

2.1.2 Uncertainty in shock tube ignition delay time measurements

The shock tube ignition delay time experiments reported in this work are performed with utmost care to avoid any systematic errors in the measurements. However, there are several sources of uncertainty in the reported ignition delay measurements. Potential sources of uncertainty in the shock tube ignition delay measurements, along with their estimated uncertainty, are reported in Table 2-1. Out of these parameters, the ignition delay times are strongly dependent upon the reflected shock temperature (T_5) because of Arrhenius (exponential) dependence of ignition kinetics on the temperature. The reflected shock temperatures are calculated using one-dimensional shock jump equations which rely

on several inputs including measured shock speed (U_{IS}), temperature and pressure inside driven section before the shock (T_1 and P_1), and the enthalpies and heat capacities to perform these calculations inferred from the NASA polynomials. Effect of stoichiometry errors ($\sim 5\%$, see next paragraph) also contributes to the uncertainty estimation of reflected shock temperature. It is worth mentioning here that the uncertainty estimates presented here are conservatively estimated, and the actual calculated uncertainty on various variables are rather low. For example, the typically calculated uncertainty on the incident shock speed calculation is less than 0.2% ; however, to allow for finite shock travel time over the pressure sensors (or the pressure rise time of these sensors), the uncertainty in the counter readings for the measurement of shock travel time between successive sensors, and the uncertainty in the location of these pressure sensors, the overall uncertainty in incident shock speed is conservatively estimated to be 0.4% . The combined effect of these parameters propagated to calculate the uncertainty in temperature, by neglecting second order interactions, result in a conservatively estimated $\pm 1\%$ uncertainty on reflected shock temperatures.

Another potential source of uncertainty in ignition delay measurements is the fuel composition inside the mixing tank and the shock tube. The mixtures reported in this work were prepared manometrically, by heating the shock tube, mixing tank and manifold to high enough temperatures to fully vaporize the fuel. Moreover, the fuel vapors were not only allowed sufficient time to fully evaporate inside the mixing vessel before making the mixtures based on stoichiometry, but also the mixtures once prepared were slowly introduced into the shock tube to avoid any condensation related issues. Conservative estimate of the overall effect of these errors in mixture composition is around 5%

uncertainty on the stoichiometry reported here.

Table 2-1: Various parameters effecting shock tube ignition measurements

Source of uncertainty	Variable effected	Conservative estimated uncertainty in the variable
Pre-shock Temperature in driven section	T_1 [K]	± 2 K
Pre-shock Pressure in driven section	P_1 [torr]	± 0.2 %
Fuel composition inside mixing tank and shock tube	ϕ [-]	± 5 %
Incident shock speed	U_{IS} [m/s]	± 0.4 %
NASA polynomials	Heat capacity [J/mol-K] and enthalpy [J/mol]	± 0.5 %
Calculated reflected shock Temperature	T_5 [K]	± 1 %
Calculated reflected shock Pressure	P_5 [bar]	± 1.8 %

Equation 2-1 is used to estimate the effect of uncertainties on various parameter discussed above on the ignition delay measurements, where τ is the ignition delay time, $t_{t=0}$ is the time zero and $\tau_{determination}$ is the method (pressure or emission) used to infer ignition. In addition to the parameters discussed above, two new parameters are included in Equation 2-1. These are the uncertainty in the determination of time zero from the pressure traces and the uncertainty in the determination of the onset of ignition from the pressure and OH* emission traces. The rise time of the Kistler 603B type pressure transducers used to monitor the pressure in this work is rather small, and in the measurements reported here the rise time was around 15 – 25 micro-seconds (shock bifurcation effects, if any, also affect pressure transducer rise time; see section 2.1.3). For high-temperature ignition delay time measurements, where ignition delay times are relatively short (on order of 100 micro-second), this error in the determination of time zero

may alone result in 15 – 25 % uncertainty in the ignition delay measurements. So to avoid these large errors in ignition delay measurements, no ignition delay measurement below 100 micro-seconds is reported in this work. For longer ignition delay times (longer than 1 ms), where most of the data are reported in this work, this error in the determination of time zero becomes negligible (~ 1 – 2 %). The pressure and OH* emission signal, for the fuel/air mixtures reported here, show very steep pressure and emission rise at ignition and both methods agree well, within 2% of each other. As mentioned before, the uncertainty in the estimates of reflected shock temperature is the largest source of uncertainty in ignition delay times, and based on the n-heptane ignition delay simulations as the reference, it is estimated that a 1% reflected shock temperature uncertainty conservatively results in around 15% uncertainty in ignition delay times. Similarly, it is determined that pressure and equivalence ratio results in around 2% uncertainty each in ignition delay times. Finally combining all these effects in Equation 2-1, the conservatively estimated uncertainty in ignition delay times are 28% for ignition delay times less than 1 ms and around 16% for longer ignition delay times. Therefore, here we have reported an average conservative estimate of our shock tube ignition delay measurements of around 20 – 22 %.

$$\Delta\tau = \sqrt{\left(\frac{\partial\tau}{\partial T_5} dT_5\right)^2 + \left(\frac{\partial\tau}{\partial P_5} dP_5\right)^2 + \left(\frac{\partial\tau}{\partial \Phi} d\Phi\right)^2 + \left(\frac{\partial\tau}{\partial t_{t=0}} dt_{t=0}\right)^2 + \left(\frac{\partial\tau}{\partial \tau_{determination}} d\tau_{determination}\right)^2}$$

Equation 2-1

2.1.3 Reflected shock bifurcation

Reflected shock bifurcation occurs when the boundary layer (behind the incident shock wave) doesn't have enough momentum to pass through the normal reflected shock

wave, resulting in oblique shock patterns formation [47]. Petersen et al. [47] developed experimental correlations to determine the size and duration of disturbed region due to bifurcation. They reported that such disturbances are related to specific heat ratios, molecular weight and incident shock Mach number; and such disturbances are aggravated for large proportion of di- and poly-atomic test gases. They also showed that such non-idealities are a weak function of reflected shock pressures and hence are equally susceptible to appear in both high and low pressure shock tubes experiments. They further showed that, for bifurcated cases, the reflected shock pressure rise, instead of single pressure jump, show two clear demarcations due to oblique shock related pressure rise. Therefore, pressure transducers, monitoring the pressure in the test section, are a good indicator of assessing the severity (and existence) of shock bifurcation.

Reflected shock bifurcation for HPST measurements (Chapter 3 – Chapter 5)

As mentioned before, the typical rise time of the pressure sensor at the arrival of reflected shock wave in all the HPST ignition delay experiments reported here (Chapter 3 – Chapter 5) is between 15 – 25 micro-seconds. Obviously, this rise time, may also include the shock bifurcation effects in addition to inherent pressure sensor rise time. The sensor's inherent response frequency is 300 kHz (3.3 micro-seconds) and so the inherent rise time of the sensor by itself, taking into account the finite shock wave travel time over the 5 mm diameter sensor active area, and other transducer non-idealities, may alone result in 10 – 15 micro-seconds of pressure rise time. However, for HPST ignition experiments, no shock bifurcation (a two-step like reflected shock pressure rise) was experimentally observed on the pressure traces. Hence, shock bifurcation effects on the HPST ignition measurements can be neglected and may only play a role for the determination of short ignition delay

times (these effects of shock bifurcation, in terms of pressure sensor rise time, at high temperatures and short ignition delay times have already been included in the uncertainty analysis). To further assess reflected shock bifurcation, here the correlations proposed by Petersen et al. [47] are utilized to determine the bifurcation step height (l , $l \propto M_s^{1.07} \gamma_2^{-2.66} M_{avg}^{-0.37}$) and the normal shock part of the bifurcation step passage time (dt_{AO} , $dt_{AO} \propto M_s^{0.66} \gamma_2^{-7.1} M_{avg}^{-0.57}$). For a typical shock tube Fuel/ air ignition delay experiment, at reflected shock temperature and pressure of around 800 K and 40 bar respectively, the bifurcation step height is around 1 mm and the normal shock passage time is around 3 – 5 micro-seconds. Thus, for a 10 cm diameter HPST shock tube, a bifurcation step height of 1 mm (in terms of perimeter $2\pi r$) will effect less than 1% of total flow area near the endwall observation location. The small bifurcation time also clearly show that, either a bifurcation doesn't exist, as also observed experimentally, or will very quickly reach reflected shock pressure (and temperature) conditions. Selected pressure traces from HPST ignition measurements are reported in APPENDIX B.

Reflected shock bifurcation for LPST measurements (Chapter 4 and Chapter 6)

Like HPST, the LPST Argon diluted ignition and speciation experiments reported in Chapter 4 also don't show any signs of reflected shock bifurcation.

However, the pre-ignition effected shock tube ignition delay experiments reported in Chapter 6 does show some weak effects of shock bifurcation in measured pressure traces. Figure 2-5 shows the shock bifurcation effects on the measured pressure profile. The reactive mixture for these experiments is 2% n-heptane, 44% O₂, Ar and reflected shock temperature and pressure are $T_5 = 1124$ K, $P_5 = 1.6$ bar. The measured pressure trace not only show shock weak bifurcation (two step-like pressure increase due to oblique reflected

shock), but also the rise time of the pressure transducer to achieve these reflected shock conditions is relatively larger (~ 50 micro-seconds). Using the same correlations as for the HPST measurements, it is determined that for these experiments, the bifurcation step height is around 3 mm and the normal shock passage time is around 10 micro-seconds. Thus, for a 14 cm diameter LPST shock tube, a bifurcation step height of 3 mm (in terms of perimeter $2\pi r$) will effect around 2% of total flow area near the endwall observation location. The relatively large bifurcation time also show the existence of shock bifurcation for these conditions. These experiments suffer from pre-ignition and localized flame initiation, and the shock bifurcation may also have an effect on the initiation and propagation of pre-ignition modes (see Chapter 6Chapter 6).

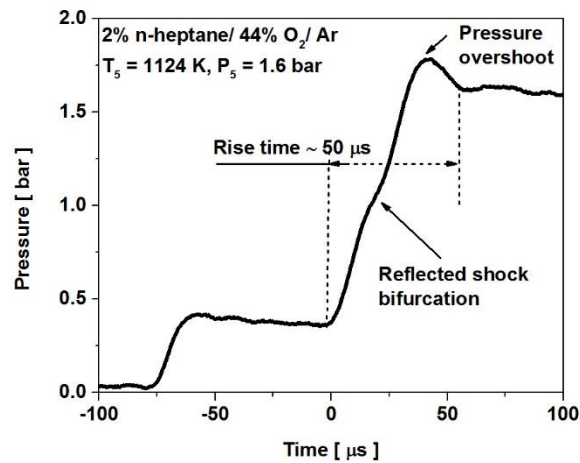


Figure 2-5: Measured pressure profile showing weak shock bifurcation effects. Mixture: 2% n-heptane, 44% O₂, Ar. T₅ = 1124 K, P₅ = 1.6 bar.

2.2 Rapid compression machine facility and ignition measurements

The KAUST rapid compression machine (RCM) is based on a twin opposed piston design, similar to that used at NUI Galway [48]. A twin-piston configuration offers better mechanical balance and lower compression times than a single piston configuration. The

chamber bore is 50.8 mm, and the stroke length of each piston is 169 mm. With the current configuration, volumetric compression ratios up to 16.8 can be achieved. The duration for the final 50% of the pressure rise in the compression stroke is approximately 3 ms. The pistons are driven by a pneumatic mechanism coupled with a hydraulic system to lock the pistons in place at the end of the compression. The desired conditions at the end of compression can be achieved by varying the compression ratio, the initial pressure (p_0), the initial temperature (T_0) and the diluent gas compositions. Equation 2-2 shows the compressed gas temperature, T_c , calculated using the adiabatic core hypothesis:

$$\int_{T_0}^{T_c} \frac{\gamma}{\gamma - 1} \frac{dT}{T} = \ln\left(\frac{p_c}{p_0}\right) \quad \text{Equation 2-2}$$

where p_c refers to the measured pressure at the end of compression and γ is the ratio of specific heats. The entire combustion chamber is covered with custom-made heating jackets to pre-heat the reacting mixture. A Kistler 6045A pressure transducer mounted on the chamber wall is used to record the experimental pressure traces. The ignition delay time is defined as the time between the end of compression (EOC) and the onset of ignition; both events were measured by a step-change in the pressure. A typical RCM ignition delay time measurement is shown Figure 2-6. Creviced piston heads are used to avoid vortex formation, and the crevice volume is $\sim 10\%$ of the total post-compression chamber volume [49]. If RCM experiments are to be successfully modeled, it is necessary to compensate for heat loss from the chamber, which is simulated as an adiabatic expansion using a volume profile calculated from pressure measurements in non-reactive experiments (conducted by replacing O_2 with N_2 in the reactive mixture, see dotted lines in Figure 2-6) [50]. The estimated uncertainty in RCM ignition delay measurements is $\pm 15 - 20\%$.

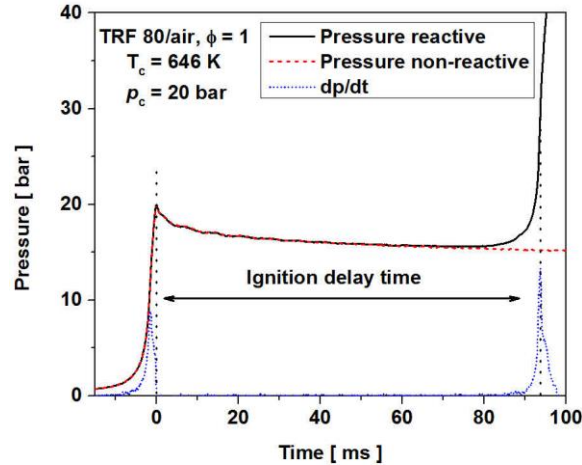


Figure 2-6: Representative RCM pressure trace during ignition delay experiment.

2.2.1 Uncertainty in RCM ignition delay time measurements

As mentioned before, ignition kinetics is strongly dependent on temperature. Hence, like for shock tube ignition measurements, the biggest source of uncertainty in RCM ignition measurements is the uncertainty in the calculation of compressed gas temperature (T_c). Equation 2-2 shows various parameters involved in the calculation of T_c . The uncertainty in T_c calculation arises from the uncertainty in measured initial temperature T_0 ($\pm 2K$), uncertainty in measured initial pressure p_0 ($\pm 0.2\%$), uncertainty in the heat capacity ratio γ calculated using NASA polynomial ($\pm 0.5\%$), uncertainty in the measured mixture composition ($\pm 5\%$ in terms of ϕ), and most importantly the uncertainty in the determination of compressed gas pressure p_c ($\pm 2.5\%$) from the measured pressure trace. Out of all these parameters, the uncertainties in the determination compressed gas pressure and the mixture composition contributes most significantly to the uncertainty to the compressed gas temperature calculation, with respective contributions of 0.7% and 0.5% . Including all these parameters, the prescribed uncertainty on compressed gas temperature calculation is around $\pm 1\%$ resulting in conservatively estimated uncertainty in RCM

ignition delay times of around 15 – 20 %.

2.3 Lasers diagnostics

The chemical kinetics and laser sensors laboratory features a wide range of laser sensors covering a wide range of spectra for various applications. Here, only a brief overview of the laser sensors used in this work is provided below.

IR absorption of CO using a DFB QCL:

Carbon monoxide concentration is monitored near 2193.36 cm^{-1} in the fundamental vibrational band of CO using a distributed-feedback (DFB) quantum cascade laser (QCL). The line-broadening parameters for this line were measured by Ren et al. [51] and line-strength values were obtained from the HITRAN database [52]. A small amount of absorption interference is caused by CO₂ at high temperatures. This is corrected by measuring CO₂ absorption cross-section at this wavelength (2193.36 cm^{-1}) in separate CO₂/Ar shock-heated experiments. The CO₂ interference is then subtracted from the measured CO absorption profiles using the CO₂ mole fraction measurements.

IR absorption of CO₂ using an external-cavity QCL:

An external-cavity QCL is used at a fixed wavelength for laser absorption of CO₂. The R(76) line at 2390.52 cm^{-1} in the ν_3 vibrational band of CO₂ was selected due to its relatively high lower-state energy and minimal interference from other species. High-temperature cross-sections of CO₂ at the peak of the transition were measured in our shock tube using CO₂/Ar mixtures and verified with previous measurements by Ren et al. [53, 54].

IR absorption of H₂O using a DFB diode laser:

H₂O concentrations are monitored using a distributed feedback (DFB) diode laser

operating at 3416.16 cm^{-1} in the ν_3 vibrational band of H_2O . This line provides increased absorption strength compared to the transitions used in previous H_2O sensing work [55, 56]. Absorption cross-sections for this transition were measured in separate experiments of shock-heated mixtures of $\text{H}_2\text{O}/\text{Ar}$.

UV absorption of OH using a ring-dye laser:

Hydroxyl concentrations are measured using frequency doubling of 613.4 nm cw light generated by a Spectra Physics ring-dye laser system. This ring-dye laser system is pumped by a Coherent Verdi laser operating at 532 nm. The $R_1(5)$ transition near 306.7 nm in the OH A-X (0, 0) absorption band is probed to measure OH mole fraction [57]. Negligible interference absorption is observed during OH measurements for FACE A and PRF 84 (see Chapter 4) oxidation. However, small interference absorption is detected at 306.7 nm during FACE C ignition experiments. This interference is corrected for by making off-line measurements, 5 cm^{-1} away from the peak of selected OH absorption transition.

Chapter 3: IGNITION STUDIES OF LOW OCTANE GASOLINES AND SURROGATES

In this chapter, ignition delay times of low octane gasolines are reported. Low octane gasolines are prospective fuels for advanced combustion engine technologies, and chemical kinetics (autoignition) is one of the primary control mechanisms in such engine combustion modes. Ignition delay data for low octane gasolines are scarce in the literature. The data presented here are one of the first ignition delay data for low octane gasolines. The rest of the chapter is organized as follows; firstly, a detailed characterization of our test fuels, light naphtha and FACE gasoline I and J, and surrogate formulation for them is presented. Next, ignition delay times of these fuels, measured in shock tube and rapid compression machine (RCM), are presented and discussed in detail. Finally, chemical kinetics analysis is used to explain the ignition delay results and also to shed some light on the surrogate requirements of these fuels in homogeneous shock tube/RCM environments.

3.1 Introduction

The transportation sector accounts for around half of global oil consumption and around 23 % of global CO₂ emissions [2, 3]. Post COP 21 (Paris 2015) world calls for stringent restrictions on emissions and associated environmental impact. Thus improvements in the transportation sector are necessary to reduce its environmental footprint. Gasoline is widely used light duty transportation sector fuel hence improving the fuel efficiency of gasoline-fired engines is of utmost importance. Several futuristic gasoline compression ignition (GCI) engine technologies such as homogeneous charge compression ignition (HCCI), dual-fuel reactivity controlled compression ignition (RCCI), partially

premixed compression ignition (PPCI) and other variants have potential to increase the efficiency of traditional gasoline engines [6].

GCI engines have several advantages over conventional spark ignition gasoline engines. These engines will operate at higher compression ratios and thus will improve the overall thermal efficiency and make it comparable to diesel compression ignition technologies [58]. Researchers have shown that such GCI engines will operate at their optimum with gasoline being in 50 – 70 octane (research octane number RON and motor octane number MON) range [59-61]. This low octane requirement, compared to conventional gasolines whose RON are typically greater than 90, can significantly reduce the refinery costs and emissions by eliminating the catalytic reforming and isomerization units required for the production of high octane gasolines. Life cycle analysis [2] of GCI engines employing low octane fuels further shows around 25% energy consumption reduction and around 23% CO₂ emissions reduction compared to convention spark ignition engines and gasolines. Moreover, there is growing disparity in the demand of diesel and gasoline fuels resulting in lighter fractions of hydrocarbons (the so-called “homeless hydrocarbons”) being left unused. Such imbalance can also be potentially solved by employing GCI engine technologies that operate with lighter hydrocarbon streams and hence can reduce the pressure faced by many refineries around the world.

Chemical kinetics is one of the primary combustion phasing control mechanisms in the GCI technologies [62]. Correct representation of the fuel ignition kinetics is key if such systems are to be successfully modeled. Due to limitations of computational resources, simulations often rely on binary or multi-component fuel surrogates to mimic the behavior of the real fuel. Low octane gasolines are relatively less studied in the literature compared

to conventional gasolines. Experimental investigations of low octane gasolines are scarce [63-68] and the autoignition characteristics of such fuels have not been studied previously in fundamental combustion experiments. Chang et al. [63, 64] studied light and heavy naphtha in PPCI engines and found that the use of petroleum naphtha in PPCI mode can indeed result in overall efficiency improvements and reductions in pollution. Yang et al. [67] showed that hydrobate (RON ~ 69) was less reactive than the corresponding PRF mixture under HCCI conditions. Yang et al. [65, 66] utilized double and multiple injection strategies on a single cylinder diesel engine operating with straight-run naphtha fuel (RON ~ 58.8) and showed that multiple injection strategies are advantageous for NO_x reduction and efficiency improvements. Javed et al. [69] and Abbad et al. [70] have also provided a wide range of ignition delay data for Toluene/PRF (TPRF) (see 0) and PRF blends for fuels ranging from RON 70 – 97.5 which can be used to model low octane (RON ~ 70) gasolines. Detailed experimental and CFD investigations (with surrogate fuels) are needed if petroleum naphtha is to be introduced as a viable future fuel in the transportation sector.

Primary reference fuel (PRF) surrogates (mixtures of n-heptane and iso-octane), are the simplest and most widely investigated gasoline surrogates. Since a PRF surrogate is composed only of paraffinic fuels, it has zero sensitivity. Sensitivity is defined as the difference between the research (RON) and motor (MON) octane numbers, and is a measure of the non-paraffinic nature of a fuel. Commercial gasolines can have a high content of aromatics (~ 20-30 %) and other non-paraffinic (~ 5-10 %) species [71], giving the fuel high sensitivity. More complex surrogates are needed to represent the reactivity of high-sensitivity fuels. Typically, toluene is added to PRF mixtures as a substitute for the aromatic compounds present in commercial gasolines. These three-component surrogates

are referred to as ternary (or toluene) reference fuels. For a typical ternary surrogate, the toluene concentration is fixed at around 10 – 20 % by volume, to achieve an H/C ratio close to that of real gasolines [72], and the PRF composition is then varied to match the octane rating (RON/MON). Gauthier et al. [23] studied the auto-ignition characteristics of RD387 gasoline and a ternary surrogate (63% iso-octane, 20% toluene, 17% n-heptane by volume) at high pressures behind reflected shock waves. They showed that the ternary surrogate adequately captured the auto-ignition behavior of a full-blend gasoline at high temperatures ($T > 850$ K). Chaos et al. [72] studied a ternary surrogate in a variable pressure flow reactor and developed an optimized kinetic mechanism. Kukkadapu et al. [27] extended the ignition studies of RD387 gasoline to low temperatures in a rapid compression machine. Kukkadapu et al. [28, 73] reported better agreement of a four-component surrogate (iso-octane, n-heptane, toluene and 2-pentene) with low-temperature ignition delay times for RD387, compared to the ternary surrogate used by Gauthier et al. [23].

More systematic approaches to formulate surrogates based on targeted optimization of palette species yield multi-component (three or more components) surrogates [74-78]. Dooley et al. [74, 75], in their works on jet fuel surrogate formulation, have proposed a strategy to emulate the active radical pool formed after initial fuel consumption. Their methodology does not require detailed a priori knowledge of the fuel composition, and the surrogate is formulated by optimizing the average molecular weight (MW), H/C ratio, derived cetane number (DCN), and threshold sooting index (TSI) of those palette species that produce a noticeably different radical pool from each other. Mueller et al. [76] have framed an approach to formulate diesel surrogates based on targeted nonlinear multi-objective optimization of fuel composition, ignition quality, volatility, and density. Ahmed

et al. [77] have developed a novel computational architecture that couples CHEMKIN-PRO with an optimization scheme to formulate surrogates that emulate physical and chemical properties of real fuels.

The purpose of the present work is to investigate the auto-ignition characteristics of low-octane fuels and to propose a suitable kinetic surrogates for them. Ignition delay times are measured for Saudi Aramco's light naphtha fuel and for Conoco Philipps Chemical Company's FACE gasoline I and J over a wide range of test conditions using a high pressure shock tube and a rapid compression machine. Measured data are compared against the simulations of simple PRF surrogate and carefully assembled multi-component surrogate. Chemical kinetic analyses are utilized to explain the trends seen in ignition delay experiments and to understand the key differences between the surrogates.

3.2 Methodologies

3.2.1 Light naphtha fuel characterization and surrogate formulation

The light naphtha fuel used in this work was supplied by Saudi Aramco and its composition was characterized at their Research and Development Center (R&DC) using detailed hydrocarbon analysis (DHA) with standard ASTM D6733 and D6730 methods. These methods allow full resolution of all chemical functionalities present in the fuel, such as n-paraffins, iso-paraffins, olefins, naphthenes and aromatics (PIONA), as well as carbon number analysis of individual functionality. The RON and MON of light naphtha were also measured at Saudi Aramco R&DC in accordance with standards ASTM D2699 and ASTM D2700, respectively. The results of these tests are summarized in Table 3-1. Light naphtha is a lightweight (avg. mol. wt. = 78.4), low-octane (RON = 64.5), and low-sensitivity

(sensitivity = RON – MON = 1) fuel. The DHA shows the fuel to have a highly paraffinic nature with > 90 mol% paraffins (~ 55.4% C₅ – C₆ n-paraffins and 35.9% C₆ – C₇ iso-paraffins). Naphthenes (cycloalkanes) are also present in light naphtha (about 6.7%) and the aromatic content of this fuel is a mere 1.32%. The detailed DHA of light naphtha is included as Appendix (Table A1).

Table 3-1: Properties of light naphtha and its surrogates. Hydrocarbon types are given in mol%.

	Light naphtha	LN- KAUST	PRF 64.5
RON	64.5	63.3	64.5
MON	63.5	61.5	64.5
Sensitivity	1	1.8	0
H/C ratio	2.34	2.32	2.26
Avg. mol. wt.	78.4	77.42	108.9
<i>n</i> -alkanes	55.4	55.0	38.0
<i>iso</i> -alkanes	35.9	35.0	62.0
Cycloalkanes	6.7	10.0	0.0
Aromatics	1.32	0.0	0.0

Two surrogate mixtures were evaluated for light naphtha in this work. A PRF surrogate matching the RON of light naphtha (PRF 64.5; 64.5% vol iso-octane/ 35.5% vol n-heptane) was utilized as the simplest surrogate. The Lawrence Livermore National Laboratory (LLNL) gasoline surrogate mechanism (hereafter referred to as LLNL mech) [79] was used for the PRF 64.5 simulations. A multi-component surrogate for light naphtha (denoted as LN-KAUST) was formulated based on the methodology of nonlinear constrained optimization to match target properties of the real fuel [68, 77]. This methodology relies on optimization of palette species based on target properties. At KAUST, a palette of 10 species has been identified as potential surrogate candidates, with

major criteria being the availability of detailed and validated chemical kinetic mechanisms for the species and also relevance to gasoline like fuels. This palette include paraffins (n-butane and n-heptane), i-paraffins (2-methylbutane, 2-methylhexane, i-octane), olefin (1-hexene), naphthenes (cyclopentane, cyclohexane) and aromatics (toluene, 1,2,4-trimethylbenzene); hence covering various PIONA classes present in commercial gasoline like fuels. The optimization scheme utilized H/C ratio (governs equivalence ratio), density (governs viscosity, spray formations, flow characteristics and mixing behavior), RON and MON (gasolines like fuels are rated on RON and MON standards), volatility characteristics [80] (governs vaporization), carbon type distribution [81] (governs chemistry) and average molecular weight as constraints. The resulting surrogate consisted of five components: 55 mol% n-alkanes (43% n-pentane, 12% n-heptane), 35 mol% iso-alkanes (10% 2-methylhexane, 25% iso-pentane) and 10 mol% cyclopentane. It can be seen from Table 3-1 that this optimized surrogate closely matches basic physical and chemical properties of light naphtha. A detailed comparison of the properties of light naphtha and this multi-component surrogate (LN-KAUST) are given in the Appendix (Tables A1 – A2, Figure. A1 – A4). Ignition delay simulations for this surrogate are performed using a newly assembled gasoline surrogate mechanism (denoted as FACE gasoline mechanism) [30].

3.2.2 FACE gasoline I and J fuel characterization and surrogate formulation

The US Department of Energy and the Coordinating Research Council comprising of research institutes, automotive and oil companies have recently formulated a set of fuels, known as Fuels for Advanced Combustion Engines (FACE). One of the basic aims of formulating these FACE fuels is to provide a consistent set of fuels with well-characterized properties and compositions, making it easy to compare research results at various

institutions and facilities.

The FACE gasolines I and J were acquired from Conoco Philipps Chemical Company and their compositions are shown in Table 3-2. It can be seen that FACE I is highly paraffinic (~ 84 mol %) and have some aromatic (~ 5 mol %) and olefinic (~ 7 mol %) content as well. FACE J also has high paraffinic (~ 64 mol %) content, but it also consists of high aromatic (~ 30 mol %) content as well. Octane measurements of these fuels are also shown in Table 3-2. It can be seen that both gasolines are low sensitivity fuels. It can be further seen from the table that the two gasolines, with widely different compositions, have a quite similar anti-knocking index ($AKI = \frac{RON+MON}{2}$) of around 70. Therefore, a PRF 70 surrogate is used in this work to compare with the FACE gasoline I and J data.

Multi-component surrogates formulated for FACE I and FACE J, henceforth referred to as FG-I and FG-J respectively, are also shown in Table 3-2 and Table 3-3. The FG-I (seven component) and FG-J (five component) were formulated using the surrogate formulation methodology developed at KAUST by Ahmed et al. [77]. This methodology has been previously used to formulate the multi-component surrogates for FACE gasolines A and C [29], FACE gasolines F and G [30] and for light naphtha [31], to say a few. It can be seen from the tables that FG-I and FG-J closely matches various targets of FACE I and FACE J respectively; whereas, a simple PRF 70 surrogate only matches the octane number of the fuels. Here, ignition delay times of FACE I and FACE J will be compared with the experimentally measured ignition delay times of PRF 70 and with the simulations of PRF 70, FG-I and FG-J surrogates. FACE gasoline mechanism [30] is used for ignition delay times simulations in this study.

Table 3-2: Properties of FACE gasoline I and J and multi-component and Primary Reference Fuel (PRF) surrogates. Hydrocarbon types are given in mol%.

	FACE I	FG-I surrogate	FACE J	FG-J surrogate	PRF 70 surrogate
RON	70.3	70.7	71.8	71.7	70
MON	69.6	68.4	68.8	67	70
Sensitivity	0.7	2.3	3	4.7	0
AKI	69.95	69.55	70.3	69.4	70
Avg. mol. wt.	95.5	98.9	94.7	93.1	109.7
<i>n</i> -alkanes	14	12	31.5	32.3	33.0
<i>iso</i> -alkanes	70	72	32.4	33.1	67.0
Cycloalkanes	4	6	2.4	-	0.0
Aromatics	5	4	30.6	34.6	0.0
Olefins	7	6	0.6	-	0.0
Unidentified	-	-	2.5	-	-

Table 3-3: Composition of the multi-component and PRF surrogates. Note that compositions are listed as mole fractions here.

	FG-I surrogate	FG-J surrogate	PRF 70 surrogate
n-butane		0.13	-
2-methylbutane	0.11	-	-
2-methylhexane	0.27	0.25	-
1-hexene	0.06	-	-
n-heptane	0.12	0.2	0.33
2,2,4-trimethylpentane	0.34	0.08	0.67
cyclopentane	0.06	-	-
toluene	0.04	0.34	-

3.3 Results and discussion

Ignition delay measurements were performed behind reflected shock waves in a high-pressure shock tube (HPST) and a rapid compression machine (RCM) at King Abdullah University of Science and Technology (KAUST). Throughout this section, solid symbols represents ignition delay results from HPST and open symbols are ignition delay data from RCM. For experimental and simulation details see Chapter 2.

3.3.1 Ignition delay times of light naphtha and surrogates

HPST ignition delay times and simulations

High-pressure shock tube (HPST) ignition delay times for light naphtha / air mixtures are shown in Figure 3-1 (a) – (c) (solid squares). Ignition delay times decrease with an increase in pressure for all equivalence ratios. The data show typical high-temperature ($T > 900$ K) Arrhenius behavior and negative temperature coefficient (NTC) behavior at intermediate temperatures ($800 < T < 900$ K). We also note that ignition delay times decrease with increasing equivalence ratio at each pressure (not shown), with fuel-rich ($\phi = 2$) mixtures being fastest. In a separate experimental campaign, shock tube ignition delay times were measured for a PRF 70 blend at $\phi = 0.5$ and 1. Ignition delay times for light naphtha and PRF 70 show reasonable agreement (Appendix Figure A5). However, in the NTC region at 20 bar, the PRF 70 data are slightly slower than the light naphtha data. Mehl et al. [82] have shown that the ignition delay times at 825 K and 20 bar can be correlated with the research octane number of the fuel, with fuels of higher octane rating yielding longer ignition delay times. The small differences in ignition delay between light naphtha and PRF 70 can therefore be attributed to their different octane ratings (RON 64.5 vs. 70).

Ignition delay shock tube simulations of the PRF 64.5 surrogate (using LLNL mech,

dotted lines) and LN-KAUST surrogate (using FACE gasoline mechanism, solid lines) are also shown in Figure 3-1 (a) – (c). Both the LN-KAUST and PRF 64.5 surrogate simulations are in reasonable agreement with each other except at $\phi = 2$, where the PRF 64.5 simulations show shorter ignition delay times compared to the multi-component surrogate simulations. Moreover, both simulations are in good qualitative and quantitative agreement with the measured light naphtha shock tube ignition delay data and capture the pressure, temperature and equivalence ratio trends of the experiments. These experimental and simulated observations are consistent with those reported by Sarathy et al. [29], who showed that for highly paraffinic gasolines, a PRF surrogate suffices for the ignition requirements in the high temperature and NTC regions.

RCM ignition delay times and simulations

Rapid compression machine (RCM) ignition delay times for light naphtha / air mixtures are shown in Figure 3-1 (a) – (c) (open squares). Both HPST and RCM data show excellent consistency and have some overlapping data points as well. The RCM data, particularly at lower temperatures, show very weak pressure dependence, with ignition delays at 40 bar being only marginally shorter than at 20 bar. We also note that the low-temperature RCM data show negligible dependence on the equivalence ratio (not shown).

Ignition delay RCM simulations of the PRF 64.5 surrogate (using LLNL mech, dotted lines) and LN-KAUST surrogate (using FACE gasoline mechanism, solid lines) reproduce weak dependence on pressure and equivalence ratio observed in experiments. It can be seen clearly that at these low-temperature ($T < 714$ K) RCM conditions, the PRF 64.5 simulations show significantly shorter ignition delay times compared to the multi-component simulations, in particular at $\phi = 1$ and 2. The LN-KAUST surrogate simulations

closely capture the measured ignition delay data of light naphtha. This points to the fact that, at low temperatures, reactivity of a lightweight fuel (Avg. Mol. Wt. light naphtha = 78.4) matches best with the surrogate that most closely mimics the compositional makeup of the fuel, and a simple binary PRF surrogate may not fulfil the low-temperature ignition requirements even for a highly paraffinic lightweight.

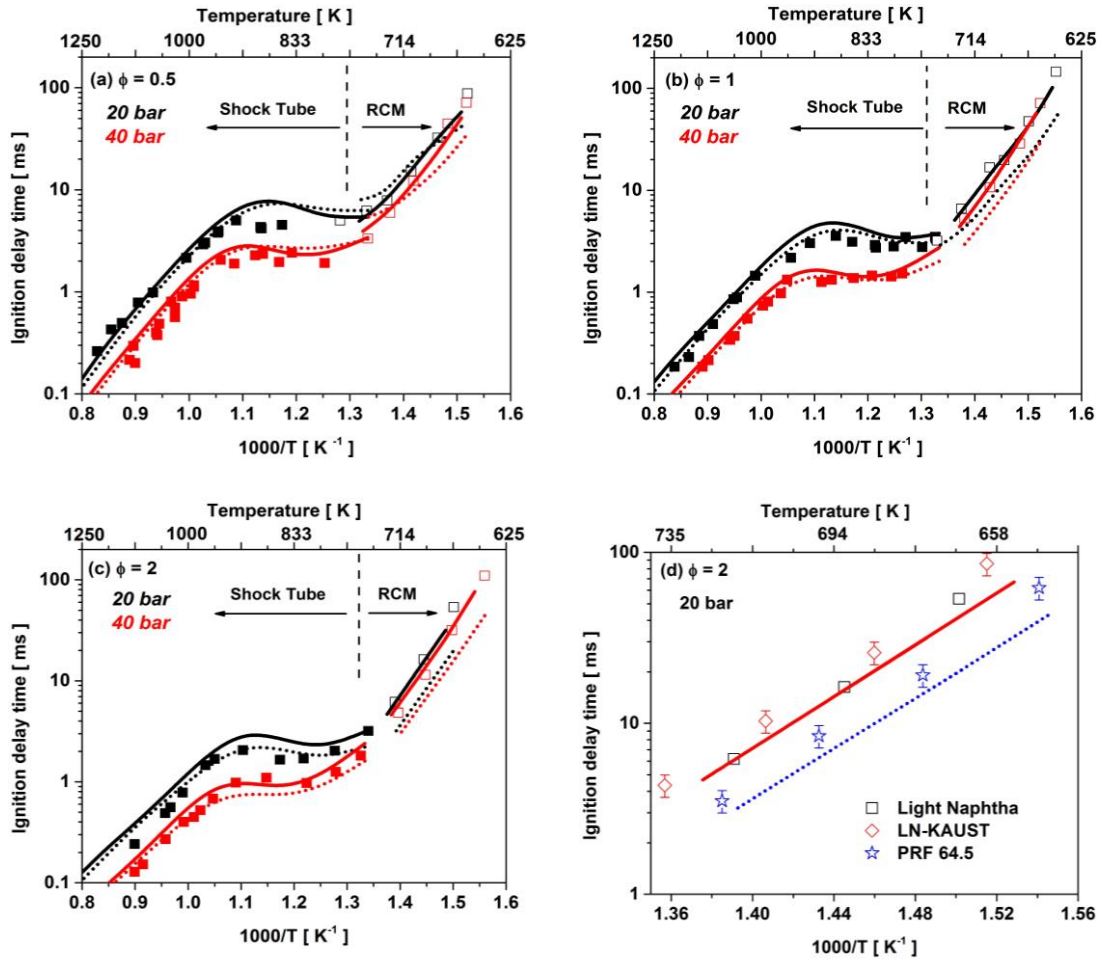


Figure 3-1: Measured and simulated ignition delay times for: (a) light naphtha at $\phi = 0.5$, (b) light naphtha at $\phi = 1$, (c) light naphtha at $\phi = 2$, and (d) light naphtha, LN-KAUST and PRF 64.5 surrogates at $\phi = 2$. Solid symbols: shock tube data, open symbols: RCM data. Solid lines: LN-KAUST surrogate simulations, dotted lines: PRF 64.5 simulations.

To explore the differences in reactivity at low temperatures, further RCM ignition

experiments were performed for the PRF 64.5 and LN-KAUST surrogate mixtures; the results are plotted in Figure 3-1 (d). These experiments were carried out at 20 bar and under rich conditions ($\phi = 2$), where the greatest differences were seen (Figure 3-1 (c)). The measured ignition delays confirm the simulated trends of the two surrogates. There is approximately a factor of two difference in the reactivity of light naphtha (black squares) and PRF 64.5 (blue stars). Ignition delay times for the LN-KAUST surrogate (red diamonds) are in good overall agreement with the light naphtha experimental data and with the LN-KAUST simulations (solid red line).

3.3.2 Ignition delay times of FACE gasoline I and J and surrogates

HPST and RCM ignition delay times

Figure 3-2 shows the ignition delay measurements of FACE I (circles) and FACE J (squares) at 20 and 40 bar and at an equivalence ratio of 1 (Figure 3-2 (a)) and 0.5 (Figure 3-2 (b)). It can be seen from the figure that, in general, the two gasolines with vastly varying compositions and similar octane ratings, FACE I and FACE J ignition delay times are in good agreement with each other over the entire temperature range. Furthermore, it can be seen that both fuels exhibit full NTC behavior in temperature range of $\sim 750 - 850$ K. These results are in line with literature findings [29, 31] that two gasolines with similar octane numbers and low sensitivity also exhibit very similar ignition delay times. Small differences in octane numbers (RON and MON) of these two gasolines and their effect on ignition delay times are also evident in these measurements (albeit scatter and consistency of these fine trends over wider range in these measurements may render the current differences as minor effects). Mehl et al. [83, 84] have shown that ignition delay times correlates well with RON of the fuel in the NTC region (825 K, 25 atm) with lower RON

resulting in lower ignition delay times; our data at 20 bar, especially for $\phi = 1$ (Figure 3-2 (a)), shows that FACE I with slightly smaller RON than FACE J (RON 70.3 vs 71.8) has also faster ignition delay times. Sarathy et al. [30] have shown that fuel with high sensitivity (lower MON) exhibit lower ignition delay times in 800 – 900 K temperature range (out of NTC region) compared to low sensitivity gasoline of similar AKI; our RCM data at $\phi = 0.5$ (Figure 3-2(b)) exhibit this trend with FACE J (MON = 68.8) being slightly faster than FACE I (MON = 69.6). Nonetheless, it is acknowledged here that neither the octane number differences between these gasolines are larger enough, nor the data is scatter free and consistent in these fine trends over a wider range to ascertain these points with same conviction as done in previous studies [30, 83, 84].

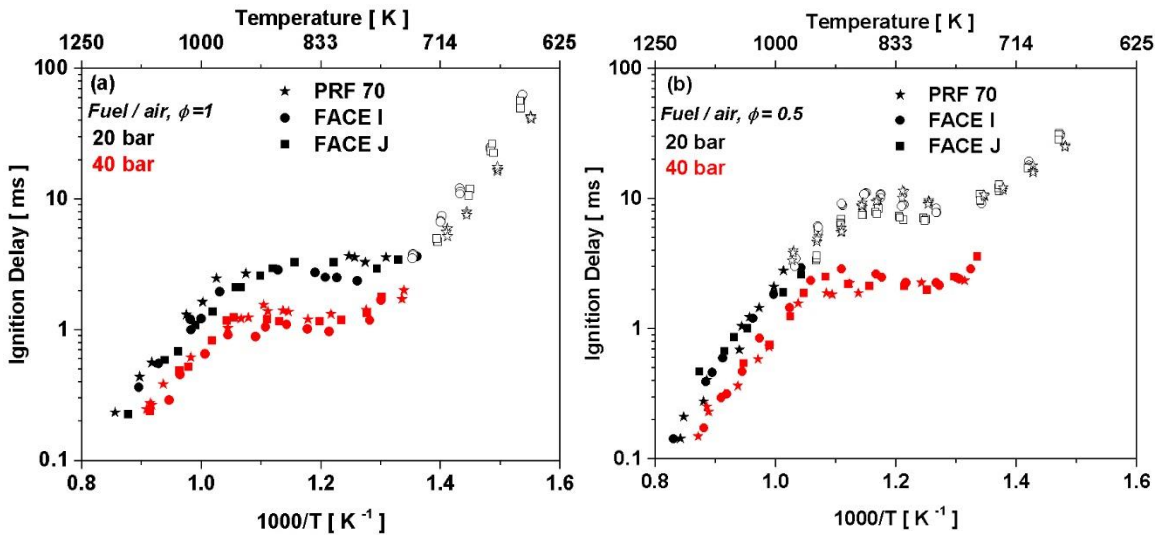


Figure 3-2: Ignition delay times of PRF 70, FACE I and FACE J at 20 and 40 bar for equivalence ratios of (a) 1 and (b) 0.5.

Figure 3-2 further shows a comparisons between the ignition delay times of these gasolines with PRF 70 (stars) surrogate. It can be seen from the figure that PRF 70 surrogate, matching the AKI of these low sensitivity gasolines, is sufficient to capture the

reactivity trends of FACE I and FACE J. Only at low temperatures RCM conditions, PRF 70 is marginally faster than the gasolines. These findings are consistent with our previous work [29, 31] and further strengthens the effectiveness of a simple bi-component PRF surrogate in capturing the reactivity of low sensitivity ($S < 3$) full boiling range gasolines.

Ignition delay simulations

Along with PRF 70 simulations, multi-component surrogate simulations (FG- I and FG-J) are also presented here. The purpose of presenting (and developing) multi-component surrogate simulations is our objective to provide guidelines for surrogate requirements for engine applications. As mentioned in the introduction section, low octane gasolines (FACE I, FACE J, naphthas, etc.) are expected to operate in GCI engine mode. Researchers at KAUST (Internal communication PhD student Nimal Nasir at KAUST) have recently conducted an interesting study. They performed HCCI and PPCI engine experiments using FACE I as fuel. They have shown that, under HCCI conditions (which are more representative of homogenous shock tube and RCM like conditions and are reactivity controlled), a PRF surrogate matches the combustion phasing targets of FACE I. However, under PPCI conditions (where spray formation and mixing plays an important role), a simple PRF surrogate fails to capture the combustion phasing targets of FACE I. This brings about an interesting research question to forefront that what complexity in a surrogate is required to capture combustion phasing targets in a particular engine operating mode; we at KAUST are undertaking an extensive study to answer this important question (see section 7.2.2). Nonetheless, this also highlights the importance of more stringent surrogate formulation methodologies (similar to the one developed at KAUST [77]) to take various engine mode relevant targets into consideration rather than simply matching the

octane numbers.

Comparisons of measured ignition delay times with simulations are shown in Figure 3-3 and Figure 3-4. It can be seen from the figures that PRF 70 simulations (blue lines) captures the reactivity of the gasolines and the PRF 70 data reasonably well at high ($T > 900$ K) and low temperatures ($T < 700$ K), but are slower compared to measured data in the NTC region ($T \sim 750 - 850$ K). FG-I (black lines) surrogate simulations shows quite similar trends to PRF 70 simulations. FG-J (red lines) surrogate simulations show similar trends to PRF 70 and FG-I at low temperatures, have a good agreement with data in the NTC region, and finally at high temperatures they overpredict the ignition delay times of FACE J (and other fuels as well).

The FACE gasoline mechanism developed by Sarathy et al. [30] (KAUST, NUIG, LLNL collaboration) was purposely put together for gasoline and surrogates simulations and to take into account various gasoline surrogate palette species. This mechanism is constantly being upgraded to improve its predictions, and the latest update (internal communication Prof. S. M. Sarathy; not shown here) improves the PRF simulations significantly over wide range of data measured in this study and other studies from our group [31, 70]. To improve the predictions for FG-I (7 component) and FG-J (five component) requires a concerted effort and integration of various sub-models and is beyond the scope of this work. Here (in section 3.3.4), the mechanism will be used as it is, to explain some interesting trends where a good agreement between the simulations and the data is seen.

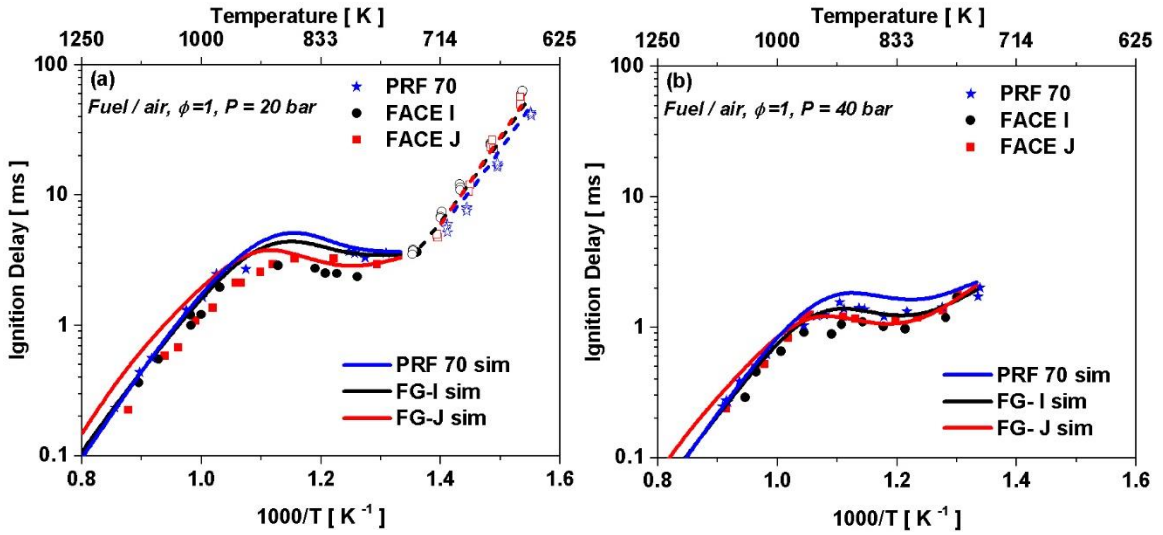


Figure 3-3: Comparison of experiments (scatter) and simulations (lines) for equivalence ratio 1 at (a) 20 bar and (b) 40 bar. Simulations done using FACE gasoline mechanism [30].

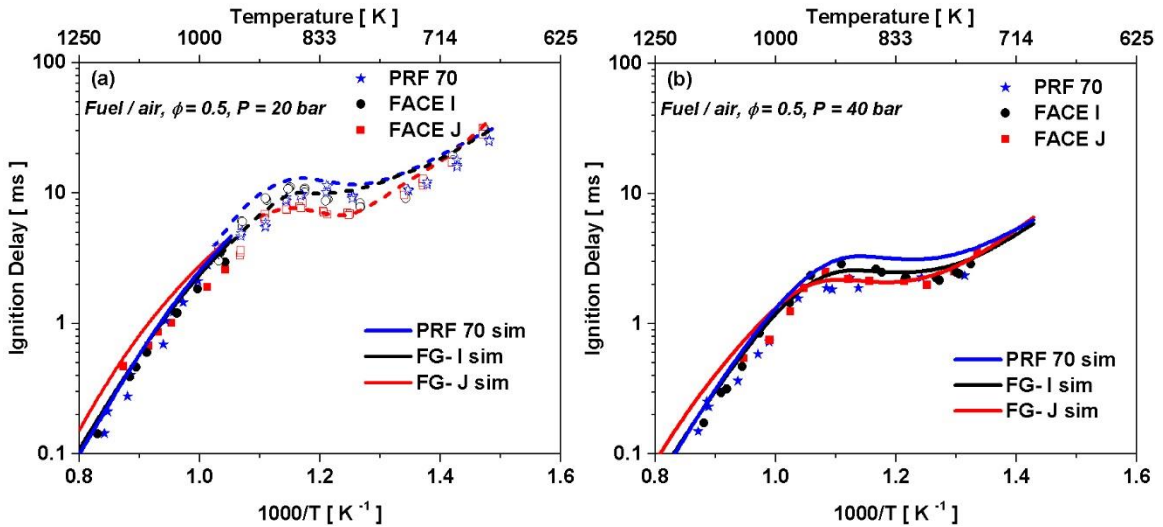


Figure 3-4: Comparison of experiments (scatter) and simulations (lines) for equivalence ratio 0.5 at (a) 20 bar and (b) 40 bar. Simulations done using FACE gasoline mechanism [30].

3.3.3 Chemical kinetic analyses for light naphtha and surrogates

In section 3.3.1, it was shown that a PRF surrogate fails to capture the ignition requirements of a lightweight highly paraffinic fuel (light naphtha Avg. Mol. Wt. = 78.4).

It was also shown that in the high and NTC temperature regimes, a PRF surrogate satisfactorily captures the ignition requirements of a highly paraffinic fuel. Here we will utilize kinetics analysis to explain these trends.

Low temperature ($T < 700$ K) trends

At low temperatures, fuel is primarily consumed through hydrogen abstractions by HO_2 and OH radicals. Although hydrogen abstraction by HO_2 is slower than that by OH, the relative concentration of HO_2 is significantly higher at early reaction times, and thus both radicals contribute to fuel consumption [85, 86]. The fuel radicals (R) react with O_2 to form alkylperoxy radicals (ROO), which then undergo a series of isomerization and O_2 addition reactions to form ketohydroperoxides (KHPs) and OH radicals; the decomposition of KHPs produces additional OH radicals, resulting in an exponential growth of OH radicals. Chain propagation (cyclic ether formation) and chain termination (concerted elimination of HO_2) reactions compete with the aforementioned low-temperature chain branching reactions and inhibit the reactivity of the system. Figure 3-5 shows the evolution of OH (solid lines) and HO_2 (dotted lines) during the oxidation of the PRF 64.5 (red lines) and LN-KAUST (black lines) surrogates at 650 K, 20 bar, $\phi = 2$. The simulations indicate a single-stage ignition process, which is in agreement with experimentally measured pressure profiles (Appendix Figure A6). The mole fraction of OH grows exponentially until it reaches a critical value ($\sim 1\text{E-}8$); at this point thermal runaway and ignition occur. It can be seen that the rate of OH and HO_2 radical growth during PRF 64.5 oxidation is much faster than in LN-KAUST surrogate oxidation, resulting in shorter overall ignition delay times for the former (see Figure 3-1 (d)). This difference in reactivity is due to the large difference in underlying chemical composition of the two surrogate mixtures.

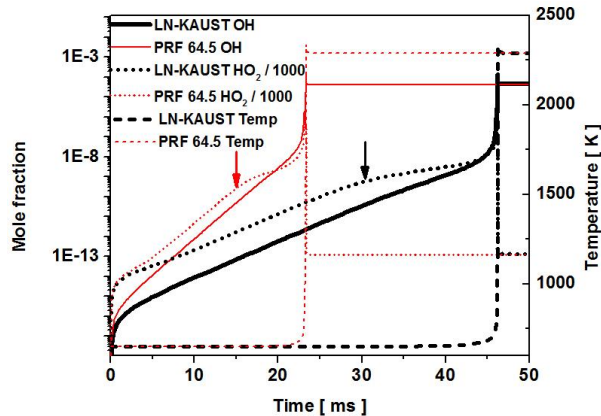


Figure 3-5: Simulated constant volume temperature, OH and HO₂ profiles during the oxidation of PRF 64.5 and LN-KAUST surrogates. Initial conditions: T = 650 K, P = 20 bar, φ = 2. FACE gasoline mechanism is used for simulations. The arrows are drawn at $2/3 \tau_{\text{ign}}$.

A rate of production (ROP) analysis was carried out during the exponential growth phase of OH and HO₂ radicals to demonstrate the effects of the underlying chemistry on ignition delay times. The ROP analysis was performed at about $2/3$ of the total homogenous ignition delay time which roughly corresponds to the pre-ignition HO₂ peak. The arrows drawn in Figure 3-5 show this time. The results of the ROP analysis are shown in Figure 3-6 (upper panel: LN-KAUST surrogate, lower panel: PRF 64.5 surrogate). Production pathways for OH and HO₂ are quite different for the two surrogates as these pathways depend strongly on the compositional makeup of the surrogate. Structural formulas of the species appearing in the ROP analysis are included in the Appendix (Table A3).

The PRF 64.5 surrogate consists of n-heptane and iso-octane, while the LN-KAUST surrogate consists primarily of pentane isomers (normal, iso, cyclo). In the PRF 64.5 surrogate, the n-heptane low-temperature chemistry dominates the OH radical buildup, while the chemistry of the pentane isomers controls the OH radical growth for the LN-KAUST surrogate. It can be seen from Figure 3-6 (a) and (c) that H-abstraction by OH

from the secondary sites of n-pentane and n-heptane to produce n-pentyl and n-heptyl radicals are the most dominant OH consumption pathways for the LN-KAUST and PRF 64.5 surrogates, respectively. Sivaramakrishnan et al. [87] and Badra et al. [88] have shown that H-abstraction by OH from secondary C-H₂ sites is dominant over abstractions from primary C-H₃ sites. The total rate of H-abstraction increases as the carbon-chain length increases, due to the presence of additional secondary sites. Therefore, n-heptyl radicals (primarily C₇H₁₅-2 and C₇H₁₅-3) in the PRF 64.5 surrogate are produced faster than n-pentyl radicals (primarily C₅H₁₁-2) in the LN-KAUST surrogate. Once fuel radicals are formed, a series of low-temperature reactions produce OH radicals. The low-temperature chain branching pathway is accelerated by internal H-atom migration via six-membered transition state rings between secondary C-H₂ sites. n-heptane has a larger fraction of secondary C-H₂ sites compared to n-pentane, and thus the former populates the OH radical pool more quickly. The faster initial production of n-heptyl radicals over n-pentyl radicals and the more pronounced low-temperature chain branching chemistry of n-heptane compared to n-pentane is the primary reason for the shorter ignition delay times of the PRF 64.5 surrogate compared to the LN-KAUST surrogate.

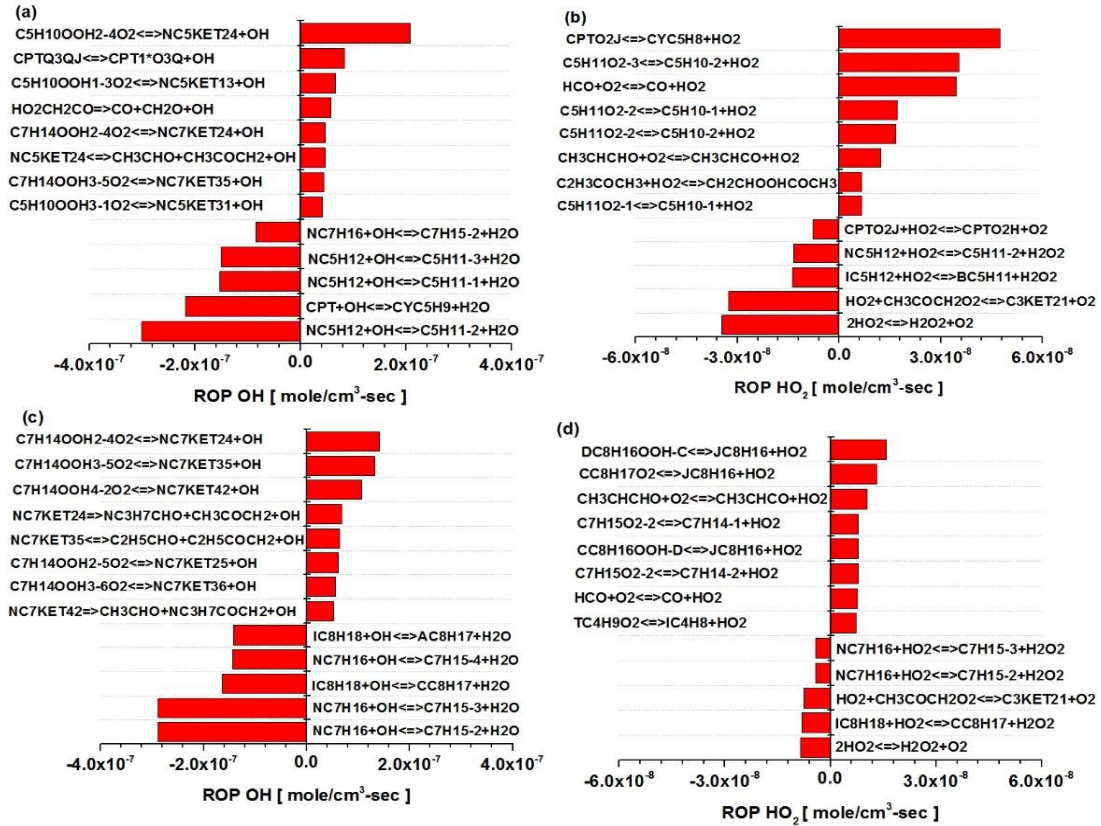


Figure 3-6: Rate of production (ROP) analysis of OH (a, c) and HO₂ (b, d). Upper panel: LN-KAUST surrogate, Lower panel: PRF 64.5 surrogate. T = 650 K, P = 20 bar, $\phi = 2$. FACE gasoline mechanism is used. ROP analysis was performed at $2/3 \tau_{\text{ign}}$.

NTC ($T \sim 750 - 850 \text{ K}$) region trends

The ROP analysis for HO₂ is shown in Figure 3-6 (b) and (d) for the LN-KAUST and PRF 64.5 surrogates, respectively. The recombination of HO₂ radicals to form H₂O₂ ($2\text{HO}_2 \leftrightarrow \text{H}_2\text{O}_2 + \text{O}_2$) and the decomposition of H₂O₂ to two OH radicals lead to the ignition event (H₂O₂ is relatively stable below 900 K). These reactions become more important in controlling ignition when the HO₂ concentration and temperature are higher. Hydrogen abstraction by HO₂ to produce n- or iso- alkyl radicals are important fuel-specific consumption channels, while concerted elimination reactions from alkylperoxy radicals to produce alkenes and HO₂ are important production channels ($\text{RO}_2 = \text{alkene} + \text{HO}_2$).

Figure 3-6 (b) and (d) show that concerted elimination from cyclopentyl peroxy and n-pentyl peroxy radicals are important in the LN-KAUST surrogate, which results in longer ignition delay times.

The present experimental and kinetic analyses demonstrate that multi-component surrogates better reproduce the low-temperature reactivity of a low octane, highly paraffinic lightweight fuel, and that such systematic surrogate formulations provide a deeper understanding of the low-temperature reactivity of these fuels.

3.3.4 Chemical kinetics analysis for FACE I and J and surrogates

High temperature ($T > 1000$ K) trends

It is previously [29-31, 69] that at high temperatures ($T > 1000$ K), ignition delay times of practical fuels are not sensitive to octane numbers. This is because, at high temperatures, chain branching is controlled through $\text{H}_2\text{O}_2 (+\text{M}) \leftrightarrow \dot{\text{O}}\text{H} + \dot{\text{O}}\text{H} (+\text{M})$ reaction and is favored more or less equally for a wide range of practical fuels/surrogates. Here we have seen similar trends (Figure 3-2), that at high temperatures, FACE I, FACE J and PRF 70 exhibit similar experimentally measured ignition delay times. Also the simulations (Figure 3-3 and Figure 3-4), with exception of FG-J simulation being slightly slower, captures the experimental data.

Low temperature ($T < 700$ K) trends

In the work on TPRF surrogates (see 0) [69], it will be shown that, at low temperatures ($T < 700$ K), fuels with low RON and sensitivity show weak effects of octane numbers on ignition delay times. Moreover, it will be also shown that, fuels with high RON and sensitivity ($S > 7$), where sensitivity is attributed to high Toluene (aromatics) content, are less reactive at low temperatures compared to low RON and low sensitivity fuels. In

the present work, it can be seen that (20 bar data in Figure 3-2 (a) and (b)) all the three fuels studied here, exhibit similar reactivity at low temperatures. The fuels studied here have similar octane ratings and modestly low sensitivities ($S < 3$), yet their compositions are widely different. Table 3-2 shows that FACE I is highly paraffinic (~ 84 mol %) and have some aromatic (~ 5 mol %) and olefinic (~ 7 mol %) content as well; whereas FACE J also has high paraffinic (~ 64 mol %) content, but it also consists of high aromatic (~ 30 mol %) content. On the other hand, PRF 70 surrogate is 100 % paraffinic with zero sensitivity. Here the hydroxyl (OH) rate of production (ROP) analysis is utilized by following the same guidelines as in our previous works [31, 69] (see also 3.3.3 for ROP analysis details) to explain why similar reactivity is observed at low temperatures times for the three fuels with varying composition and similar octane ratings.

The ROP analysis is performed at a time corresponding to 2/3 of the first stage OH peak, and hence have negligible effects of temperature rise associated with ignition (first and second stage). Figure 3-7 shows the ROP OH analysis for PRF 70, FG-I and FG-J surrogates. This analysis was conducted at 700 K, 20 bar and at an equivalence ratio of 1. Out of all the reactions influencing ROP OH, top 12 reactions promoting and inhibiting ROP OH were selected for each surrogate. Furthermore, various pathways of a similar reaction class were coupled in a single representative reaction pathway for brevity. For example, hydrogen abstraction through secondary sites of n-heptane (NC_7H_{16}) can proceed through five secondary sites to produce n-heptyl (C_7H_{15}) radicals, the effective ROP OH of all these pathways (pathways which appear in top 12 ROP OH) is coupled in generic reaction to produce n-heptyl radical. It can be seen from the figure that hydrogen abstraction by OH to produce n-heptyl radicals ($\text{NC}_7\text{H}_{16} + \text{OH} \rightleftharpoons \text{C}_7\text{H}_{15} + \text{H}_2\text{O}$) is

important consumption (negative ROP) pathway for all the fuels. These n-heptyl radicals can add on O_2 and go through internal isomerizations to produce ketohydroperoxide radicals ($C_7H_{14}OOH(a)-(b)O_2 \Leftrightarrow NC_7KET(ab) + OH$) which can further decompose to OH radicals hence completing low temperature chain branching process. Similarly, FG-I and FG-J surrogate, because of the presence of 2-methylhexane (C_7H_{16-2}) in them, can consume OH to produce branched heptyl (C_7H_{15-2}) radicals, these branched heptyl radicals follow similar low temperature chain branching pathways ($C_7OOH(a)-(b)O_2-2 \Leftrightarrow C_7KET(ab)-2 + OH$). Hence, important OH consumption pathways include hydrogen abstraction by OH from secondary sites of n-heptane (and its isomers) and are quite similar in their rates for all the fuels. Also, the production pathways follows the formation of C_7 ketohydroperoxides whose rates are quite comparable for all the fuels as well. Therefore, the largely varying differences in the compositions of these fuels doesn't have much effect on their reactivities (and octane numbers) at low temperatures. Combined the current findings and those of literature studies [30, 69] (see also findings related to octane dependence of on ignition delay times of TPRFs in 0), it can be stated that low temperature reactivity differences for practical full boiling range fuels only become significant for larger sensitivities ($S > 7$).

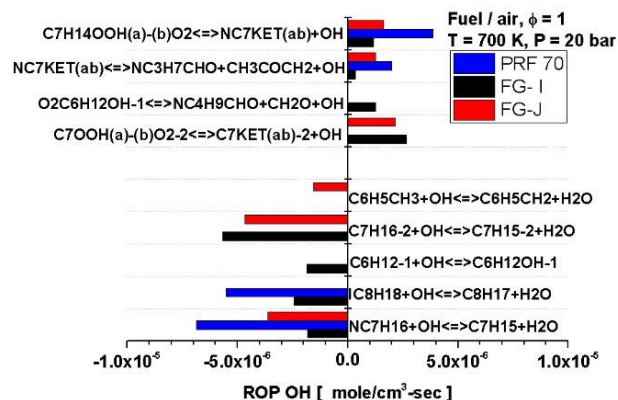


Figure 3-7: ROP OH analysis at for various fuel/air mixtures at an equivalence ratio of 1. T = 700 K, P = 20 bar.

To experimentally verify the above assertion, that only high sensitivity full boiling range fuels exhibit reactivity differences at low temperatures, Figure 3-8 shows the experimentally measured low temperature ignition delay times of a wide range of fuels at 20 bar and $\phi = 1$ conditions. First lets' look at low to mid ($S < 7$) sensitivity fuels. It can be seen from the figure that FACE A and C ($S \sim 0$), PRF 84 ($S = 0$), TPRF70 ($S = 4$), TPRF 80 ($S = 5.7$), and FACE I ($S = 0.7$), FACE J ($S = 3$) and PRF 70 ($S = 0$) all exhibit similar ignition delay times. Next, high sensitivity fuels ($S > 7$), TPRF 97.5 ($S = 10.9$), FACE G ($S = 11$) and TPRF 91 ($S = 7.6$) all show different levels of octane dependences and are slower compared to rest of low sensitivity fuels. The only exception here is FACE F ($S = 5.6$), which despite being mid sensitivity, show octane dependence at low temperatures. The data presented in the figure is from three different RCM facilities (KAUST (FACE I, FACE J and PRF 70), NUIG (TPRF 70 – 97.5), UCONN (FACE A, FACE C, PRF 84, FACEF and FACE G)) and further supports the above assertion.

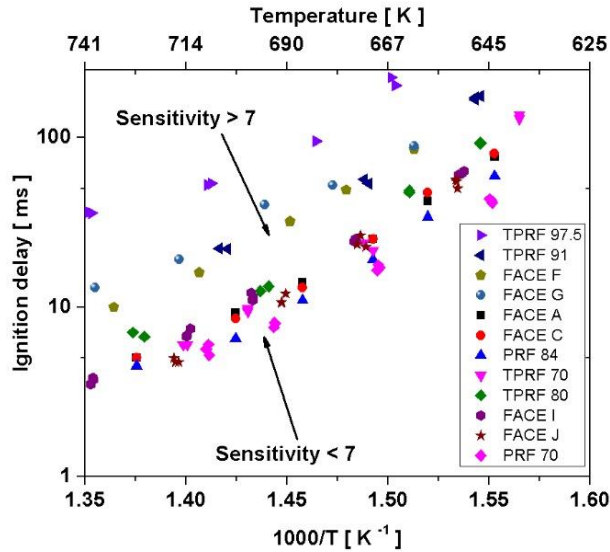


Figure 3-8: Experimentally measured low temperature ignition delay data for a wide range of fuels at 20 bar and $\phi = 1$. FACE A, FACE C and PRF 84 data taken from [29], TPRF 70 – 97.5 data taken from [69], FACE I, FACE J and PRF 70 (current study), and FACE F and G data taken from [30].

NTC ($T \sim 750 - 850$ K) region trends

In the NTC region ($T \sim 750 - 850$ K), it could be seen (Figure 3-2 (a) and (b)) in the experimentally observed ignition delay times that all fuels exhibit similar reactivity (albeit some minor distinctions). However, the simulations show clear trends, that FG-J surrogate simulation is faster compared to FG-I and PRF 70 surrogate simulations and exhibit less NTC behavior. The two surrogates formulated for simulating current data have following predicted octane ratings: FG-I RON = 70.7, MON = 68.4, S = 2.3; FG-J RON = 71.7, MON = 67, S = 4.7. The lesser NTC observed for the FG-J simulations could be explained by the fact that FG-J surrogate has larger predicted sensitivity and we have shown previously that larger sensitivity fuels exhibit lesser NTC behavior [69]. These reactivity differences seen in simulations among various may be an artifact of mechanism discrepancy to capture the experimental data, as is the case in FG-J simulations failing to capture the high temperature reactivity as well, and could be resolved with better optimizing the chemistry of some of

the species present in these surrogates. Although an HO₂ ROP can be utilized to explain the trends in the NTC region, as done in our previous work [69], the simulated differences seen here are not consistent with experimental findings and hence such explanations of trends are not presented here.

In this chapter, the ignition delay times of low octane gasolines are reported and surrogate formulation constraints are suggested for them. It is shown that at high temperatures and NTC region, a PRF surrogate satisfactorily captures the ignition requirements of these gasolines. At low temperatures, a PRF surrogate fails to capture the reactivity of lightweight fuel (light naphtha); however, for full boiling range low sensitivity gasolines like FACE I and J, a PRF surrogate performs reasonably at low temperatures as well.

Chapter 4: SPECIATION AND IGNITION STUDIES OF MID OCTANE GASOLINES AND SURROGATES

In this chapter, laser absorption based species time histories during the combustion of two mid-octane highly paraffinic (Sensitivity ~ 0) gasolines, FACE gasoline A and C, are presented. Speciation data can be used to impose stringent constraints on a chemical kinetics mechanism. Moreover, ignition delay times of these gasolines are also reported to complement speciation data. The two gasolines have similar antiknock index (AKI ~ 84) but have widely different compositions; therefore, it is interesting to see if these disparity in their compositions have any effect on speciation and global reactivity (ignition delay times). These datasets are one of the first measurements of species of shock heated fully blended gasolines and are expected to be used widely as validation targets for gasoline surrogate mechanism development.

4.1 Introduction

The commercial transportation-grade gasoline is a complex mixture of hundreds of hydrocarbons including linear and branched paraffins, naphthenes, olefins and aromatics. It becomes extremely inefficient to accommodate all of these species in any real world computational/experimental scenario. These difficulties can be overcome by considering a surrogate mixture of a few well-known components in a well-defined composition to emulate the target properties of the real fuel. Generally, these target properties include desired combustion characteristics (ignition delay, flame speed, etc.) and/or physical properties (molecular weight, H/C ratio, distillation curve, etc.). However, it should be noted that a given surrogate may not be able to match all physical and kinetic targets

simultaneously. A conventional scale for rating the ignition properties of gasoline fuels is the research octane number (RON) and/or the motor octane number (MON) based on blends of gasoline primary reference fuels (PRF), n-heptane and iso-octane. Blends of primary reference fuels have previously been used as gasoline surrogates. The chemical kinetics of PRFs has been studied quite comprehensively over the last decade or so. Work by Curran et al. [7, 8] on n-heptane/iso-octane and by Mehl et al. [79] on gasoline surrogates provides good account of the experimental and chemical kinetic modeling studies of primary reference fuels. Ignition delay times of PRF blends have been measured previously by few groups [14, 15, 89]. More complex multi-component gasoline surrogates have been proposed in ignition delay studies under HCCI-like conditions [23, 28, 90].

In the current study, the oxidation characteristics of FACE gasoline A and C are investigated. Table 4-1 shows some of the key features of these two fuels, more detailed compositional analysis of different FACE gasoline and diesel fuels can be found in [29, 91]. Both gasolines have very similar octane rating but they differ in their compositions; FACE C has more than double the amount of n-paraffins than FACE A. Also, small amount (~ 4%) of aromatics are present in FACE C but are almost negligible in FACE A. The two gasoline fuels are compared here against a PRF blend of 84% iso-octane / 16% n-heptane (by volume), referred to as PRF 84 in this work.

Table 4-1: Properties of FACE gasoline fuels and PRF surrogate. The hydrocarbon types for FACE

A and C were determined by Detailed Hydrocarbon Analysis (DHA) technique.

Fuel Properties	FACE Gasoline A	FACE Gasoline C	PRF 84
RON	83.5	84.7	84
MON	83.6	83.6	84
Sensitivity	-0.1	1.1	0
Avg. mol. wt.	97.8	97.2	112
Hydrocarbon Type, liquid mol%			
n-Paraffins	13.2	28.6	17.6
iso-Paraffins	83.7	65.1	82.4
Aromatics	0.3	4.4	0
Alkenes	0.4	0.4	0
Cycloalkanes	2.4	1.5	0
H/C ratio	2.29	2.27	2.26

Chemical kinetic models are often validated against global kinetics targets such as ignition delay and flame speed data obtained from shock tubes, rapid compression machines, and simple canonical flames. Such data provide an overall view of the kinetic mechanism behavior and its ability to predict fuel reactivity but these data cannot be used to validate complex reaction pathways which are important, for example, in predicting emissions. The detailed chemical kinetics also play important role in controlling the fuel reactivity under HCCI- or PCCI- like conditions. Comprehensive validation of detailed chemical kinetic mechanism would benefit greatly by experimentally measured species time-history profiles. Shock tube / laser absorption experiments are particularly well-suited for acquiring species time-history data [92-96] because of the step change in test conditions behind shock waves, the highly uniform temperatures and pressures, and the fast time response of laser absorption diagnostics.

Figure 4-1 shows the predictions for the evolution of five major species formed

during the oxidation of PRF 84. Simulations are carried out using gasoline surrogate mechanism of Mehl et al. [79] with constant internal energy and volume (constant UV) gasdynamic model in Chemkin-Pro [97]. The fuel decomposes immediately within the first 10 – 50 μs producing fuel fragments, $\text{C}_1 - \text{C}_4$ intermediate species and an active radical pool. The concentrations of the reaction progress markers (CO , H_2O and CO_2) increase slowly at early times, over the 50 – 450 μs window in this example, until there is an exponentially fast growth of OH radicals and significant energy release from the $\text{CO} + \text{OH} \leftrightarrow \text{CO}_2 + \text{H}$ reaction. Post-ignition CO_2 and H_2O concentrations will eventually approach their equilibrium values governed primarily by their thermochemical properties. Details of the species time-histories in the pre-ignition region are very important, and can provide very stringent constraints on mechanism predictions and validations.

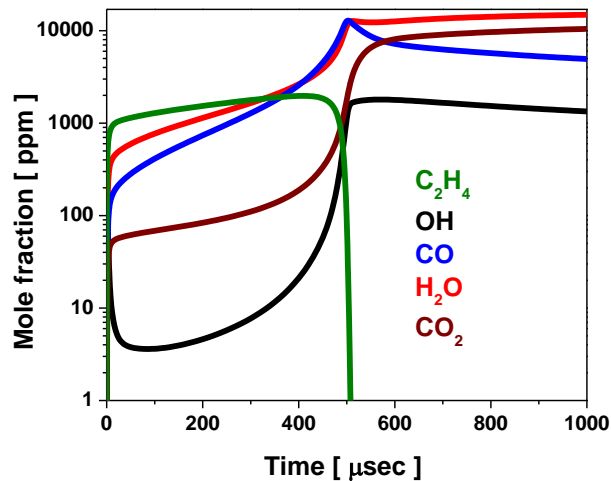


Figure 4-1: Simulated profiles of major species formed during the oxidation of PRF 84. Mixture: 0.2% PRF84/ O_2 / Ar ($\Phi = 1$), $T = 1500 \text{ K}$, $P = 2 \text{ atm}$. Constant internal energy and volume (constant UV) simulations performed in Chemkin-Pro [97] using Mehl et al. mechanism [79].

Here, species time-history and ignition delay time measurements for FACE gasolines A and C as well as a PRF 84 surrogate are presented. The low pressure shock tube ignition

delay experiments were carried out with the fuel concentration of 0.2% diluted in Argon for $\phi = 1$ at 2 atm. Species time-histories of OH, CO, CO₂ and H₂O were measured using laser-based UV and IR absorption spectroscopy at same conditions. Further ignition delay experiments were performed for 0.4% fuel diluted in Argon at $\phi = 0.5$ and 1 at 10 atm. The reactivity and speciation of the three fuels were compared based on the fuel composition. Ignition delay data for these fuels, at a wide range of practical conditions, taken from the literature, is also shown for a complete picture.

4.2 Methodology

4.2.1 Ignition delay measurements

Two types of ignition measurements are presented here. Firstly, highly diluted experiments (Argon dilution) with fuel concentration of 0.2% at 2 atm and $\phi = 1$, and 0.4% at 10 atm at $\phi = 0.5$ and 1 are carried out in KAUST low pressure shock tube. Next, high pressure shock tube and RCM data is taken from the literature [29] to present a complete picture of global reactivity (ignition delay time). For details of shock tube and RCM ignition delay experiments please refer to Chapter 2.

4.2.2 Laser absorption measurements

Four laser absorption diagnostics were used to simultaneously monitor the concentration time-histories of CO, CO₂, H₂O and OH. These diagnostics have either been validated previously (CO, OH) or were characterized in separate non-reactive experiments conducted in our shock tube facility (CO₂, H₂O). These diagnostics enabled us to make extremely sensitive measurements with relatively low detection limits at the conditions of our experiments: ~1 ppm for OH, ~10 ppm for CO and ~100 ppm for CO₂ and H₂O. The

overall uncertainty in these speciation measurements is $< 5\%$ and primarily comes from uncertainty in absorption cross-section, post-shock temperature (T_5) and calculation of temperature time-history. Highly diluted conditions (Argon dilution) with fuel concentration of 0.2% at 2 atm and $\phi = 1$ were used to perform laser absorption speciation measurements. Details of each diagnostic is provided in Chapter 2.

4.2.3 Calculation of temperature time-history

Beer-Lambert law for spectrally narrow radiation can be written as $I/I_o = \exp(-SPL\phi_\nu X)$, where I/I_o is the ratio of transmitted and incident laser intensities, $S(T)$ is the line-strength, P is the total pressure, L is the laser path-length, $\phi_\nu(T,P)$ is the line-shape function and X is the mole fraction of the absorbing species. The line-strength and line-shape are temperature-dependent quantities and their variation with temperature is either known from a spectral database or determined via line characterization experiments. For shock tube experiments, the temperature behind reflected shock wave (T_5) is calculated from the measured incident shock speed and thermodynamic parameters of the gas mixture. In non-reactive shock tube experiments, the T_5 remains almost constant throughout the test time (~ 2 ms). However, in reactive experiments, energy release from exothermic combustion reactions can cause the temperature to increase substantially during and after the ignition event. Thus a temperature time-history is needed to accurately calculate the mole fraction time-history using Beer's law. In the absence of direct temperature measurement, a temperature profile simulated by a chemical kinetic mechanism is used for the calculation of temperature-dependent spectroscopic quantities, i.e., line-strength and line-shape functions. Shock tubes are usually modeled with constant volume and constant internal energy (constant UV) constraints. However, these constraints are not suitable for

situations where sufficient energy release takes place. In this work, we imposed the measured-pressure profile in Chemkin-Pro [97] and solved the energy equation to calculate temperature time-history. This modeling approach, referred to as UMP (constant internal energy with measured pressure profile), is used throughout the paper to generate temperature time-histories for converting measured absorbance profiles to concentration time-histories. This approach is demonstrated in Figure 4-2, and compared with calculations using constant UV constraints and the ChemShock code proposed by the Stanford University group [98]. As expected, the constant UV simulations greatly overpredict the temperature and pressure. The temperature time-histories calculated using UMP and ChemShock are essentially similar, though the UMP approach is easier to implement.

4.2.4 Validation of laser diagnostics

Since chemical kinetic mechanisms for n-heptane are very well-validated, species time-history profiles were initially measured during the oxidation of n-heptane stoichiometric mixtures to validate the laser diagnostics and the temperature modeling strategy. Measurements were carried out in a mixture of 0.2% n-heptane/oxygen/argon over a range of temperatures (1350 – 1500 K) and pressures near 2 atm. A representative dataset is shown in Figure 4-3 at a reflected shock temperature of 1440 K. The measured and simulated profiles (using Mehl et al. [79] mechanism) are generally in good agreement with some minor differences. For example, the mechanism overpredicts H₂O production and underpredicts CO production at relatively early times of 50 – 100 μ s. It is expected that all of the fuel carbon will get converted to CO and CO₂ in the post-ignition region. Carbon balance can be calculated in the post-ignition region for validating the CO and CO₂

diagnostics. At an elapsed time of 700 μs , the sum of measured CO and CO₂ mole fractions is 13100 ppm which is within 6.5% of the initial fuel carbon (14000 ppm).

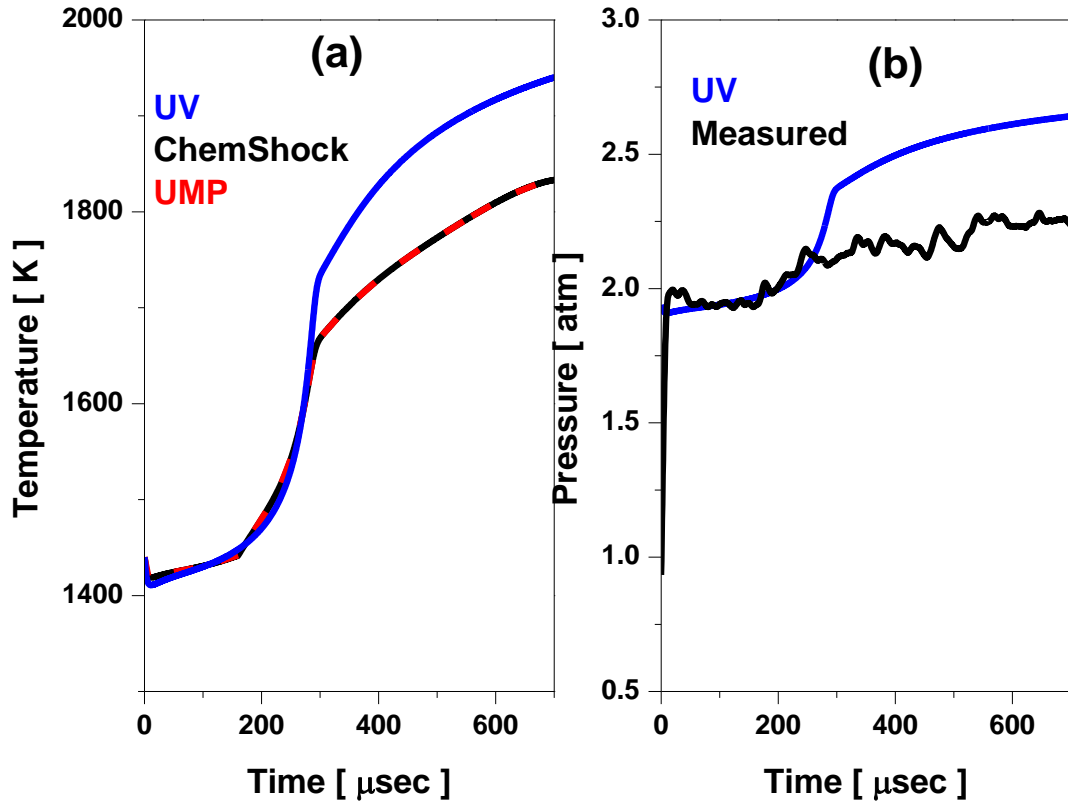


Figure 4-2: Comparison of modeled (a) temperature and (b) pressure using various gasdynamic models (UV = constant internal energy and volume, UMP = constant internal energy with measured pressure) during the oxidation of 0.2% n-heptane/ O₂/Ar ($\Phi = 1$), $T = 1440$ K , $P = 1.94$ atm. Temperature output using ChemShock [98] code is also shown. Simulations performed using Mehl et al. [79] mechanism.

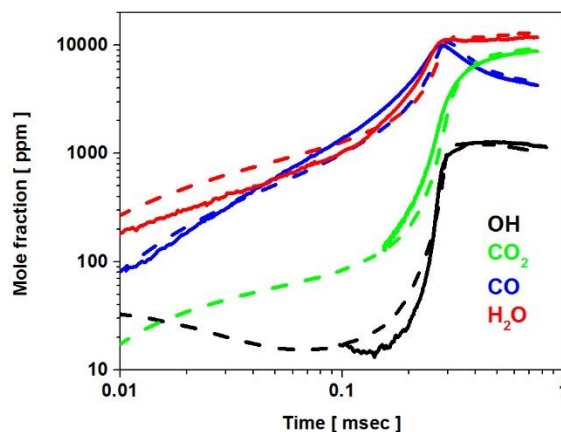


Figure 4-3: Comparison of model prediction with experimentally measured species profiles for 0.2% n-heptane/O₂/Ar ($\Phi = 1$), $T = 1440$ K, $P = 1.94$ atm; solid lines: experimental profiles, dashed lines: Constant UV simulations using Mehl et al. [79] mechanism.

4.3 Results and discussion

4.3.1 Ignition delay times of FACE gasolines and PRF surrogate

Ignition delay times were measured for the two FACE gasolines and PRF 84 blend over a temperature range of 1330 – 1550 K and pressures near 2 atm; results are shown in Figure 4-4. FACE gasoline A and C have the same overall reactivity indicated by very similar ignition delay times within the uncertainty limits of these experiments (~15 %). It is well known [99-101] that increasing the branched hydrocarbon and/or aromatic content in the fuel decreases overall reactivity while n-paraffins increase the reactivity. FACE gasoline C has almost double the amount of n-paraffins compared to FACE gasoline A. However, FACE gasoline C has about 5% aromatics which balances out the higher reactivity due to increased n-paraffins, resulting in similar octane rating and similar ignition delays for both gasolines. Also evident in Figure 4-4 is that PRF 84 surrogate captures the reactivity of these gasoline fuels over the entire temperature range of this study. This can be explained by the fact that both gasolines and the PRF blend are primarily paraffinic in

nature (~ 95% paraffinic content) and thus exhibit similar reactivity. This is consistent with surrogate fuel formulation strategy proposed by Dooley et al. [74] for jet fuels. They argued that the composition of the surrogate does not necessarily need to emulate all of the functional classes present in the real fuel. The composition of the surrogate should be such that it is able to emulate closely the development of the active radical pool and C₁-C₄ intermediate species which control the chemical kinetics phenomena at high temperatures.

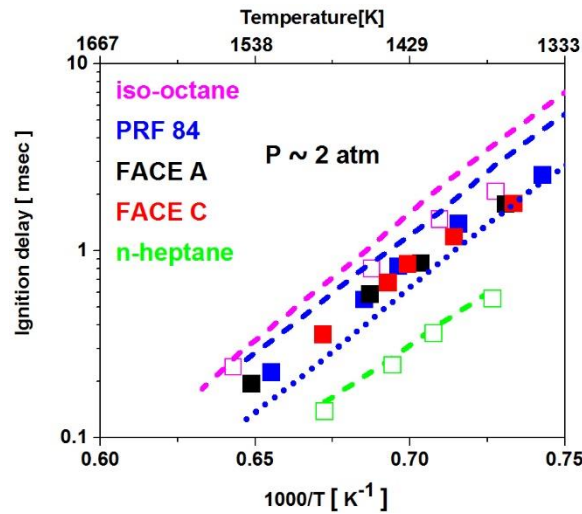


Figure 4-4: Ignition delay times during the oxidation of stoichiometric mixtures with 0.2% fuel (iso-octane, PRF 84, FACE A, FACE C, n-heptane) / O₂ / Ar, P ≈ 2 atm; Scatter: Experimental, Dashed lines: Mehl et al. [79] mechanism. Dotted line: Bieleveld et al. mechanism [102]

Comparisons of measured ignition delay times with predictions from Mehl et al. [79] and Bieleveld et al. [102] gasoline surrogate mechanism are also shown in Figure 4-4. The primary difference between the two mechanisms is that Bieleveld et al. [102] use lumped component/reaction method (methods developed by Ranzi and coworkers [103]) whereas Mehl et al. [79] consider all isomers and reaction pathways. Mehl et al. [79] mechanism overpredicts the experimental ignition delay times of the PRF surrogate and the two FACE gasolines over the entire temperature range of this study, whereas Bieleveld et al. [102]

mechanism underpredicts the experimentally measured ignition delay times. It can also be seen from Figure 4-4 that the Mehl et al. [79] mechanism predictions are closer to the experimental data at higher temperatures but exhibit relatively large deviations as temperature decreases. On the contrary, Bieleveld et al. [102] mechanism is closer to the experimental data at lower temperatures. The high-temperature chemistry is generally considered to be well established for reference fuels, such as n-heptane and iso-octane. Therefore, it is surprising that both mechanisms are unable to accurately predict the high-temperature ignition delay times of the PRF blend. Also shown in Figure 4-4 are the experimental ignition delay times measured in our laboratory for n-heptane and iso-octane stoichiometric mixtures under similar conditions. Mehl et al. [79] mechanism captures n-heptane reactivity very well but overpredicts iso-octane ignition delay times. Thus it can be argued that the Mehl et al. [79] overprediction of PRF 84 ignition delay times is caused by iso-octane kinetic mechanism or the blending of n-heptane and iso-octane chemistry. The kinetics of iso-octane and related smaller branched intermediates, like iso-butene, must be evaluated further to improve the discrepancy between the measurements and the model.

To present a complete picture on the global reactivity (ignition delay times) of these fuels, Figure 4-5 and Figure 4-6 show further ignition data of these fuels. It can be seen from Figure 4-5 that at 10 atm diluted conditions, the two gasolines (FACE A and C) and the PRF 84 exhibit similar reactivity at high temperatures. Furthermore, Figure 4-6 shows ignition data for these fuels at practical conditions (low to high temperature, fuel / air mixtures, at 20 and 40 bar). It can be seen from Figure 4-6, that the two gasolines exhibit similar reactivity at a wide range of test conditions and PRF 84 surrogate satisfactorily captures their ignition requirements. PRF surrogate is only marginally faster (~ 25 %)

compared to the gasolines at low temperatures.

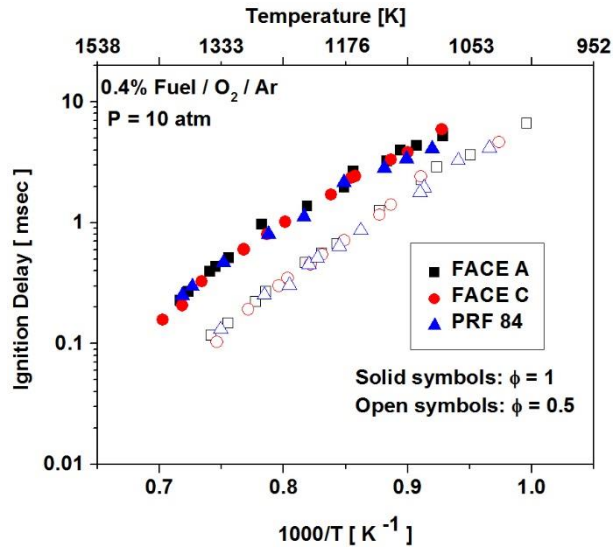


Figure 4-5: Ignition delay times during the oxidation of 0.4% fuel (iso-octane, PRF 84, FACE A, FACE C, n-heptane) / O₂ / Ar, P = 10 atm at $\phi = 0.5$ and 1. Data obtained in KAUST low pressure shock tube and presented in [29].

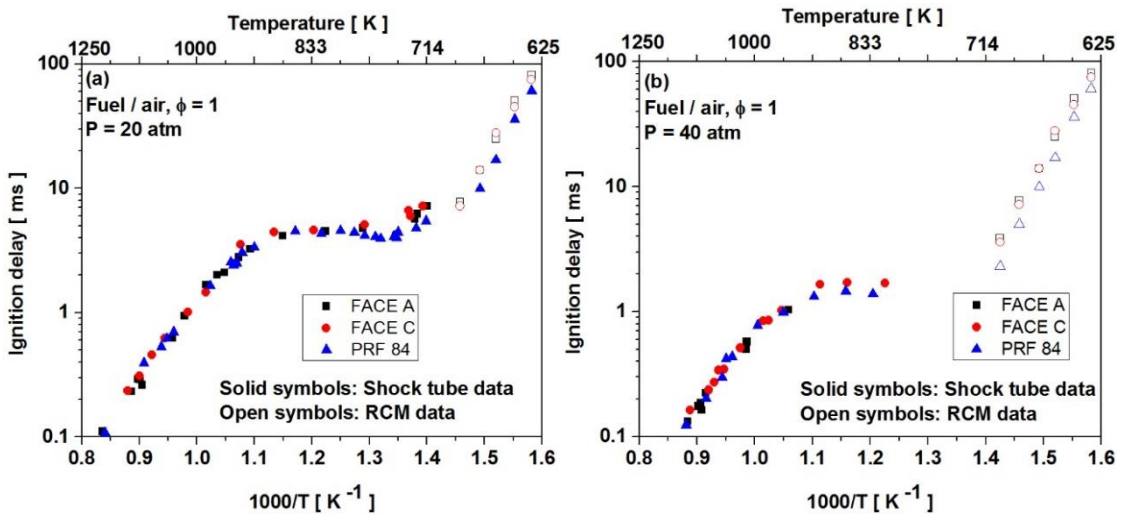


Figure 4-6: Ignition delay times during the oxidation of stoichiometric fuel / air mixtures (iso-octane, PRF 84, FACE A, FACE C) / at (a) 20 atm and (b) 40 atm. Data taken from [29].

4.3.2 Species time-histories of FACE gasolines and PRF surrogate

Species time histories were measured for the two FACE gasolines and the PRF

surrogate over 1350 – 1550 K and nominal pressures of 2 atm. Figure 4-7 shows the measured profiles of OH, CO, H₂O and CO₂ during the stoichiometric oxidation of 0.2% fuel (PRF 84, FACE A, FACE C) at a representative temperature of 1450 K. Although all four species are measured simultaneously for a specific fuel, the profiles shown for different fuels were measured in separate experiments; thus the actual reflected shock temperatures are 1450 ± 10 K. Both FACE A and C show very similar trends in all four species profiles. Also, PRF 84 surrogate captures the speciation profiles of both gasoline fuels reasonably well. These trends are consistent with the similarities found in ignition delay (Figure 4-4 and Figure 4-5) of all three fuels studied here. The chemical kinetics phenomena at high temperatures are primarily controlled by the presence of active radical pool such as OH, CH₃, H, and HO₂. If two fuels produce very similar active radical pool, it is expected that the fuels will then exhibit similar reactivity. Thus the PRF surrogate needs to reproduce the active radical pool of the real fuel as closely as possible in order to capture the chemical kinetics of the real fuel. It can be seen from Figure 4-7 (a) that both gasoline fuels and PRF 84 show very similar trends in OH formation and consumption. The pre-ignition OH concentrations for PRF 84 and FACE A oxidation are in close agreement whereas the OH concentration for FACE C is lower by about 30% during the first 100 μs. Similar n- and iso-paraffin content present in PRF 84 and FACE A leads to similar OH profiles. The lower OH concentration for FACE C over the early time, however, does not appear to significantly affect the ignition delay time.

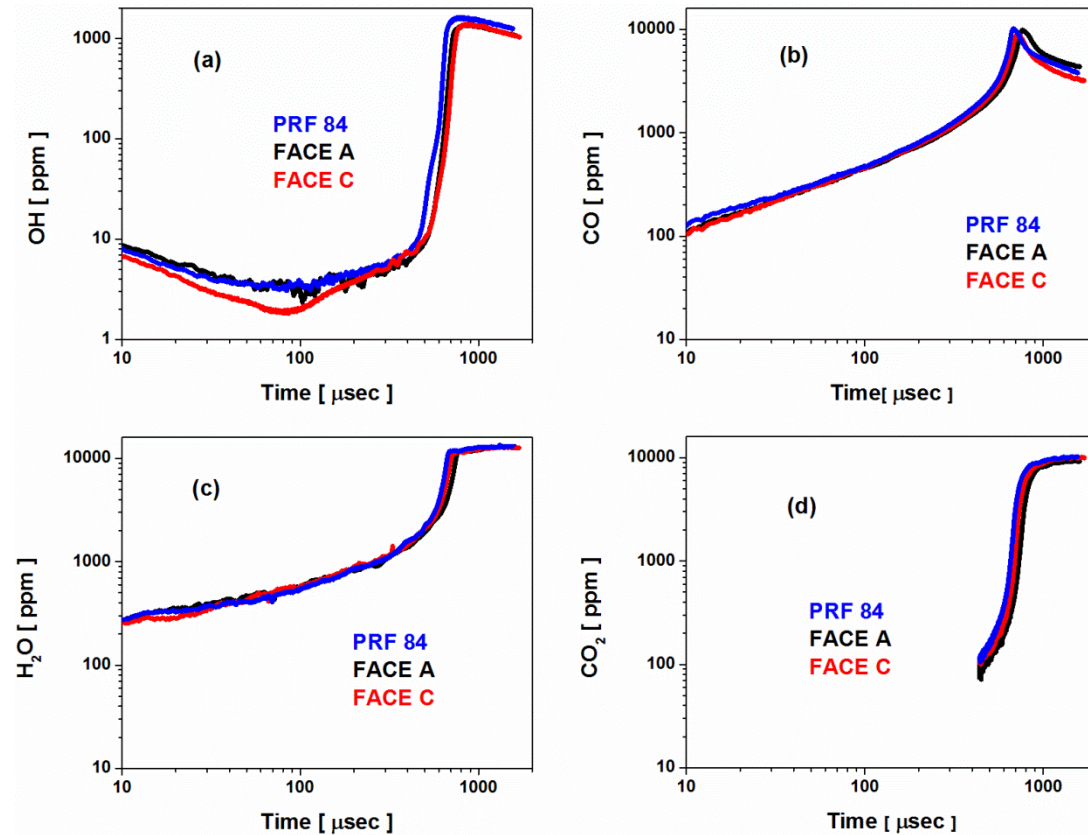


Figure 4-7: Measured species profiles during the oxidation of 0.2% fuel, $\Phi = 1$, $P \approx 2$ atm; Reflected-shock temperatures are PRF 84: 1459 K; FACE A: 1455 K; FACE C: 1443 K. Note that the CO_2 data are not available at early times due to the 100 ppm detection limit of the CO_2 diagnostic used here.

The three stable molecules measured here, CO , H_2O and CO_2 , are important reaction progress markers. It can be observed from Figure 4-7 (b-d) that these species evolve quite similarly in time for all three fuels studied. Post-ignition plateau values of these species are slightly higher for PRF 84 compared to FACE A, with OH , CO and CO_2 being 15%, 9% and 6% higher, respectively. The similarities in global reactivity of the three fuels, indicated by similarities in ignition delay (Figure 4-4 and Figure 4-5), can now be explained based on the observation that the local reactivity markers also evolve similarly during the induction period. These fuels may exhibit some differences in higher carbon-containing species produced during initial fuel decomposition, but these differences did not affect the

global reactivity as well as the local reactivity markers (Figure 4-4, Figure 4-5 and Figure 4-7) in this high-temperature study.

Measured PRF 84 species profiles are compared with those predicted by Mehl et al. [79] gasoline surrogate mechanism and Bieleveld et al. [102] PRF mechanism in Figure 4-8. The correct prediction of OH radicals is very important, particularly in high temperature regime. The rates of production (ROP) of reaction progress markers, such as H₂O (OH + H₂ ↔ H + H₂O, CH₄ + OH ↔ CH₃ + H₂O) and CO₂ (CO + OH ↔ CO₂ + H), are strongly dependent on the OH radical concentration at these high temperatures. It can be seen from Figure 4-8 that Mehl et al. [79] mechanism (dashed lines) captures the OH experimental profile very well at the highest temperature of this study (1526 K), although there is considerable under-prediction (~ 50%) at earlier times (20 – 100 μsec). Bieleveld et al. [102] mechanism (dotted lines in Figure 4-8) significantly overpredicts the early-time concentration of all measured species and thus gives much shorter ignition delay time.

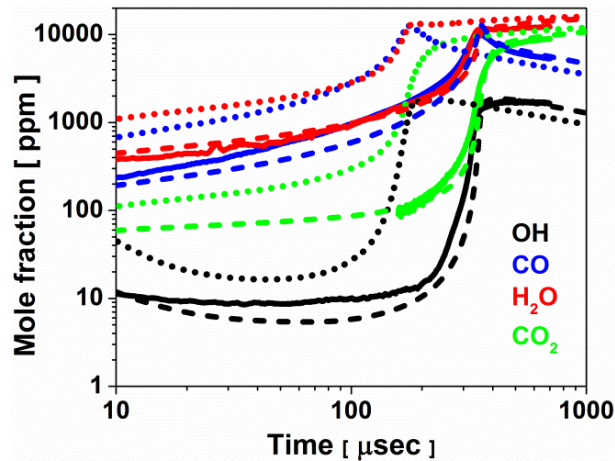


Figure 4-8: Comparison of multi-species measurements with kinetic simulations during the oxidation of 0.2% PRF84/O₂/Ar ($\Phi = 1$), T = 1526 K, P = 2 atm. Solid lines: Measurements, Dashed lines: Mehl et al. [79] simulations, Dotted lines: Bieleveld et al. [102] simulations.

Figure 4-9 shows Mehl et al. [79] model predictions for different species as a function

of temperature. As temperature is decreased, the OH model predictions start to deviate further from the OH experimental profiles; see the comparison at 1459 K, 1436 K and 1397 K. Similar observations can be made for time-histories of CO, H₂O and CO₂. At 1526 K, Mehl et al. [79] mechanism overpredicts CO at early times, though excellent agreement can be seen between the simulated and experimental CO₂ and H₂O profiles. Importantly, the model fails to capture any of the reaction progress markers at lower temperatures. These trends are also depicted in Figure 4-4 and Figure 4-5, where the discrepancy between PRF 84 measured and Mehl et al. [79] simulated ignition delay times increases as temperature decreases.

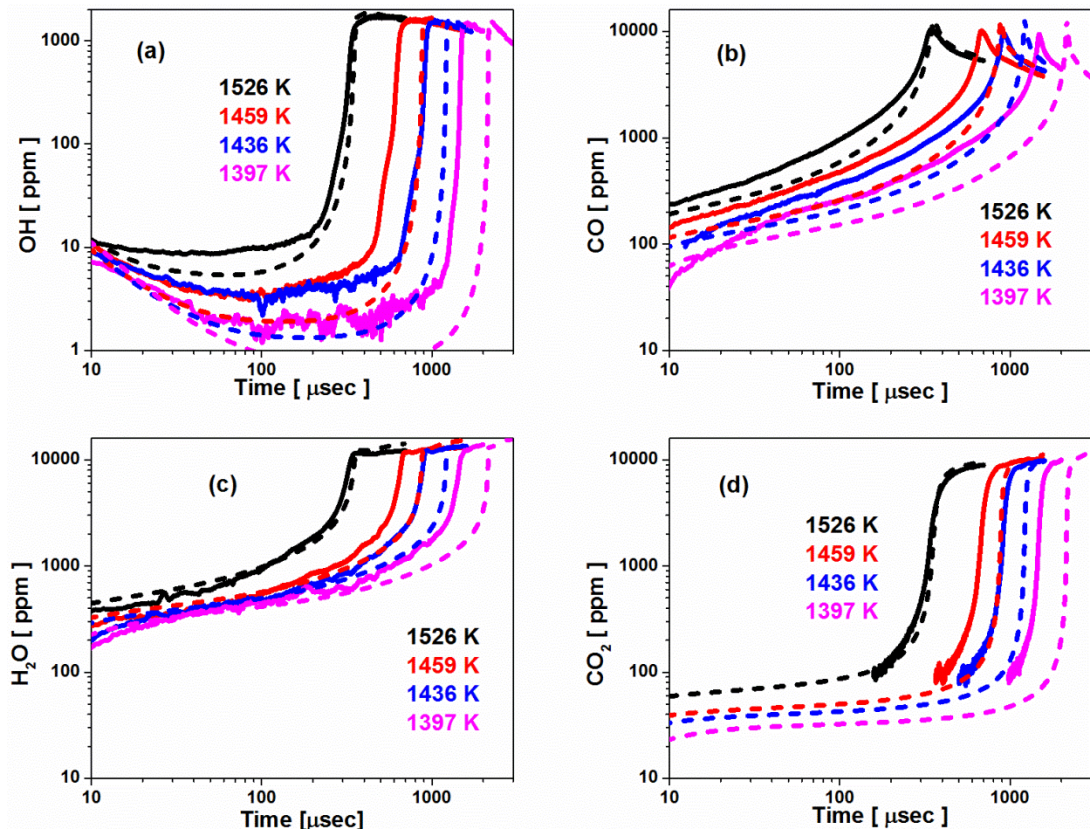


Figure 4-9: Comparison of measured profiles with kinetic simulations during the oxidation of 0.2% PRF84/O₂/Ar ($\Phi = 1$), Solid lines: Measurements, Dashed lines: Mehl et al. [79] simulations.

Hydroxyl sensitivity (Figure 4-10) and rate-of-production (not shown here) analyses

performed for PRF 84 show that OH is consumed by propene and iso-butene after the initial fuel decomposition and abstraction reactions. Propene and iso-butene are thus OH radical scavenging species and produce resonantly-stabilized allyl ($C_3H_6 + OH \leftrightarrow C_3H_5-A + H_2O$) and relatively unreactive allene ($IC_4H_8 + OH \leftrightarrow IC_4H_7 + H_2O$, $IC_4H_7 \leftrightarrow C_3H_4-A + CH_3$), respectively. Thus the rates of reactions involving propene, iso-butene, allyl, and allene can affect the overall fuel reactivity. The uncertainty in unimolecular decomposition and hydrogen abstraction rates of these species may contribute to the differences between the experimental and modeled speciation trends. Mehl et al. [79] gasoline surrogate mechanism captures n-heptane reactivity quite accurately (Figure 4-3, Figure 4-4), and thus the discrepancy between measured and simulated PRF profiles can be the result of deficiencies in the iso-octane sub-mechanism or synergetic effects between the n-heptane and iso-octane chemistry.

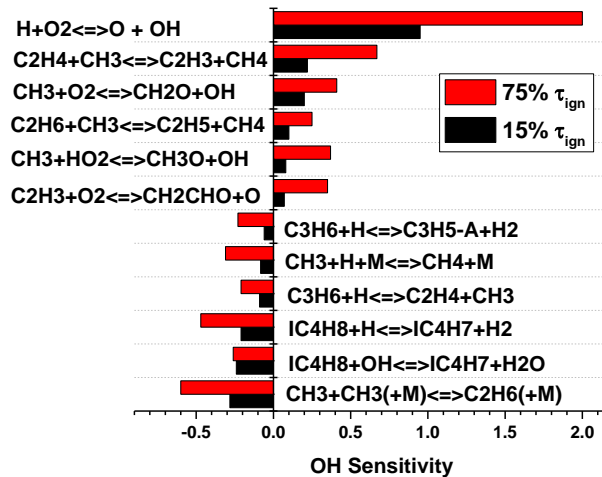


Figure 4-10: Hydroxyl sensitivity at two instants: 15% and 75% of the predicted ignition delay time.

0.2% PRF84/O₂/Ar ($\Phi = 1$), T = 1430 K, P = 2 atm.

In this chapter, the ignition delay times and species time histories of two highly paraffinic (low sensitivity) mid-octane gasolines and their PRF surrogate are presented.

Using the species and ignition data, it is shown that a PRF data satisfactorily captures the ignition requirements of these highly paraffinic gasolines. The trends seen in species data nicely complement the ignition delay trends. It is shown that, at high temperatures, where ignition delay times of gasolines and surrogates are similar, their speciation trends are also quite similar with important reaction progress and completion markers evolving quite consistently for the gasolines and surrogates. From the current study, it can be concluded that a PRF surrogate, having similar octane rating, can be used to capture the global reactivity of a predominantly paraffinic gasoline fuel (low sensitivity) under a wide range of test conditions.

Chapter 5: IGNITION STUDIES OF HIGH OCTANE GASOLINES AND SURROGATES

In this chapter, ignition delay times of ternary blends of toluene/*n*-heptane/iso-octane (TPRFs) are presented. Simple Primary Reference Fuel (PRF) surrogates, by definition, can not take into account the non-paraffinic content present in commercial gasolines. Commercial high octane gasolines have high non-paraffinic content (Sensitivity > 7). Therefore, TPRFs surrogates are used to adequately represent the sensitivity requirements of commercial high octane gasolines. A wide range of TPRF ignition data was collected using shock tube and rapid compression machine. The data is analyzed based on its pressure, equivalence ratio and octane dependence. Chemical kinetics analysis is used to explain experimental trends. The data are also compared with ignition delay data of certified high octane gasolines.

5.1 Introduction

Primary reference fuel (PRF) surrogates are among the simplest surrogates employed to emulate gasoline ignition. A PRF is a bi-component mixture of *n*-heptane (octane number defined to be 0) and iso-octane (octane number defined to be 100), with PRF xx meaning xx% iso-octane and 1 – xx% *n*-heptane by volume. Gasoline fuels are knock rated, having both a Research Octane Number (RON) and a Motor Octane Number (MON), based on comparisons with PRF blends in a cooperative fuels research (CFR) engine. Due to the traditional use of *n*-heptane and iso-octane as gasoline surrogate components, several experimental [15, 104, 105] and modeling efforts [8, 9, 106, 107] are available in the literature describing the ignition of *n*-heptane and iso-octane. A few chemical kinetic

modeling and experimental studies have also focused on describing the ignition of PRF blends [15, 17, 20, 25, 108-110].

It has been shown that a PRF surrogate captures the ignition of a high-paraffinic content gasoline reasonably well at temperatures above 850 K [29] (see also 0 and Chapter 4). Sarathy et al. [29] showed that for two highly paraffinic gasoline fuels, FACE (Fuels for Advanced Combustion Engines; Conoco Philips) gasoline A and C, a PRF surrogate was slightly more reactive at low temperatures (< 750 K) compared to the gasoline fuels. Moreover, Sarathy et al. [30] showed that for high sensitivity gasolines (FACE F and G), a PRF surrogate fails to capture many trends (both qualitatively and quantitatively) in the ignition delay times at NTC and low temperatures.

Commercial high octane gasoline fuels generally have high aromatic content ($\sim 20 - 30$ %) and some other non-paraffinic ($\sim 5 - 10$ %) components [4]. Consequently, such fuels tend to have a high sensitivity ($S = \text{RON} - \text{MON}$) which can be considered as a measure of the non-paraffinic content of the fuel. A PRF surrogate by definition has zero sensitivity and will not be able to emulate the ignition behavior of a real gasoline fuel. Kalghatgi and coworkers [111, 112] demonstrated that PRF surrogates cannot be used to rate a gasoline based on the primitive RON and MON testing methods. This discrepancy is due to the fact that real gasoline, due to its high sensitivity ($S \sim 10$), matches different PRF blends at different engine operating conditions. They proposed the use of toluene/*n*-heptane [111] and toluene/*n*-heptane/iso-octane [112] blends as more suitable gasoline surrogates. Kalghatgi et al. [112] developed correlations to calculate the composition of a toluene/*n*-heptane/iso-octane surrogate to match the RON and sensitivity of a target gasoline for a wide range of octane numbers. By matching both RON and sensitivity, the

surrogate is expected to capture the real fuel reactivity over a wide range of conditions.

There have been a few fundamental ignition studies of surrogates comprising three or more components. Gauthier et al. [23] studied the auto-ignition characteristics of *n*-heptane/air, RD387 gasoline/air, and ternary surrogate/air (63% iso-octane / 20% toluene / 17% *n*-heptane by volume) mixtures in a shock tube facility. They showed that the auto-ignition behavior of the RD387 gasoline was well-reproduced by the ternary surrogate. Vanhove et al. [25] studied an iso-octane/1-hexene/toluene ternary blend in a rapid compression machine, interestingly preferring 1-hexene over *n*-heptane to produce low-temperature reactivity. Kukkadapu et al. [27] measured ignition delay times of RD387 in a rapid compression machine and the results agreed well with the work of Gauthier et al. [23]. In further studies, Kukkadapu et al. [28, 73] reported better agreement of a four component (iso-octane/*n*-heptane/toluene/2-pentene) surrogate with ignition delay times of RD387 at lower temperatures compared to the ternary surrogate proposed by Gauthier et al. [23]. Sarathy et al. [29] used five- (*n*-butane/iso-pentane/2-methylhexane/*n*-heptane/iso-octane) and six- (*n*-butane/iso-pentane/2-methylhexane/*n*-heptane/toluene/iso-octane) component surrogates to simulate low-temperature ignition of FACE gasolines A and C, respectively. Sarathy et al. [30] used a TPRF surrogate and a multi component surrogate to adequately model the NTC and low temperature ignition delay trends of FACE F using a seven component (*n*-butane/2-methylbutane/2-methylhexane/Cyclopentane/1,2,4-trimethylbenzene/1-Hexene/*i*-octane) surrogate and FACE G using a eight component (*n*-butane/2-methylbutane/2-methylhexane/Cyclopentane/1,2,4-trimethylbenzene/1-Hexene/*i*-octane/Toluene) surrogate.

Previous work has thus shown that ternary blends of toluene/*n*-heptane/iso-octane

(henceforth referred to as TPRF) can serve not only as adequate gasoline surrogate candidates on their own but may also be major constituents of the more complex multi-component surrogates. This is because TPRF surrogates can emulate the aromatic, *n*-paraffinic and iso-paraffinic content present in a real gasoline, where these three classes represent > 90% of the chemical content of commercially available distillate gasoline fuels. However, wide-ranging fundamental studies of TPRF ignition and chemical kinetic development are not available in the literature. The objective of the current work is to provide a large dataset of experimental ignition delay times of TPRF blends for use in the refinement and development of surrogate kinetic models.

Here, ignition delay times of four TPRF mixtures (RON = 70, 80, 91 and 97.5; S = 4, 5.7, 7.6 and 10.9) have been measured in a shock tube (ST) and in a rapid compression machine (RCM). These measurements were performed at pressures of 10 (RCM), 20 and 40 bar (RCM and ST) in the temperature range 650 – 1250 K and at equivalence ratios of 0.5 and 1.0. The TPRF mixtures were formulated to match the RON and sensitivity of two certified gasoline and two prospective naphtha-like fuels (see Figure 5-10). These data are the first of their kind and will form a highly valuable dataset for future gasoline surrogate mechanism development and validation. Furthermore, TPRF 91 and 97.5 data are compared against the ignition delay data of high octane certified gasolines.

5.2 Methods

5.2.1 TPRF Surrogate Formulation

Several methodologies have been proposed in the literature to formulate TPRF surrogates for gasoline fuels [112-114]. Morgan et al. [113] developed a second-order volume-based model to derive TPRF surrogate composition corresponding to the RON and

MON of the target fuel. Kalghatgi et al. [112], on the other hand, proposed a second-order method on molar basis. Both works relied on engine octane data to optimize the correlations. Pera et al. [114] used octane ratings and the carbon, hydrogen and oxygen content of the target gasoline (ULG 95) to optimize the TPRF surrogate. However, they used linear by volume blending method which can potentially introduce errors in determining surrogates composition [113]. The TPRF surrogates studied in this work were formulated based on the correlations developed by Kalghatgi et al. [112]. These correlations calculate the TPRF surrogate composition required to emulate the RON and sensitivity the target fuel. The surrogates tested in this work were formulated over a wide range of octane numbers (RON: 70 – 97.5) with varying degrees of sensitivity (S: 4 – 11). The RON and MON values of the TPRF surrogates were experimentally measured at the Saudi Aramco Research and Development Center in their cooperative fuel research (CFR) engine following the ASTM D6733 (RON) and D6730 (MON) standards. These surrogates are listed in Table 5-1. It can be seen that the measured and estimated (from [112]) RON and MON values are in very good agreement with each other which further fortifies the use of the correlations developed by Kalghatgi et al. [112]. For brevity, the surrogate blends henceforth will be referred to as TPRF xx where xx represents the RON of the surrogate blend.

Table 5-1: TPRF surrogates investigated in this work. See Table A4 in Appendix for compositions in mole fractions.

Surrogate	iso-octane ¹	<i>n</i> -heptane ¹	Toluene ¹	RON estimated ²	RON measured ³	MON estimated ²	MON measured ³	Sensitivity ⁴
TPRF 70	42.48	36.23	21.29	70	70	66	66	4
TPRF 80	39.85	28.58	31.57	80	80.4	74.3	75.3	5.7
TPRF 91	36.58	19.31	44.1	91	92	83.4	84.3	7.6
TPRF 97.5	11.52	18.04	70.44	97.5	98	86.6	87.1	10.9

¹ % volume

² RON and MON estimated using correlations developed by Klaghatgi et al. [112]

³ RON and MON measured in a CFR engine using ASTM standards

⁴ Sensitivity $S = \text{RON} - \text{MON}$ (estimate)

5.2.2 Experimental Details

The experiments reported in this study were performed in the high-pressure shock tube (HPST) facility at King Abdullah University of Science and Technology (KAUST) and in a rapid compression machine (RCM) at the National University of Ireland, Galway (NUIG). For details shock tube and RCM ignition delay measurements, please refer to Chapter 2.

5.3 Results and Discussion

Ignition delay times of TPRF mixtures measured in the HPST and RCM are reported in this section. These data cover a wide range of temperatures (650 – 1250 K), pressures (10, 20 and 40 bar) and equivalence ratios ($\phi = 0.5$ and 1.0). Experiments at 10 bar were only conducted in the RCM as the ignition delay times at low pressures are too long for the shock tube. Throughout this section, the scatter symbols represent the measured data (solid symbols: shock tube data, open symbols: RCM data) and the lines represent the model simulations (solid lines: shock tube simulations, dashed lines: RCM simulations). The

gasoline surrogate mechanism developed by Mehl et al. [79] (henceforth referred as ‘LLNL mech’) is used throughout this manuscript to simulate and interpret the measured data.

5.3.1 Effect of Pressure

The effect of pressure (10, 20 and 40 bar) on the ignition delay times of TPRF 70, 80, 91 and 97.5 mixtures is shown in Figure 5-1 (a) – (d) for the stoichiometric ($\phi = 1$) mixtures, and in Figure 5-2 (a) – (d) for the fuel-lean ($\phi = 0.5$) cases. The figures show, as expected, that the fuel reactivity increases with increasing pressure at both equivalence ratios. The data show Arrhenius behavior at high ($T > 900$ K) and low ($T < 725$ K) temperatures, and exhibit varying degrees of negative temperature coefficient (NTC) behavior in a temperature range of around 750 – 850 K. The NTC behavior is particularly pronounced at low pressures (10 bar) and for low octane number (and low sensitivity) mixtures (TPRF 70 and 80). The TPRF 97.5 mixture, Figure 5-1 (d) and Figure 5-2 (d), showed only marginal NTC behavior. This is due to the high concentration of toluene in the TPRF 97.5 mixture (~ 70% vol. toluene, see Table 5-1), with the low reactivity of toluene suppressing the NTC behavior at all pressures.

The shock tube simulations (solid lines) are in good agreement, both qualitatively and quantitatively, with the HPST data (solid symbols) for the wide range of varying octane number TPRF fuels, Figure 5-1 and Figure 5-2 (a) – (d), and adequately capture the pressure dependence of the HPST data. An exception to this trend is the over-prediction of the TPRF 97.5 mixture at $\phi = 1$, Figure 5-1 (d). This is likely due to the very high content of toluene in this particular mixture and points towards the high-temperature toluene reactivity being too slow in the current model.

The RCM simulations (dashed lines) over-predict the experimental RCM data (open symbols) at low temperatures, particularly for high pressure (20 and 40 bar) and high octane fuels. This over-prediction can be seen clearly for the stoichiometric TPRF 91 and 97.5 mixtures, Figure 5-1 and Figure 5-2 (c), (d). For instance, at 700 K, $p = 40$ bar and $\varphi = 1$, the mechanism over-predicts RCM ignition delay times of the TPRF 91 and 97.5 mixtures by a factor of 2 and 3, respectively. Recently, Zhandong et al. [115] discovered the third O_2 addition channels which are important in controlling the low temperature reactivity and are expected to resolve this discrepancy in the current mechanisms. At 10 bar, we observe opposite trend where the RCM simulations under-predict the ignition delay times in the NTC region and at lower temperatures. In general, the model predictions appear reasonable and perhaps require only minor adjustments at low temperatures for high toluene concentration TPRF fuels at stoichiometric and/or fuel-rich conditions (i.e. at high fuel concentrations). These adjustments may require separate optimization of the toluene sub-mechanism for an improved prediction of the TPRF blends. Toluene sub-chemistry is being separately updated by the NUIG group currently.

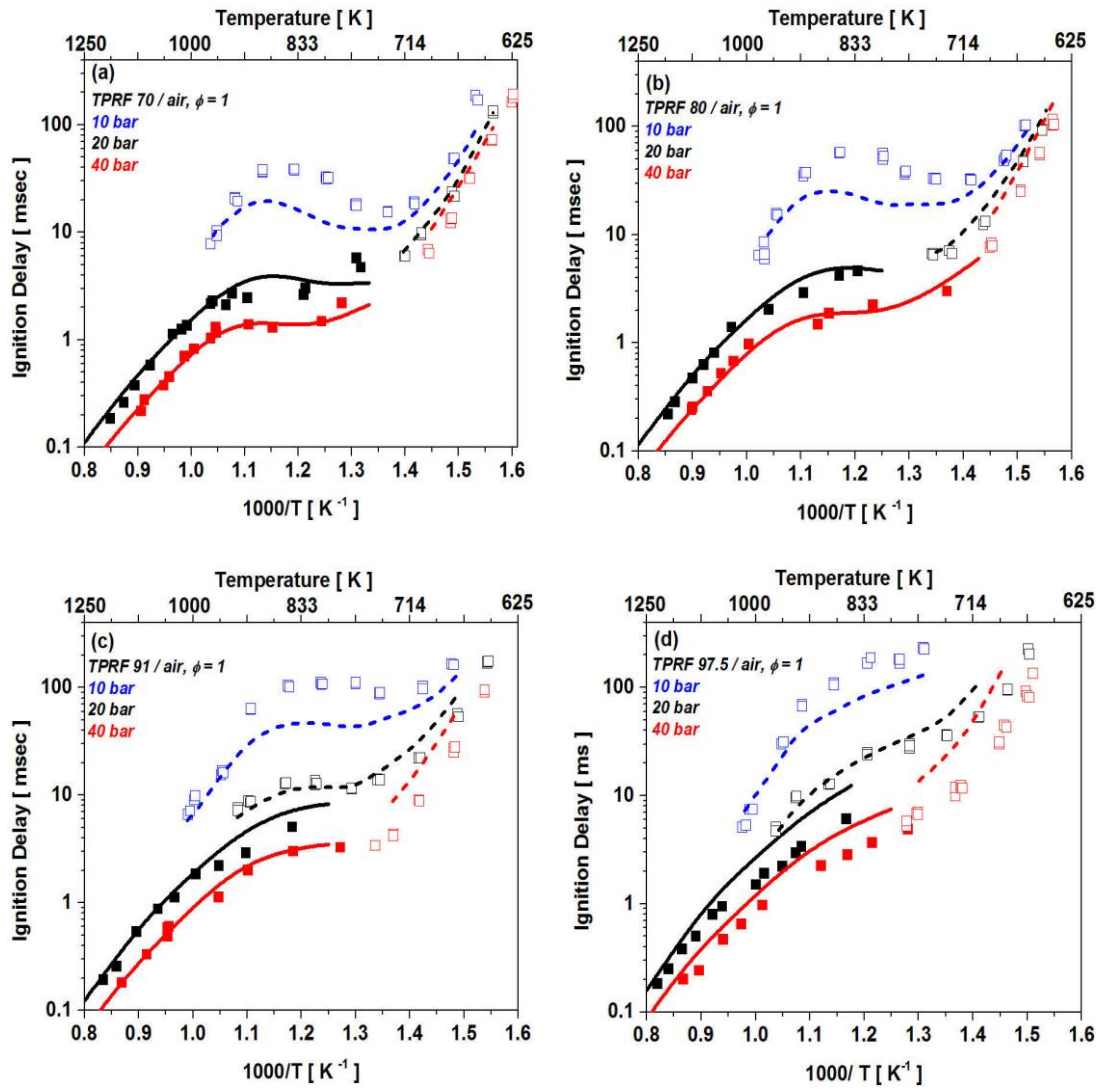


Figure 5-1: Effect of pressure (10, 20, 40 bar), at $\phi = 1$, on the ignition delay times of (a) TPRF 70, (b) TPRF 80, (c) TPRF 91, (d) TPRF 97.5. Scatter: solid symbols – HPST data, open symbols – RCM data. Lines: solid lines – shock tube simulations, dashed lines – RCM simulations. LLNL mech [79] is used for simulations.

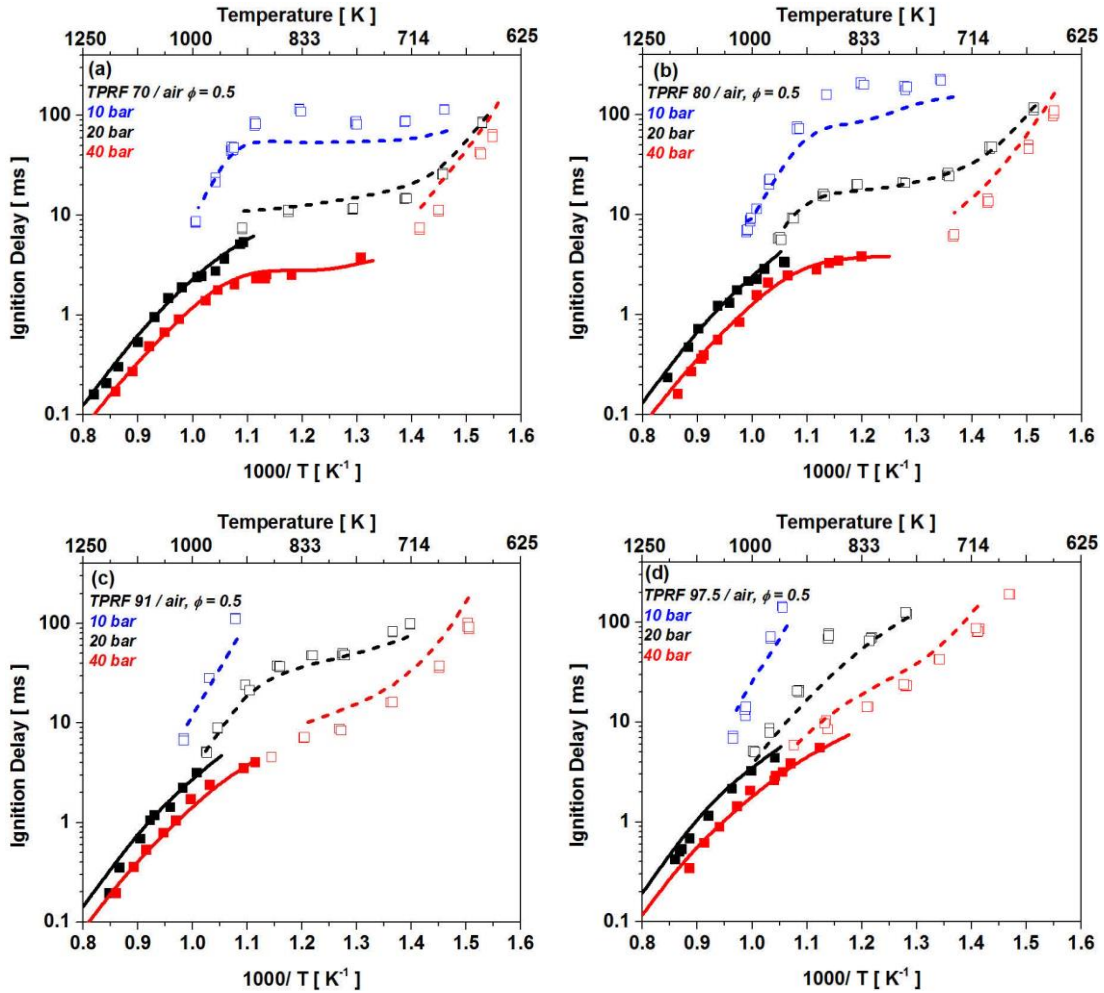


Figure 5-2: Effect of pressure (10, 20, 40 bar), at $\phi = 0.5$, on the ignition delay times of (a) TPRF 70, (b) TPRF 80, (c) TPRF 91, (d) TPRF 97.5. Scatter: solid symbols – HPST data, open symbols – RCM data. Lines: solid lines – shock tube simulations, dashed lines – RCM simulations. LLNL mech [79] is used for simulations.

Although general agreement between the ignition data from the HPST (KAUST) and RCM (NUIG) is good (Figure 5-1 and Figure 5-2), some discrepancies between the two facilities were observed. These are evident at 20 bar in the temperature range of 850 – 1000 K, particularly for the TPRF 91 and 97.5 mixtures at $\phi = 1$, Figure 5-1 (c), (d), where there is approximately a factor of two difference between the HPST and RCM ignition delay times, with the HPST data being faster. The authors of this study internally debated various

causes and remedies of these discrepancies. For example, careful cross experimentation and validations were performed at the KAUST RCM and the NUIG shock tube (see Appendix Figure A7); these experiments revealed similar discrepancies. It is important to note here that this is not the first time such discrepancies are observed between shock tube and RCM data. Recently, Sarathy et al. [30] found similar discrepancies between the shock tubes (Rensselaer Polytechnic Institute, KAUST) and RCM (University of Connecticut) ignition delay times of FACE gasoline F and G at 20 bar and 800 – 1000 K. It can be hypothesized that the homogeneous core model used to simulate RCM data is not fully valid under such conditions. On the other hand, the relatively long ignition delay shock tube data could potentially be affected by localized flame initiation and propagation [116] resulting in shortened ignition delay times (see Appendix Figure A8). The discrepancies between shock tube and RCM data under specific conditions are being investigated in a larger collaborative framework and is beyond the scope of this work. Nonetheless, it is important to highlight systematic differences seen between commonly used fundamental experimental devices.

5.3.2 Effect of Equivalence Ratio

The effect of equivalence ratio ($\phi = 0.5$ and 1.0) on the ignition delay times of TPRF 70, 80, 91 and 97.5 mixtures is shown in Figure 5-3 – Figure 5-5 at 10, 20 and 40 bar, respectively. The figures show that, in general, the ignition delay times decrease with increasing equivalence ratio at all pressures and temperatures, i.e., fuel-lean mixtures are slower to ignite compared to stoichiometric ones. At higher temperatures ($T > 1000$ K), the HPST ignition delay data and the simulations show relatively weak dependence on equivalence ratio, with the stoichiometric mixtures being only marginally more reactive

compared to the fuel-lean ones at all three pressures. Moreover, this high-temperature equivalence ratio dependence is more pronounced for the high-toluene blend TPRF 97.5 at 40 bar, Figure 5-5 (d). Similarly, the low-temperature ($T < 725$ K) RCM ignition delay data and simulations show a weak dependence on equivalence ratio, and again the TPRF 97.5 mixture shows the largest variation with equivalence ratio at low temperatures. The dependence on equivalence ratio is most pronounced in the NTC region. Moreover, in this region, the ϕ -dependence correlates well with the inherent NTC nature of the fuel, i.e., TPRF 70 and 80, Figure 5-3 – Figure 5-5 (a), (b), have the most paraffinic content and, therefore, exhibit the largest dependence on equivalence ratio compared to the TPRF 97.5 mixtures, Figure 5-3 – Figure 5-5 (d), which have the highest concentrations of toluene and so exhibit the least NTC behavior and the least dependence on equivalence ratio in the NTC region.

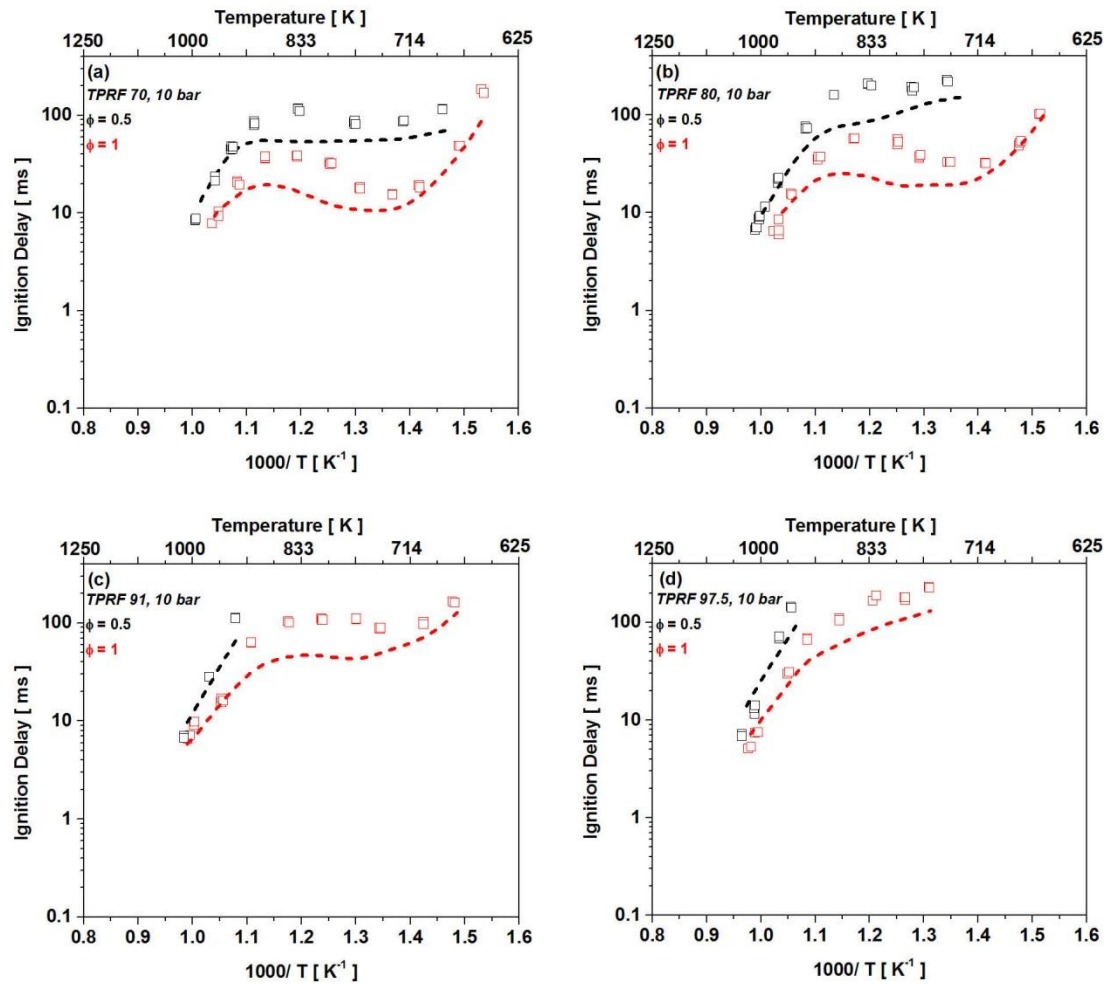


Figure 5-3: Effect of equivalence ratio ($\phi = 0.5$ and 1.0), at 10 bar, on the ignition delay times of (a) TPRF 70, (b) TPRF 80, (c) TPRF 91, (d) TPRF 97.5. Scatter: open symbols – RCM data. Lines: dashed lines – RCM simulations. LLNL mech [79] is used for simulations. Ignition delay times were not measured in the shock tube for 10 bar.

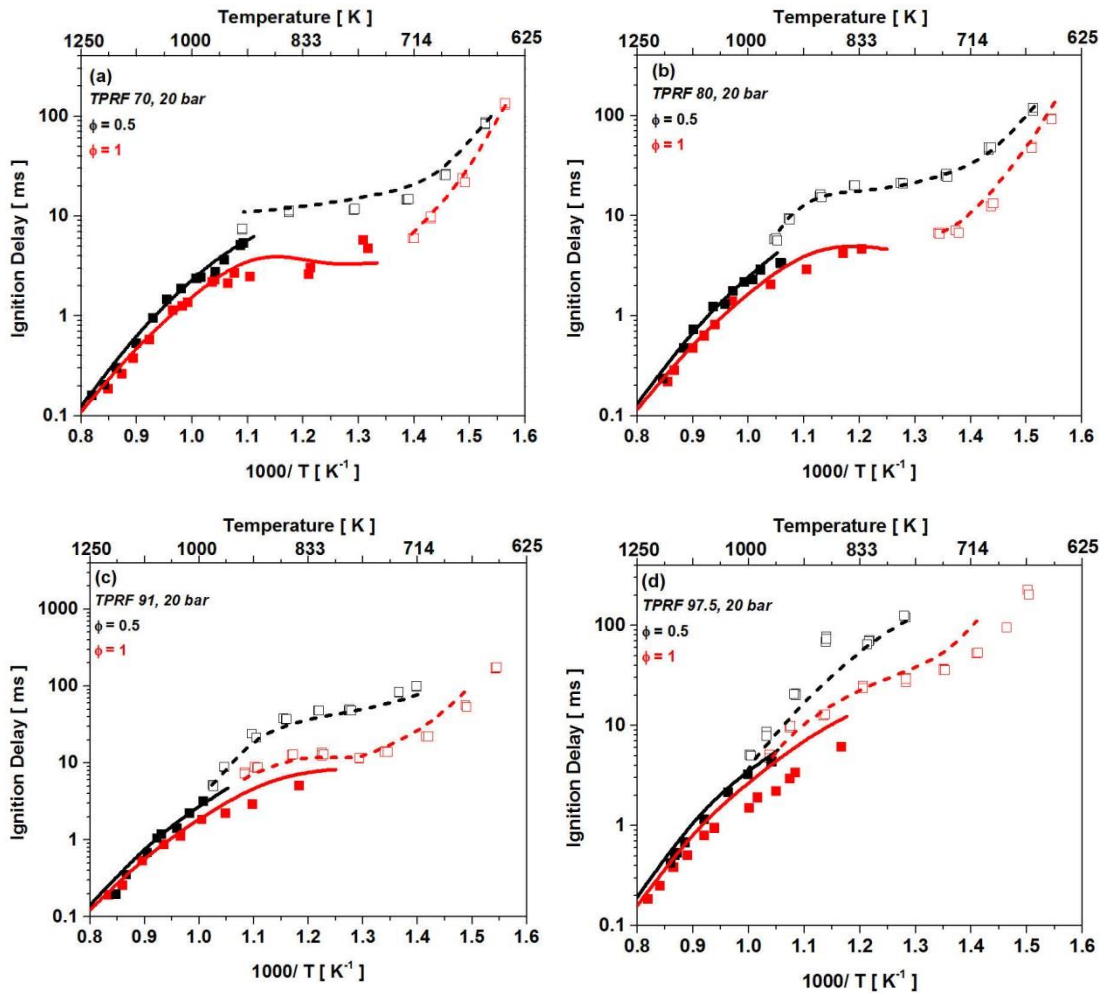


Figure 5-4: Effect of equivalence ratio ($\phi = 0.5$ and 1.0), at 20 bar, on the ignition delay times of (a) TPRF 70, (b) TPRF 80, (c) TPRF 91, (d) TPRF 97.5. Scatter: solid symbols – HPST data, open symbols – RCM data. Lines: solid lines – shock tube simulations, dashed lines – RCM simulations. LLNL mech [79]

is used for simulations.

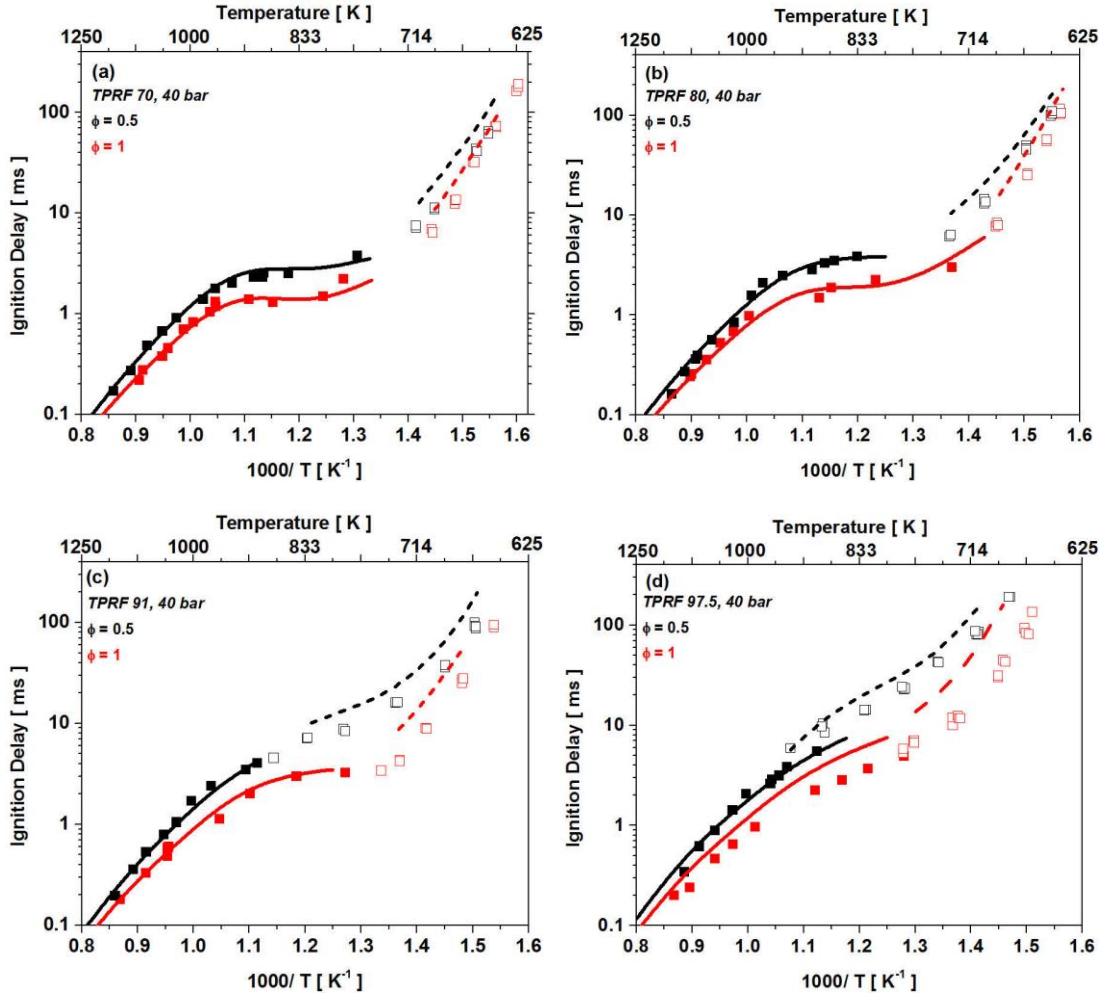


Figure 5-5: Effect of equivalence ratio ($\phi = 0.5$ and 1.0), at 40 bar, on the ignition delay times of (a) TPRF 70, (b) TPRF 80, (c) TPRF 91, (d) TPRF 97.5. Scatter: solid symbols – HPST data, open symbols – RCM data. Lines: solid lines – shock tube simulations, dashed lines – RCM simulations. LLNL mech [79] is used for simulations.

5.3.3 Effect of Octane Number

The effect of octane number on ignition delay times of TPRF 70, 80, 91 and 97.5 mixtures is shown in Figure 5-6 (for $\phi = 1$) and Figure 5-7 (for $\phi = 0.5$). The figures show that at high temperatures ($T > 1000$ K), the measured and simulated ignition delay times

of all of the fuels show very similar ignition delay times. At very low temperatures ($T < 700$ K), the measured and simulated ignition delay times show a weak dependence on the research octane number (RON) of the fuel. At low temperatures, this octane dependence is more pronounced for the higher RON fuels i.e., there is on average a factor of 2 – 3 difference between the ignition delay times of TPRF 97.5 (RON 97.5) and TPRF 91 (RON 91) mixtures. This difference diminishes as we move to lower RON fuels, as can be seen by the negligible reactivity differences between TPRF 80 (RON 80) and TPRF 70 (RON 70). Another way to consider this reactivity difference at low temperatures is by looking at the sensitivity of these fuels. The sensitivity of the studied fuels decreases from TPRF 97.5 ($S = 10.9$) to TPRF 70 ($S = 4$). This indicates that large reactivity differences at low temperatures for TPRF 97.5 and TPRF 91 mixtures compared to TPRF 80 and TPRF 70 mixtures are primarily driven by the non-paraffinic content (toluene) present in these fuels. Therefore, it can be argued that, at low temperatures, the octane dependence of TPRFs will only be significant for high sensitivity TPRF fuels, i.e., fuels composed of a large non-paraffinic content.

The largest effect of octane number on the reactivity (ignition delay times) is observed in the NTC region (near 750 – 850 K). It can be seen clearly in Figure 5-6 (for $\phi = 1$) and Figure 5-7 (for $\phi = 0.5$) that the ignition delay times correlate very well with the octane number of these fuels, i.e., the fuel with the highest octane number (RON) has the longest ignition delay times and the reactivity increases (ignition delay time decreases) with a decrease in octane number (RON). Mehl et al. [82, 84] have shown that ignition delay times in the NTC region (at 825 K and 25 atm) correlate well with the RON of fuels. Sarathy et al. [43] and Badra et al. [117] also formulated methodologies to correlate NTC

region ignition delay times to RON and MON. The results from the current study also confirm that correlations between octane ratings (RON, MON, S) and ignition delay times for TPRF surrogates can be best formulated in the NTC region.

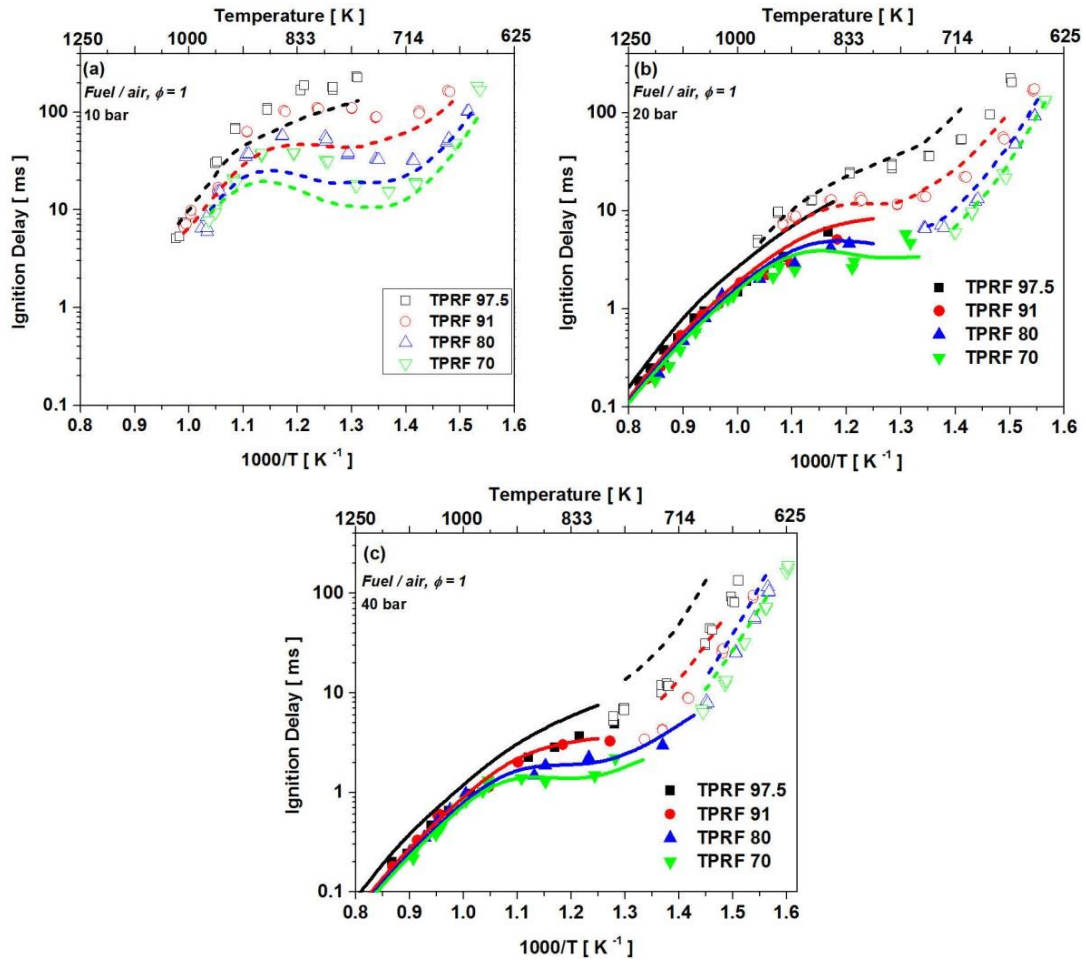


Figure 5-6: Effect of RON (97.5, 91, 80, 70), at $\phi = 1$, on the ignition delay times of TPRF 97.5 (■), TPRF 91 (●), TPRF 80 (▲), TPRF 70 (▼) at (a) 10 bar, (b) 20 bar and (c) 40 bar. Scatter: solid symbols – HPST data, open symbols – RCM data. Lines: solid lines – shock tube simulations, dashed lines – RCM simulations. LLNL mech [79] is used for simulations.

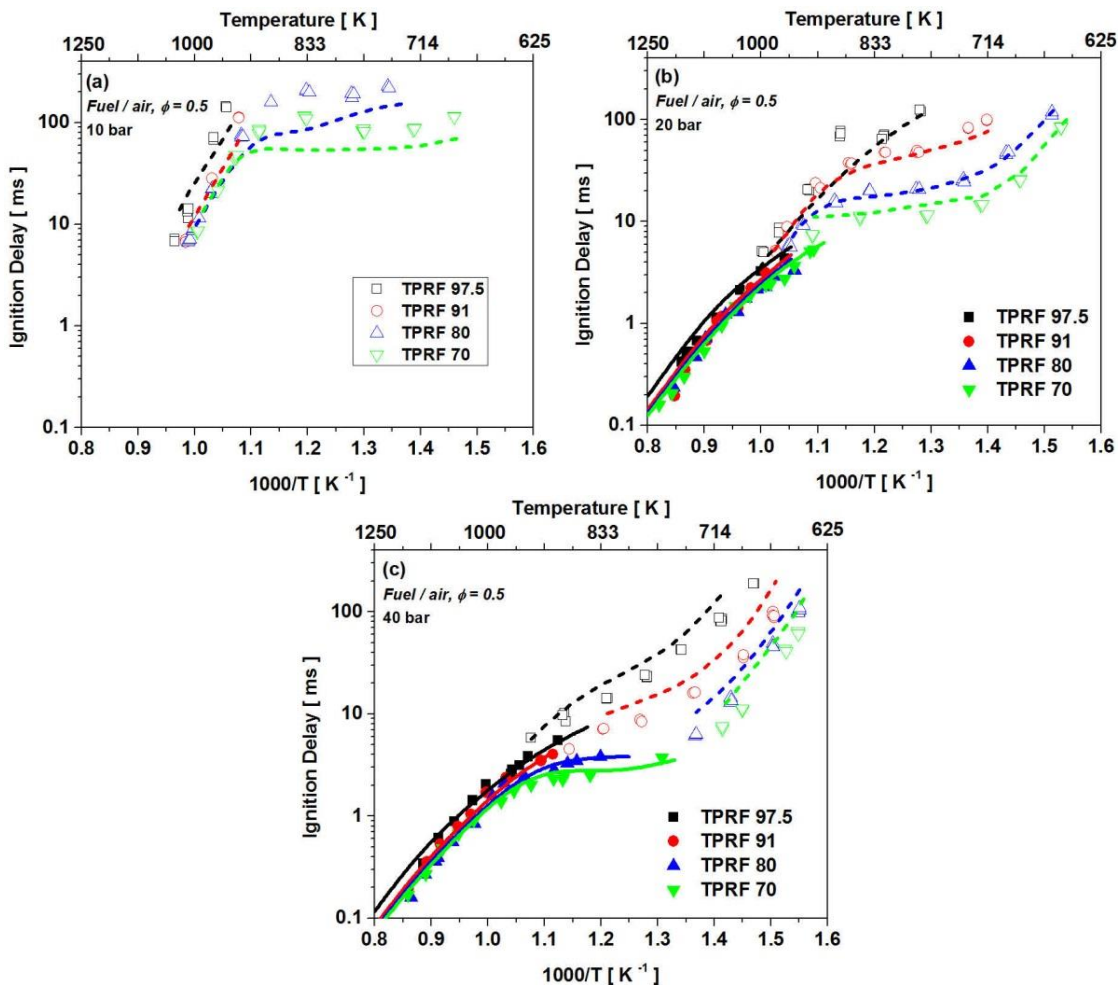


Figure 5-7: Effect of RON (97.5, 91, 80, 70), at $\phi = 0.5$, on the ignition delay times of TPRF 97.5 (■), TPRF 91 (●), TPRF 80 (▲), TPRF 70 (▼) at (a) 10 bar, (b) 20 bar and (c) 40 bar. Scatter: solid symbols – HPST data, open symbols – RCM data. Lines: solid lines – shock tube simulations, dashed lines – RCM simulations. LLNL mech [79] is used for simulations.

5.4 Chemical Kinetic Analyses

In the previous section (Section 5.3.3), several observations were made about the dependence of ignition delay times of the TPRFs on the octane number of the fuel. Firstly,

at high temperatures, very little effect of octane number on the ignition delay times was observed. Furthermore, at low temperatures, a weak octane number dependence was observed, and this dependence was pronounced for high-RON and high-sensitivity fuels (TPRF 97.5, TPRF 91) compared to low-RON and low-sensitivity fuels (TPRF 80, TPRF 70). Finally, a strong dependence of octane number on the ignition delay times was observed in the NTC region. We will now explain these trends using chemical kinetic analyses.

At high temperatures ($T > 1000$ K), ignition is primarily controlled by the thermal chain branching of H_2O_2 to produce two $\dot{\text{O}}\text{H}$ radicals via the reaction $\text{H}_2\text{O}_2 (+\text{M}) \leftrightarrow \dot{\text{O}}\text{H} + \dot{\text{O}}\text{H} (+\text{M})$, which is favored more or less equally for various fuels studied here. This results in very similar ignition delay times at high temperatures and hence an almost indistinguishable dependence of ignition delay times on octane number at high temperatures.

At low temperatures ($T < 700$ K), degenerate chain branching to produce $\dot{\text{O}}\text{H}$ radicals primarily controls the ignition of typical paraffinic fuels [86]. Therefore, rate of production (ROP) analyses based on $\dot{\text{O}}\text{H}$ radicals are utilized here (Figure 5-8) to highlight key similarities and differences between the various fuels studied here. The ROP analyses are conducted at a time corresponding to two-thirds of the exponential growth of $\dot{\text{O}}\text{H}$ radical concentration in line with the guidelines provided by Merchant et al. [85]. It can be seen that H-abstraction from the fuel (n-heptane/iso-octane/toluene) is responsible for $\dot{\text{O}}\text{H}$ radical consumption (negative ROP) for all cases. However, these consumption channels are widely different as we go from high-RON, high-sensitivity fuels (TPRF 97.5, TPRF 91) to low-RON, low-sensitivity fuels (TPRF 70, TPRF 80). Figure 5-8 (c) and (d) show

that H-abstraction by $\dot{\text{O}}\text{H}$ radicals from toluene to produce benzyl radical is the most important $\dot{\text{O}}\text{H}$ radical consumption channel for TPRF 97.5 and TPRF 91 mixtures; however, H-abstraction from secondary sites on *n*-heptane to produce *n*-heptyl radicals are the most important $\dot{\text{O}}\text{H}$ consumption pathways for the TPRF 80 and 70 mixtures (Figure 5-8 (a) and (b)). The subsequent pathways for these radicals (abstraction products) control the low-temperature ignition process. The benzyl radicals formed by H-atom abstraction are stabilized [25] at low temperatures rendering toluene or high toluene-containing fuels (like TPRF 97.5 mixtures in this case) relatively un-reactive at lower temperatures. The subsequent ignition of high toluene concentration fuels, even at low temperatures, is controlled by H_2O_2 decomposition due to the temperature increase associated with the exothermicity of the oxidation of toluene to benzyl radical (and subsequently benzaldehyde) and water [25]. On the other hand, the highly reactive *n*-heptyl radicals formed by H-abstraction by $\dot{\text{O}}\text{H}$ radicals in the TPRF 80 and 70 mixtures follow the expected low-temperature degenerate chain branching pathways [86] to produce $\dot{\text{O}}\text{H}$ radicals (positive ROP). The *n*-heptyl radicals react with molecular oxygen to form alkylperoxy radicals, which then undergo a series of isomerization and oxygen addition reactions to form ketohydroperoxides (KHPs) and $\dot{\text{O}}\text{H}$ radicals. The decomposition of KHPs produces additional $\dot{\text{O}}\text{H}$ radicals, resulting in an exponential growth of $\dot{\text{O}}\text{H}$ radicals and ignition. It can be concluded from the ROP analyses that *n*-heptane primarily controls $\dot{\text{O}}\text{H}$ consumption for TPRFs with low sensitivity / low RON (TPRFs 70 and 80) and, therefore, relatively weak octane dependence is seen at low temperatures for these low sensitivity TPRFs. On the other hand, significant octane dependence observed for the high sensitivity / high RON TPRFs may be attributed to the toluene kinetics.

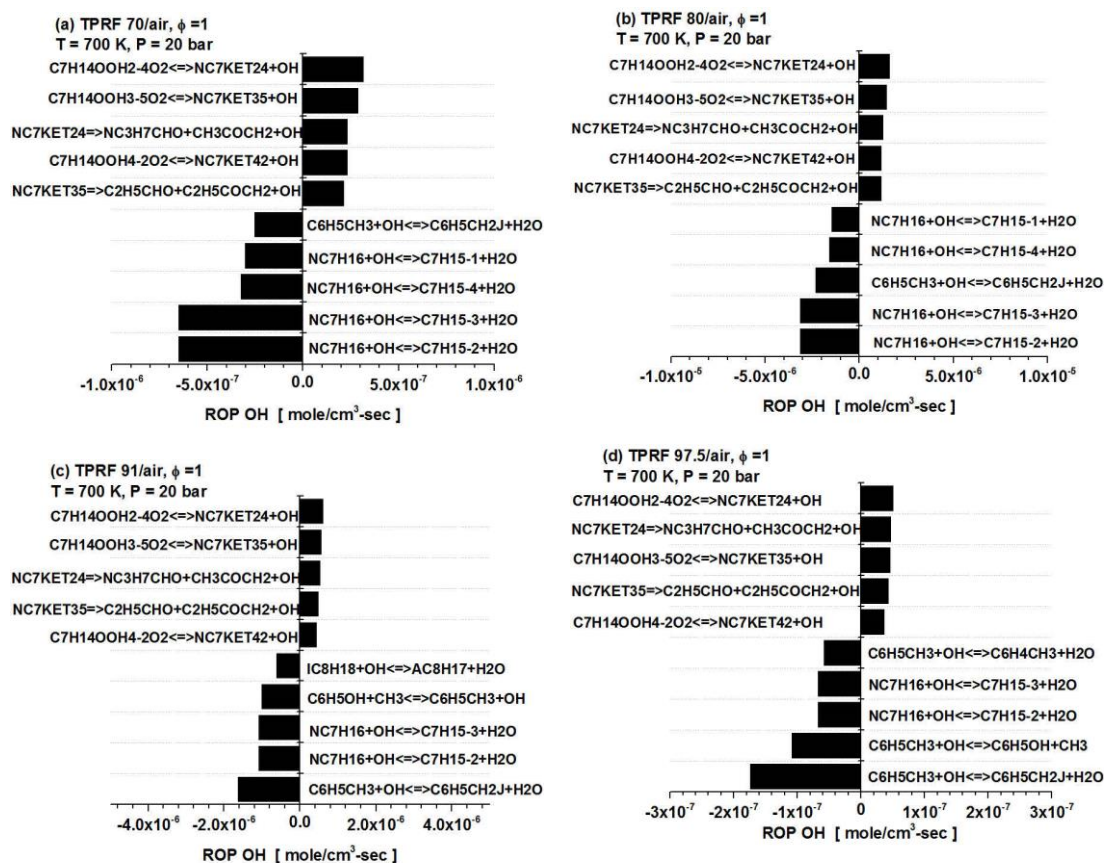


Figure 5-8: ROP analyses of $\dot{O}H$ radical at $T = 700 \text{ K}$, $p = 20 \text{ bar}$, $\phi = 1$; (a) TPRF 70/air, (b) TPRF 80/air, (c) TPRF 91/air, and (d) TPRF 97.5/air mixtures. LLNL mech [79] is used for ROP analyses. The ROP analyses are conducted at a time corresponding to two-thirds of the exponential growth of $\dot{O}H$ radical concentration.

At intermediate temperatures (750 – 850 K), $\dot{H}O_2$ radicals are primarily produced through ($\dot{R}O_2 \leftrightarrow \text{alkene} + \dot{H}O_2$) or ($R + O_2 \leftrightarrow \text{alkene} + \dot{H}O_2$) concerted elimination mechanisms [86]. Production of $\dot{H}O_2$ radicals, through either mechanism, renders the system unreactive and is the main cause of the NTC behavior. Once formed, $\dot{H}O_2$ radicals are mainly converted to H_2O_2 ($RH + \dot{H}O_2 \leftrightarrow R + H_2O_2$), and, therefore, the eventual chain branching of H_2O_2 to produce two $\dot{O}H$ radicals controls ignition in the NTC region. Figure 5-9 shows the $\dot{H}O_2$ ROP analyses for various TPRF fuels examined in this study. It

can be seen that $\dot{H}O_2$ radical production (positive ROP) is favored much more for the TPRF 70 mixture compared to the other mixtures, and as such it correlates well with the RON and sensitivity of the TPRF fuels (smaller the RON and sensitivity, larger the $\dot{H}O_2$ radical production). This is why both experimental data and simulations in the previous section showed enhanced NTC behavior for TPRF 70 mixtures compared to the other ternary blends. It can also be seen in Figure 5-9 that the production of $\dot{H}O_2$ radicals is much lower for TPRF 97.5 mixture compared to other fuels, and this is the primary reason for the near negligible NTC behavior for TPRF 97.5. Moreover, the figure also shows that the consumption of $\dot{H}O_2$ radicals (negative ROP) to produce H_2O_2 and its further decomposition to two $\dot{O}H$ radicals (not shown here) are much more favored for TPRF 70 mixtures compared to others. This is the primary reason for the increased reactivity (shorter ignition delay times) of TPRF 70 mixtures compared to other fuels in the NTC region.

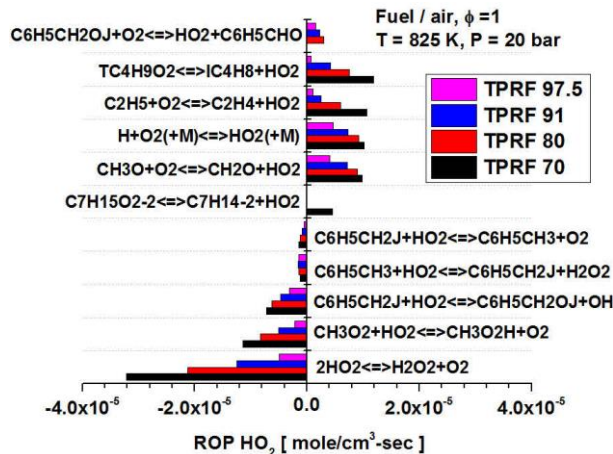


Figure 5-9: ROP analysis of $\dot{H}O_2$ radical at $T = 825$ K, $p = 20$ bar, $\phi = 1$ for TPRF 97.5/air (magenta bars), TPRF 91/air (blue bars), TPRF 80/air (red bars), and TPRF 70/air (black bars) mixtures. LLNL mech [79] is used for ROP analysis. The ROP analyses are conducted at the time corresponding to two-thirds of the exponential growth of $\dot{H}O_2$ radical concentration.

5.5 Comparisons with certified high octane gasolines

The TPRF surrogates, especially TPRF 91 and 97.5, were purposely put together to match the octane requirements of certified high octane gasolines. It can be seen from Figure 5-10 that the TPRF surrogates presented here can be used to study a wide range of certified gasolines with RON ranging from 70 – 97.5. More specifically, it can be seen from Figure 5-10 and Table 5-2 that the TPRF 91 and 97.5 surrogates matches the octane requirements of Haltermann and Coryton gasolines. It is also worth noting that both Haltermann and Coryton gasolines have some ethanol content present in them which is non-existent in TPRF surrogates by definition. Also, the octane ratings of non-oxygenate FACE gasolines F and G are in close proximity of TPRF 91 and 97.5 surrogates. Hence, a comparison of ignition delay times of these gasolines with the TPRF surrogates will be presented here. The ignition delay, octane ratings and compositions data presented in Figure 5-11 and Table 5-2 are taken from literature, for FACE F and G from [30] and that for Haltermann and Coryton gasolines from [118]. Low and NTC temperature regions, at 20 and 40 bar and stoichiometric conditions, are chosen for this comparison for consistency. The TPRF 91 and 97.5 (current work) data and Haltermann and Coryton data [118] are from NUIG RCM (which is quite similar in design and operation to KAUST RCM), and the FACE F and G data [30] are from UCONN RCM.

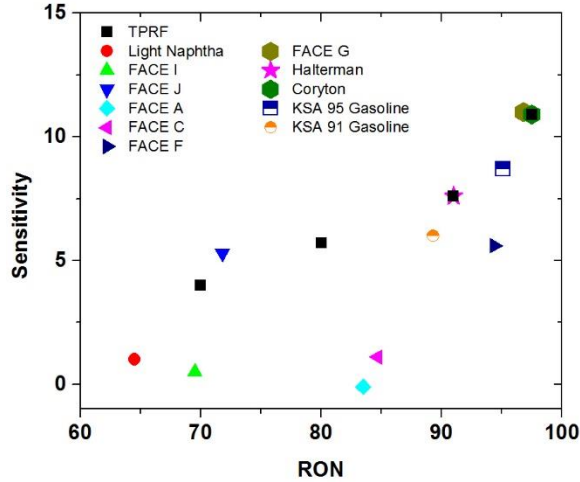


Figure 5-10: Comparison of RON and Sensitivity of TPRFs and commercial gasolines

Table 5-2: Comparison of TPRF surrogates with certified gasolines. Hydrocarbon classes are presented as mol %.

Fuel	RON	MON	S	n-Paraffins	i-Paraffins	Aromatics	Ethanol
Haltermann	91	83.4	7.6	12.2	26.1	22.9	16.8
FACE F	94.4	88.8	5.6	4.8	61	8.4	-
TPRF 91	91	83.4	7.6	17	29	54	-
Coryton	97.5	86.6	10.9	10.1	31.9	33.6	8.2
FACE G	96.8	85.8	11	7.9	38.3	31.8	-
TPRF 97.5	97.5	86.6	10.9	14.5	8	77.5	-

Figure 5-11 compares the ignition delay times of TPRF 91 and 97.5 with Haltermann and Coryton gasolines and with FACE gasoline F and G. Several interesting observations can be made from the figure. Firstly it can be seen that the ignition delay times of Haltermann and FACE F gasolines (RON 91 and 94.4 respectively) are replicated satisfactorily by TPRF 91 (RON 91). Next it can be seen that the ignition delay times of Coryton gasoline (RON 97.5) are matched well by those of TPRF 97.5 (RON 97.5) at high

temperatures and in the NTC region (especially at 20 bar Figure 5-11 (a)); flattening out of the NTC region due to high sensitivity ($S = 10.9$) of Coryton gasoline is particularly well emulated by TPRF 97.5. However, at low temperatures, TPRF 97.5 overpredicts the ignition delay times of Coryton gasoline. Ignition delay times of FACE G, in general, are overpredicted by TPRF 97.5 surrogate and are closely captured by TPRF 91 surrogate.

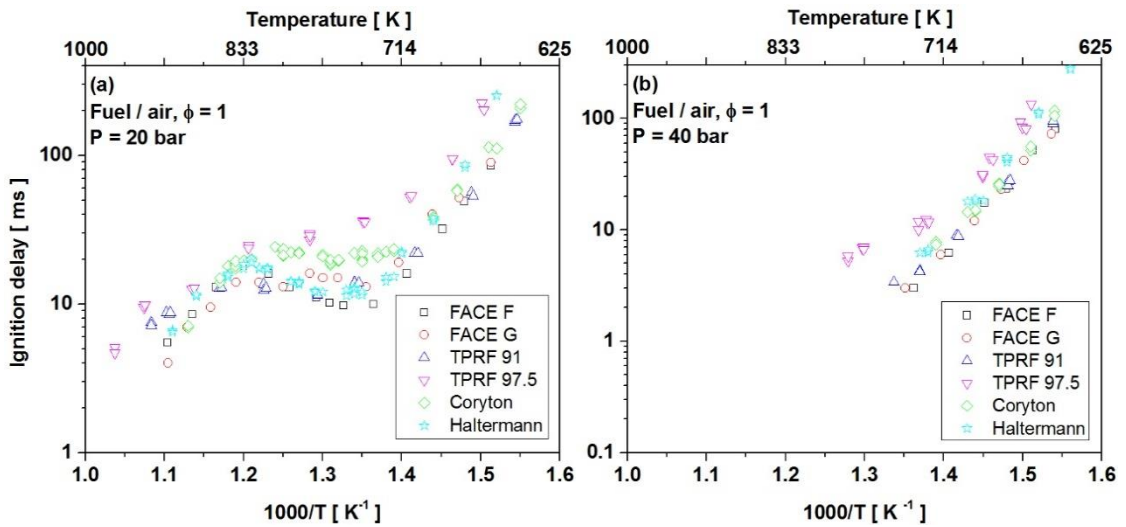


Figure 5-11: Comparison of ignition delay times of TPRF 91 and 97.5 with FACE F and G and Coryton and Haltermann gasolines at stoichiometric conditions and at (a) 20 bar and (b) 40 bar. Data for FACE F and G is taken from [30] and for Haltermann and Coryton gasolines from [118].

In this chapter, we have presented a wealth of ignition delay data for TPRF surrogates which can be used to model the reactivity of a wide range of commercial gasolines with modestly high sensitivities. It is shown that the TPRF fuels show a negligible octane dependence at high temperatures, a weak octane dependence at low temperatures and a strong octane dependence in the NTC region. At low temperatures, the octane dependence is more pronounced for the high-RON, high-sensitivity fuels and is attributed to the non-paraffinic (toluene) content. It is also shown that the TPRF surrogates can effectively match

the ignition requirements of modestly high sensitivity gasolines (Haltermann and FACE F with Sensitivities of 7.6 and 5.6 respectively). Although the TPRF surrogate captures many trends present in the ignition delay data of high sensitivity gasolines (Coryton and FACE G with Sensitivities of 10.9 and 11 respectively), the TPRF surrogate overpredicts the ignition requirements of highly sensitive ($S \sim 11$) gasolines in homogeneous shock tube/RCM environments.

Chapter 6: SHOCK TUBE IGNITION DELAY DATA AFFECTED BY LOCALIZED IGNITION PHENOMENA

In this chapter, non-idealities associated with low temperature long ignition delay times shock tube ignition data are presented. Specifically, pre-ignition of localized kernels in homogeneous shock tube core and associated flame propagation and bulk ignition advance are discussed in great details. Current study is first of its kind in specifying the ignition regimes in shock tube ignition research. The current work should pave way for more careful shock tube experimentation to avoid any non-idealities artificially expediting ignition kinetics in shock tube ignition measurements. Pre-ignition and its transition to “super-knock” is a very relevant research topic in engines research community; if properly developed, shock tube pre-ignition and associated bulk ignition advance can also help engines research community understand and control super-knock.

6.1 Introduction

Shock tubes are widely used for chemical kinetic measurements and detailed reaction mechanism development [119]. The incident and reflected shock waves instantaneously heat and compress the test gas, thereby decoupling the complex chemical kinetic phenomena from fluid dynamics and heat transfer and achieving near-uniform well-defined pressure and temperature conditions. As such, shock tube data are often reliably modeled with zero-dimensional homogeneous reactors and are considered ideal experimental devices for studying high-temperature combustion chemistry.

Advanced internal combustion (IC) engines, towards higher efficiencies and lower emissions, primarily operate at relatively low temperatures in compression-ignition modes.

In these engine concepts, fuel chemistry plays a critical role in controlling the onset of auto-ignition. Therefore, there is an increasing interest in understanding ignition and subsequent heat release characteristics at low and intermediate temperatures. Chemical kinetic studies at such conditions require long test times due to the exponential scaling of ignition delays with temperature. Conventionally, shock tubes achieved test times of about $O(1 \text{ ms})$ and were thus focused mainly on high-temperature ignition studies. As such, rapid compression machines (RCMs) have been frequently used at low temperature ignition conditions due their ability to provide longer test times up to, say, 100 ms, with their own inherent limitations. Recently, there have been efforts in extending available test times in shock tubes to overlap with RCM operating temperature range. One way to increase shock tube test times without altering the geometry is to tailor the driver gas, typically helium, with a heavier gas, such as nitrogen and carbon dioxide [44, 45].

When shock tubes are used to perform long test time experiments, some non-idealities can affect the measurements. An example is the gradual pressure increase behind the reflected shock wave, referred to as dP_5/dt . This pressure increase is accompanied with a simultaneous temperature increase and can thus expedite the homogeneous ignition event. These pressure and temperature changes can become significant for long test time ignition experiments. These effects can be accounted for by modeling the shock tube as a variable volume reactor. Heat transfer to the shock tube walls can be a concern at relatively long experimental times. However, Frazier et al. [120] showed that heat transfer effects can be ignored for large diameter shock tubes.

More recently, another non-ideality that has been reported as potentially important in affecting the ignition characteristics for low temperature shock tube measurements is

localized pre-ignition events. Hanson et al. [121] observed remote ignition for hydrogen-oxygen reactive mixtures and proposed the use of constrained-reaction-volume (CRV) strategy to eliminate remote ignition. Zhu et al. [122] applied the CRV strategy during the oxidation of 1-butanol to minimize pre-ignition energy release. Campbell et al. [123] measured ignition delay times of n-heptane/Ar mixtures over 651 – 823 K and pressures near 6 – 7 am using both conventional and CRV filling strategies. However, they only found minor differences between the two strategies. As for more convincing evidence of pre-ignition, Uygun et al. [116] observed pre-ignition pressure rises while measuring ignition delay times of 2-methylfuran and tetrahydrofuran. Using schlieren imaging, they further showed that the main ignition event was preceded by deflagrative flame kernels which, in some cases, initiated close to the shock tube end-wall.

Pre-ignition energy release in homogeneous ignition events have also been observed in RCMs. Mansfield et al. [124] reported the presence of localized ignition events through high-speed imaging, during syngas oxidation in their rapid compression facility. The phenomenon was named “weak-ignition” which was found to yield a significant advancement in ignition at low temperatures. Wang et al. [125] also investigated the pre-ignition leading to super-knock event in an RCM. They utilized an optical RCM to image the sequence of events starting from random pre-ignition spots to deflagration and eventually to detonation. Theoretical attempts were made by Im et al. [126, 127] and Grogan et al. [128] to formulate a regime diagram to predict ignition characteristics in terms of key non-dimensional parameters.

Recent studies [129-132] on autoignited lifted flames showed some discrepancies between the autoignited lifted flame heights and the calculated ignition delay times.

Experiments were conducted by ejecting fuel jet into high temperature air. For gaseous fuels [129, 130], the autoignited liftoff height correlated well with the square of calculated ignition delay times, in agreement with a theoretical derivation [129]. For pre-vaporized n-heptane and iso-octane fuels [131, 132], at atmospheric pressure and temperature range of 900 – 1000 K, the autoignited liftoff flame heights did not correlate successfully with the square of calculated ignition delays. These results pointed to either very slow reactivity in the n-heptane / iso-octane kinetic models or to some systematic shortening of ignition delays in the experiments.

Pre-ignition is also a highly relevant subject in internal combustion engine applications. Modern downsized and boosted engines have encountered premature auto-ignition, or much stronger and detrimental super-knock events [133, 134]. As such, fundamental understanding of pre-ignition phenomena has broader impact in a wide range of practical engineering applications.

The main hypothesis of the present study is that the discrepancies between the chemical kinetic mechanism predictions and the measured ignition delay times observed in the current low temperature/pressure shock tube experiments are attributed to the pre-ignition of nearly homogeneous reactant mixture under specific conditions, in analogy with the findings from the earlier shock tube and RCM studies [116, 124-128]. As a systematic validation process, experimental measurements of the ignition delay times for n-heptane and n-hexane mixtures over a wide range of temperatures and at low pressure conditions are presented. Next, it is shown that attempts to predict the observed ignition characteristics by considering various non-idealities (such as uncertainties in chemical kinetic rates and the bulk pressure rise effects) are not sufficient to reconcile the discrepancies.

Subsequently, simple computational fluid dynamic (CFD) simulations of model problems with post-shock conditions containing a hot spot, without simulating full shock boundary layer interaction and shock propagation, are presented. The effects of the pre-ignition on the overall ignition characteristics are discussed in detail.

6.2 Experimental Details

In this work, ignition delay times ranging from 200 μs to 32 ms are measured for n-heptane and n-hexane mixtures over 650 – 1250 K and pressures near 1.5 atm. A wide range of mixture compositions were investigated for n-heptane; these include 2% n-heptane / 44% O_2 / Ar ($\Phi = 0.5$), 2% n-heptane / 22% O_2 / Ar ($\Phi = 1$) and 1% n-heptane / 11% O_2 / Ar ($\Phi = 1$). Experiments for n-hexane were carried out using 5% n-hexane / 47.5% O_2 / Ar ($\Phi = 1$). All experiments were carried out in low pressure shock tube (LPST) facility at KAUST. For details regarding shock tube ignition measurements, please refer to Chapter 2.

6.3 Ignition Delay Times of n-Heptane and n-Hexane

Ignition delay times for n-heptane and n-hexane were measured over a temperature range of 650 – 1250 K and pressures near 1.5 atm. Figure 6-1 shows the results for 2% n-heptane / 44% O_2 / Ar ($\Phi = 0.5$) and 5% n-hexane / 47.5% O_2 / Ar ($\Phi = 1$) mixtures. Measured ignition delay times span from about 200 μs to 32 ms. Several observations can be made for the ignition delay results shown in Figure 6-1. Due to the higher fuel concentration of the n-hexane mixture, its ignition delay times are generally shorter than those of n-heptane in the fuel-dependent low-temperature chemistry region. The ignition delay times show expected Arrhenius behavior in the high (1050 – 1250 K) and low (650

– 750 K) temperature regimes. However, the negative temperature coefficient (NTC) behavior is hardly observed in the temperature range of 750 – 900 K. This contrasts the trends found in experiments and kinetic mechanisms reported in the literature [107, 135] which show strong NTC behavior for n-heptane.

The Chemkin-Pro package was utilized to simulate ignition delay times with constant internal energy and volume (constant UV) constraints. The chemical kinetic mechanism developed by Mehl et al. [79] was employed. Figure 6-1 shows that the model predictions and experimental data are in good agreement at high-temperatures (1050 – 1250 K), reasonable agreement can also be observed at low-temperatures (650 – 750 K). However, significant discrepancies between the model predictions and measurements are found in the intermediate-temperature range (750 – 1000 K), with the largest difference being more than an order of magnitude near 850 – 900 K. These are unexpected results as n-heptane and n-hexane kinetic models are believed to be extensively validated for ignition predictions across the entire temperature range, albeit at higher pressures. It was confirmed that the data reported in Figure 6-1 are repeatable and cannot be attributed to some random uncertainties in the measurements or the experimental set-up.

Since the large discrepancies are seen at lower temperatures (850 – 900 K), where fuel-specific reactions and RO_2 chemistry plays a critical role, additional ignition delay experiments were carried out with varying concentration of fuel and oxygen. The investigated mixtures include 2% n-heptane / 22% O_2 / Ar ($\Phi = 1$) and 1% n-heptane / 11% O_2 / Ar ($\Phi = 1$). Measured ignition delay times for these mixtures are plotted in Figure 6-2 along with the n-heptane data from Figure 6-1. As expected, the ignition delay times increases with decreasing oxygen (44% to 22%) or n-heptane (2% to 1%) concentration.

Corresponding ignition delay time predictions using Mehl et al. [79] kinetic mechanism show similar trends. However, all experimental data exhibit large deviations from the simulated ignition delay times in the temperature range of 750 – 1000 K.

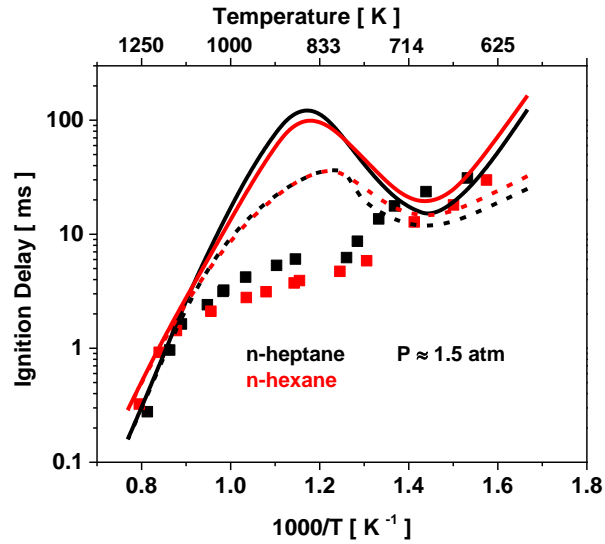


Figure 6-1: Comparison of measured ignition delay data (symbols) with predictions using the Mehl et al. [79] mechanism. Solid lines: constant volume simulations. Dashed lines: simulations with 3% dP_5/dt correction. Mixtures: 2% n-heptane / 44% O₂/Ar ($\Phi = 0.5$) and 5% n-hexane / 44% O₂/ Ar ($\Phi = 1$)

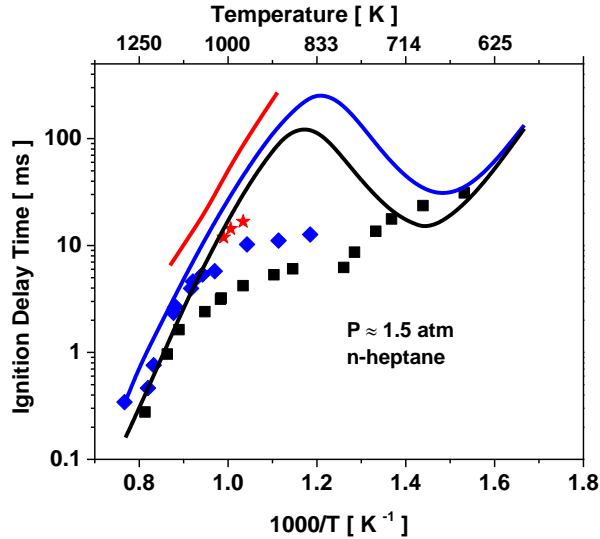


Figure 6-2: Ignition delay results for various n-heptane mixture compositions. Experimental: ■ 2 % n-heptane/44 % O₂/Ar ($\Phi=0.5$), ◆ 2 % n-heptane/22 % O₂/Ar ($\Phi=1$), ★ 1 % n-heptane/11 % O₂/Ar ($\Phi=1$). Lines: Constant UV simulations with Mehl et al. [79] mechanism.

The pressure behind the reflected shock wave gradually increases due to the interaction of the reflected shock wave with boundary layers [41]. This pressure increase, and accompanied temperature increase, can be neglected for high-temperature ignition experiments where ignition delay times are generally less than 2 – 3 ms. However, such pressure/temperature changes become significant when measuring relatively long ignition delay times. This effect is referred to as dP_5/dt and is facility-dependent with reported values in literature ranging 1 – 10 %/ms. Generally, shock tubes with smaller diameters have larger dP_5/dt . To account for this effect, the measured pressure variation over time is converted to volume variation using the isentropic relation and is included in the Chemkin-Pro simulations [39, 42, 43]. For the experiments reported here, dP_5/dt was found to vary between 1.5 to 3 %/ms. Assuming the worst case scenario, 3 %/ms dP_5/dt was imposed in the simulations, shown as the dashed lines in Figure 6-1. It is evident that, even with the pressure correction, the model calculations still substantially overpredict the measured

ignition delay times in the temperature range of 750 – 1000 K.

Since its inception in 2013, the low-pressure shock tube (LPST) facility at KAUST has been extensively validated, and the shock tube technique has been perfected in high-purity reaction rate determinations [136], species time-history measurements [137] and in ignition delay measurements [29, 43, 137], to say a few. As a further validation, additional ignition delay data for stoichiometric n-heptane/air mixtures at relatively high pressure of ~ 12 bar are presented. It can be seen from Figure 6-3 (a) show that the present 12 bar data are in excellent agreement with the recent 12 bar shock tube study of Sheen et al. [138]; reasonable agreement is also seen with the classic studies of Ciezki et al. [104] at 13.5 bar and Gauthier et al. [23] 20 bar shock tube data sets. The RCM data of Silke et al. [101] at 10 atm are also in reasonable agreement with the current validation study as well as with the literature shock tube studies. Note that the data from [23, 101, 104, 138] are normalized to 12 bar for easy comparisons with the present data. This analysis serves as further validation of the KAUST LPST facility and the shock tube ignition delay technique employed. Furthermore, the solid line in Figure 6-3 (a) represents the constant UV model predictions using Mehl et al. [79] mechanism. It can be seen that at these conditions, the mechanism captures the ignition delay data from various laboratories quite well.

Figure 6-3 (b) shows 4 bar rapid compression machine data from Minetti et al. [105], 12 bar normalized data of Figure 6-3 (a), and three additional data sets [23, 104, 138] normalized to 50 bar. It is observed that the mechanism adequately captures the ignition delay times of stoichiometric n-heptane/air mixtures over a wide range of pressures.

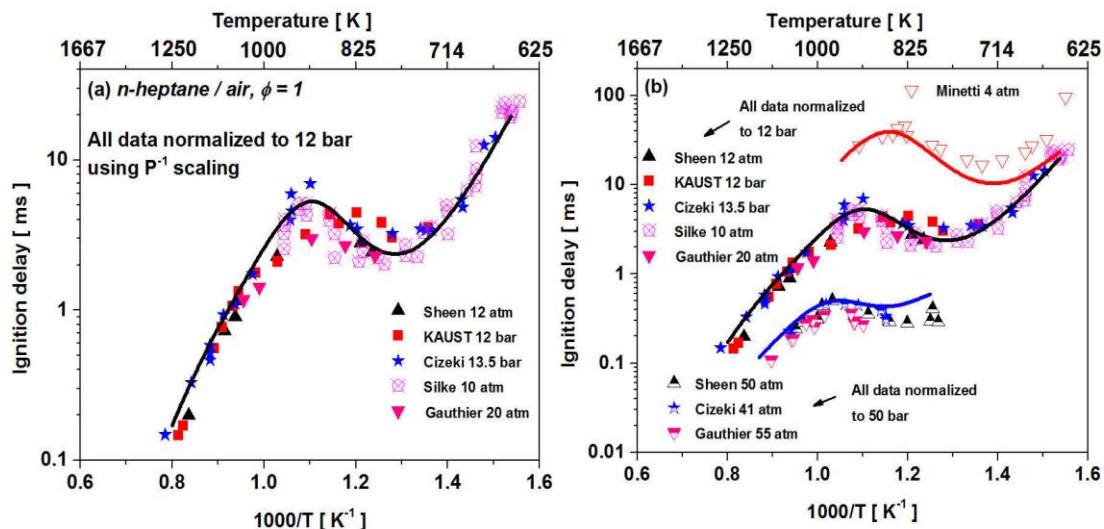


Figure 6-3: Ignition delay validation using stoichiometric n-heptane mixtures: (a) KAUST 12 bar (present study), Sheen et al. [138] 12 atm, Ciezki et al. [104] 13.5 bar, Silke et al. [101] 10 atm, and Gauthier et al. [23] 20 atm data normalized to 12 bar. (b) In addition to data plotted in (a), Minetti et al. [105] 4 atm, Shen et al. [138] 50 atm, Ciezki et al. [104] 41 atm, and Gauthier et al. [23] 55 atm data are plotted. Lines in (a) and (b) represent constant UV simulations at 4 (red line), 12 (black line) and 50 (blue line) bar using Mehl et al. [79] mechanism.

6.4 Chemical Kinetic Mechanisms of n-Alkanes

The observed discrepancies between experiments and simulations may suggest deficiencies in the chemical kinetic model employed in the present study at relatively low pressures ($P \sim 1 - 2$ bar).

To assess the possible uncertainties in the kinetic models, three additional reaction mechanisms were considered for comparison: the San Diego mechanism (University of California San Diego Mechanisms), Lawrence Livermore detailed n-heptane mechanism (LLNL NC7 detailed mech) [106], and reduced n-heptane mechanism from the Milano group (Ranzi NC7 reduced) [139]. Figure 6-4 shows the comparisons of the ignition delay

times using the four different mechanisms. While there are differences in the predictions, none of the established reaction mechanisms were able to improve the agreement with the experimental data in a significant way. It must also be noted that these mechanisms have also been validated with low-temperature oxidation experiments in jet-stirred reactors (JSR) and computational kinetic rate theory. Therefore, it is concluded that the ignition characteristics observed in the present experiment cannot be solely attributed to chemical kinetic models.

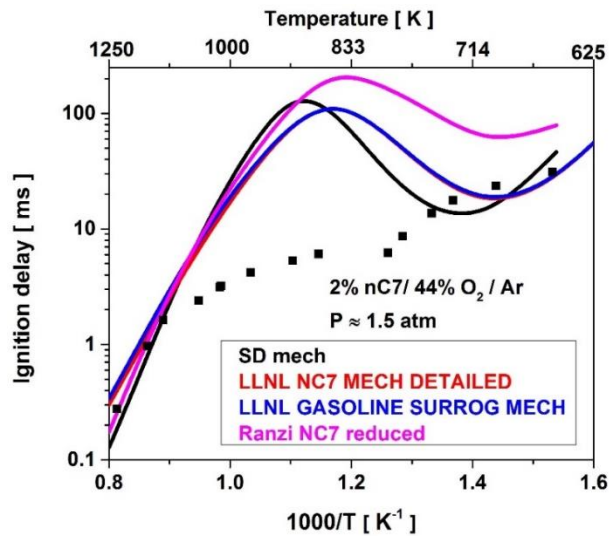


Figure 6-4: Ignition delay simulations using various mechanisms for 2 % n-heptane/44 % O₂/Ar ($\Phi = 0.5$).

The present experimental results are surprising in that no NTC behavior is observed, while previous studies reported that n-heptane displays strong NTC characteristics at lower pressures [106]. To investigate the effects of pressure on NTC behavior, Dagaut et al. [140] studied the oxidation of n-heptane/air mixtures in a JSR at pressure from 1 to 40 atm. By measuring the temperature-dependent concentration profiles for n-heptane, heptene isomers, and C₇ cyclic ether, it was shown that the NTC regime is

more prominent at low pressures. The attenuation in the NTC behavior with increasing pressure is attributed to the pressure-dependence of H_2O_2 decomposition to two OH radicals, which becomes faster at higher pressures and shifts the high-temperature oxidation regime to lower temperatures. Furthermore, at any given temperature, the stability of RO_2 radicals produced via $\text{R} + \text{O}_2$ is thermodynamically favored as pressure increases (Le Chatelier's principle); thus the subsequent production of QOOH radicals and low temperature reactivity intermediates (e.g., cyclic ethers, ketohydroperoxides) is shifted towards higher temperatures as pressure increases. Computational studies by Villano et al. [141, 142] with pressure-dependent and temperature-dependent rate constants from high-level theoretical calculations confirm that RO_2 radicals are produced in higher concentrations as pressure increases. They attributed the increasing rate of production of RO_2 radicals to both favorable thermodynamic and kinetic conditions at higher pressures. Therefore, the fact that the present experimental results hardly exhibit the NTC behavior further suggests that the main cause of the observed discrepancies is not due to chemical kinetics.

6.5 Pre-Ignition Heat Release

In the present work, four different types of pressure traces (energy release patterns) were observed. Pressure-time histories for n-heptane ignition are presented in Figure 6-5 a-c. Similar pressure traces were observed for n-hexane oxidation experiments and a representative n-hexane pressure trace at the lowest temperature of this study (635K) is shown in Figure 6-5 d.

First, at high temperatures (1100 – 1250 K), an exponential pressure rise (strong ignition) occurs due to the main homogeneous ignition event (Figure 6-5 a).

Next, at lower temperatures (850-1050 K), a gradual energy release/pressure increase is observed, which persists for about 1-2 ms, followed by the main energy release indicated by exponential rise in pressure signal (Figure 6-5 b). Such gradual energy release observed in Figure 6-5 b is consistent with the results by Uygun et al. [116], and is attributed to pre-ignition hot spots close to the shock tube end-wall. It is conjectured that the pre-ignition initiates subsequent flame/ignition front propagation, resulting in earlier pressure rise and ultimately a reduction in the overall ignition delay time. This phenomenon is particularly evident in 850 – 1000 K range where the discrepancies between the model and experimental data are largest.

At further lower temperatures (700 – 850 K), two-stage ignition (Figure 6-5 c) is observed as expected for n-heptane and n-hexane in this temperature range. It is seen that gradual pre-ignition energy release is followed by first stage energy release before the main ignition event. The second stage (main) energy release is very close to the first stage energy release. Therefore, it appears that the pre-ignition primarily affects in advancing the first stage ignition event in this specific case.

Finally, at the lowest temperatures in this study, again near-homogeneous energy release is observed (Figure 6-5 d). At these conditions, pre-ignition effects appeared to be weak. The effect is hardly noticeable and the overall ignition behavior appears to be typical of homogeneous auto-ignition.

Based on the experimental findings presented so far, it is postulated that a pre-ignition and subsequent front development can drastically advance the homogeneous (strong) ignition delay times. Since the bulk ignition advance is observed before the onset of NTC region, a localized hot-spot may be the cause of pre-ignition inside the reactive

volume, either in the interior part of the mixture or near the shock tube end-wall. It has been suggested that such hot spots may be caused by shock non-uniformities [143], interaction of reflected shock wave with contact surface and boundary layer or due to some dust or catalytic particles [144]. The occurrence of such non-ideal events was found to depend on the experimental conditions and specific reactive mixtures. The exact cause of these hot spots and localized flame kernels is an open question that needs to be explored in future studies. These non-idealities may have also arisen from weak reflected shock bifurcation (see section 2.1.3) effects. It should be pointed out that the reduced ignition delay times observed in the present work were found to be highly repeatable. The experimental lesson from the current work is that the shock tube measurements must be performed with caution especially when measuring long ignition delay times as the system, at these conditions, could be more likely to encounter hot spots and pre-ignition energy release. Another point to consider is that in the NTC region, a cold spot can also result in shorter ignition delay times [145].

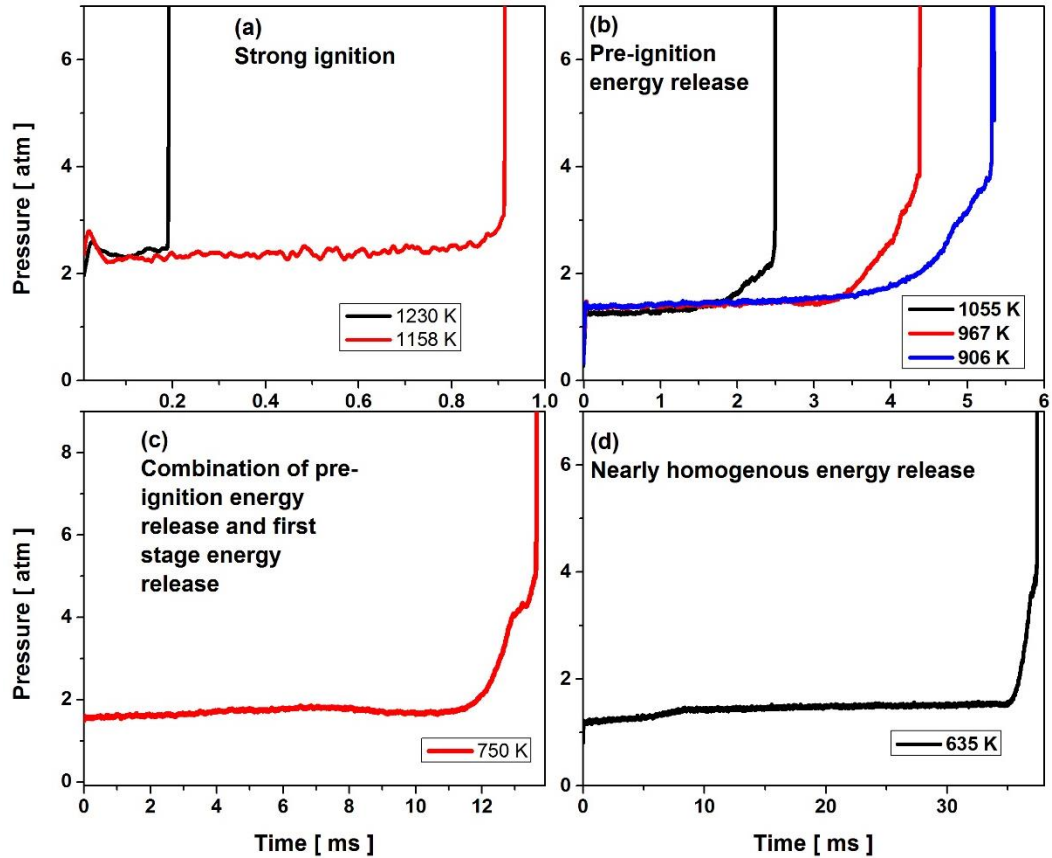


Figure 6-5: Various types of pressure profiles (energy release patterns) observed during shock tube ignition delay measurements: (a) strong ignition (b) pre-ignition energy release (c) combination of pre-ignition and two-stage behavior, and (d) near-homogeneous energy release. (a–c) are for 2% n-heptane/44% O₂/ Ar and (d) is for 5% n-hexane / 47.5% O₂/ Ar.

6.6 CFD Simulations of Pre-Ignition

6.6.1 Numerical Setup

In the preceding section, we have postulated that pre-ignition energy release and subsequent front development could drastically advance the homogeneous (strong) ignition delay times. To validate the hypothesis, simple CFD simulations were conducted for a

model configuration that represents pre-ignition induced by a hot spot within a closed volume. It must be noted here that the purpose of these CFD simulations is not to assess detailed shock propagation and shock / boundary layer interactions. Rather a commercial CFD package was used as a way to quickly simulate the phenomena of interest and to assess if the order of the experimentally observed ignition advancement may be replicated by simple hot-spot simulations. Thus the modeled problem is initiated at a time where reflected shock has already passed through the test section and thermodynamic conditions behind the reflected shock wave (T_5 , P_5) have been established.

CONVERGE software [146] was used as a simulation tool which can adequately capture the fluid dynamic and combustion behavior in a large domain size with a reasonable computational efficiency. RANS-based turbulent models were used throughout the simulations, and the SAGE detailed chemistry solver [147] along with multizone approach as a combustion sub-model was used. This approach maps the entire computational cells into a smaller number of bins in the temperature and equivalence ratio space to compute the reaction source terms. Here, a temperature bin size of 5 K and an equivalence ratio bin size of 0.05 were utilized. A reduced reaction mechanism for the primary reference fuel (PRF) developed by Andrae et al. [148] was used.

To represent the shock tube test section near the end wall, the computational configuration was set up as a cylinder of 5 cm in length and 2 cm in diameter for the results presented in the following sections. One of the primary advantages in using CONVERGE was its efficient grid management capabilities. Grid generation is done during run-time by utilizing both fixed embedding of cells and adaptive mesh refinement (AMR) based on key criteria. A 4 mm base mesh size was chosen, which was found to be sufficient to resolve

the nearly uniform mixture fields. When a pre-ignition energy source was imposed in the middle of the domain, a spherical fixed embedding of 4 levels and a diameter of 2 mm was implemented around the ignition source. This results in a minimum cell size of 0.25 mm within the sphere of interest. Furthermore, adaptive mesh refinement of 4 levels (0.25 mm minimum cell size) was utilized based on temperature gradient of 2.5 K, which allowed adaptive grid generation following the flame propagation. A snapshot of the grid in the domain is shown in Figure 6-6. Fully implicit time integration was employed with minimum and maximum time steps of 10 ns and 1 μ s, respectively.

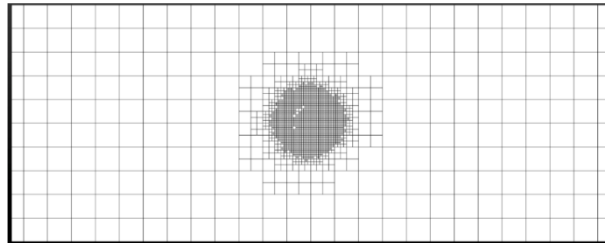


Figure 6-6: Two-dimensional (2D) cut-plane of the numerical domain showing the grid refinement in the area of interest.

A typical three-dimensional (3D) simulation of the given domain size took 12 CPU hours to solve for 10 ms on a 20-core workstation. While the domain size is smaller than the actual dimension of the shock tube test section, the choice was based on the computational consideration. To ensure that the results are not affected by the domain size, additional simulations using a 2D domain of 50 cm \times 14 cm and 1 m \times 14 cm were also conducted for the identical parametric conditions for several representative 2D cases. It was confirmed that the results, in terms of the ignition delay times and front propagation characteristics, remain reasonably similar.

Several parametric studies were conducted to ascertain the ignition sensitivity on the

magnitude, size and timing of the pre-ignition energy source. It is worth mentioning here that the purpose of this study is not to find the exact nature of pre-ignition energy source, but to demonstrate that a pre-ignition source can qualitatively results in comparable ignition advance as experimentally observed in this study. The aim of these CFD simulations is not to capture the full shock wave dynamics, shock wave boundary layer interaction and other non-idealities within the shock tube, but is to show the effect of pre-ignition energy release on homogeneous ignition delay times.

6.6.2 CFD Modeling Results

Figure 6-7 shows the comparison of the ignition delay times measured by the shock tube experiments and predicted by the CONVERGE simulations, for the conditions shown in Figure 6-4. To ensure that CONVERGE predicts consistent chemical kinetics behavior, the homogeneous ignition delay time calculations for the constant UV conditions were also reproduced by CONVERGE and the results were overlaid with the CHEMKIN-Pro data. For both simulations, the reduced chemistry model of Andrae et al. [148] is used. While the 3D pre-ignition simulations with the 5 cm domain size were considered the final results, results from additional 2D simulations at different domain lengths are also shown in order to ensure that the results are not sensitive to the domain size.

Figure 6-7 further shows a remarkable agreement between the CONVERGE pre-ignition results (dashed and dotted lines), with the pre-ignition energy set at 25 mJ and active during 2 – 6 ms and the experimental measurements throughout the entire temperature range. Note that in the high temperature range of ($T > 1050$ K) and in the low temperature range ($T < 700$ K), the hot-spot does not have a significant effect on ignition delay times compared to constant volume cases, while there is appreciable difference in

the temperature range of 750 – 1000 K. These respective behaviors will be elaborated later. The overall result clearly substantiate our hypothesis in that the pre-ignition event does advance the overall ignition delay times appreciably in the temperature range of 750 – 1000 K at the level nearly identical to the experimental observations. It can be seen that 2D ignition advance is slightly less than that of 3D, however the ignition advance in 2D is again fairly identical to experimental observations, and these minor differences does not alter the conclusions drawn in further discussion.

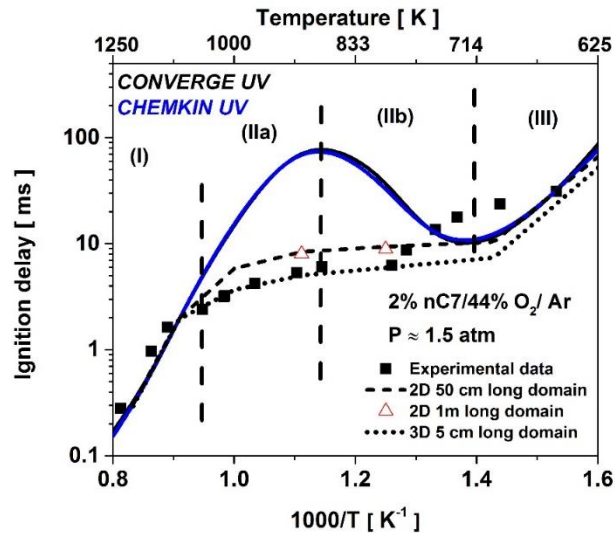


Figure 6-7: Comparison of the ignition delay times from experimental measurements (solid squares), constant-UV calculations using CHEMKIN (solid blue line), CONVERGE-UV calculations (solid black line), and CONVERGE pre-ignition simulations with 2D 50 cm domain length (dashed lines), 2D 1m domain length (open triangles) and 3D 5 cm domain length (dotted lines). The pre-ignition source is active from 2 – 6 ms with 25 mJ total energy. Reactive mixture is 2% n-heptane / 44% O₂ / Ar, and pressure at 1.5 atm.

The sensitivity on the magnitude of pre-ignition energy source is assessed by performing simulations for a range of energy source magnitudes (0.1 to 75 mJ). The result

in Figure 6-8 shows that for small values (< 5 mJ), the ignition delay predictions are close to the homogeneous simulations (dashed line) for $T < 900$ K. For higher energy source magnitudes (over 15 mJ), the ignition delay advancement reaches near asymptotic behavior. Therefore, a pre-ignition energy source of 25 mJ was selected to adequately represent the energy source in the remainder of this study. This value reproduces the ignition advance seen experimentally and is also close to the minimum ignition energy requirement [149, 150] for typical hydrocarbon fuels to ignite and sustain combustion. The 25 mJ energy source value also results in comparable local temperature gradients as those reported in [145, 151].

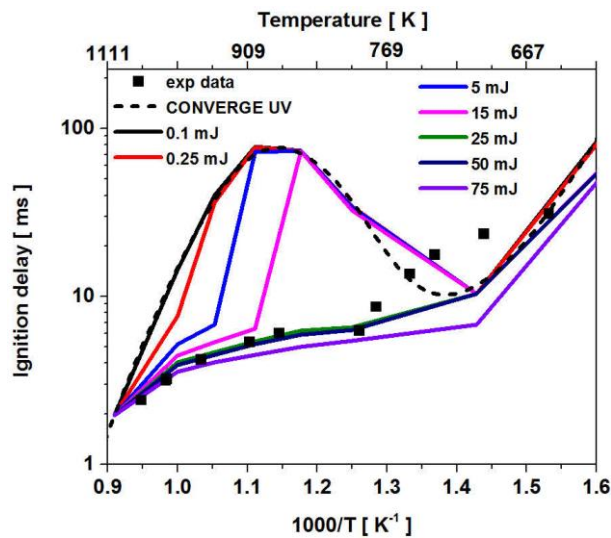


Figure 6-8: Parametric study on the magnitude of pre-ignition energy source. Reactive mixture is 2% n-heptane / 44% O_2 / Ar, and pressure at 1.5 atm.

As a further confirmation that the results are not affected by the initial time and duration of the ignition source, additional parametric tests were carried out with the 3D 5 cm domain size case. The diameter, location, start time, and duration of the energy source were varied. The details of the tested energy sources are listed in Table 6-1, and the results are shown in Figure 6-9. As in the other tests discussed above, the variations in the ignition

source location, timing and duration within the extent shown in Table 6-1 yielded minimal differences in the total ignition delay time predictions. A pre-ignition energy source active from 2-6 ms is used in subsequent simulations reported in this study.

Table 6-1: Details of the various pre-ignition energy sources used in the CFD simulations.

Diameter (mm)	Location in domain	Time duration of the energy source (ms)
2 mm	Left, Right and Center	1-3, 1-4, 2-4 and 2-6
1 mm	Left, Right and Center	1-3, 1-4, 2-4 and 2-6
0.5 mm	Left, Right and Center	1-3, 1-4, 2-4 and 2-6

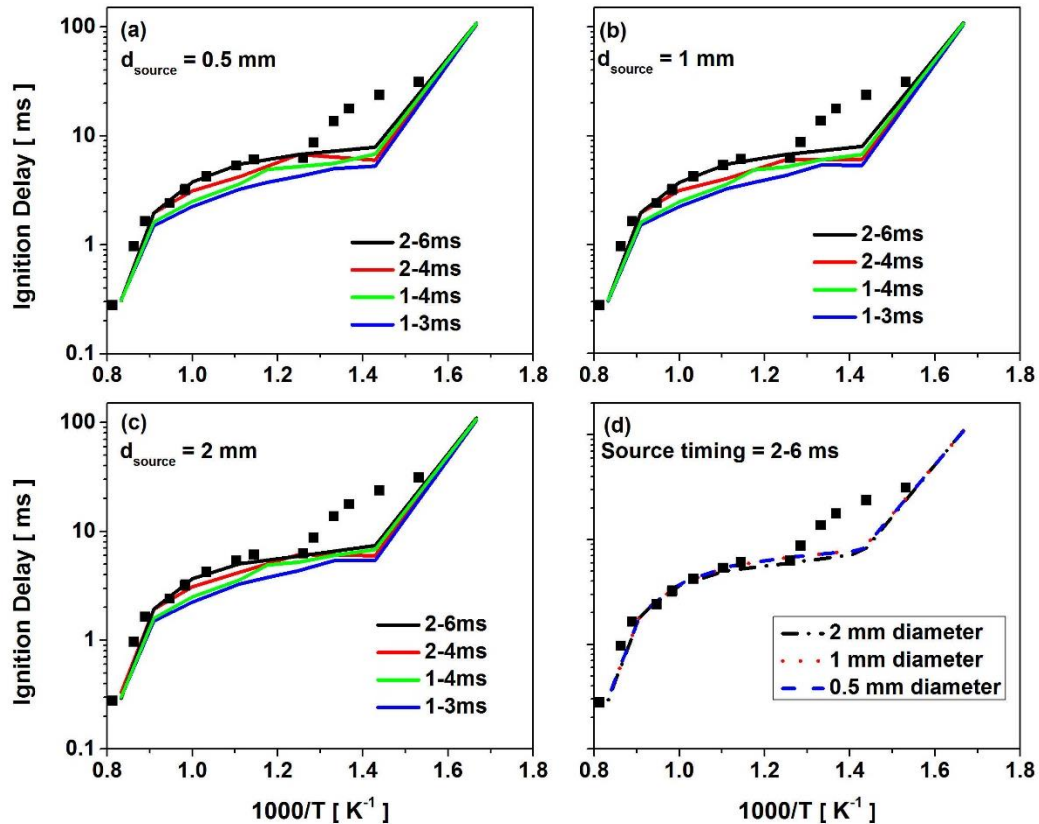


Figure 6-9: Parametric study on the pre-ignition source (a) source diameter 0.5 mm (b) source diameter 1 mm (c) source diameter 2 mm, and (d) comparison of various energy source diameters for 2 – 6 ms duration. For each source size, source initiation and duration times are parameterized. Square symbols represent measurements. Reactive mixture is 2% n-heptane / 44% O₂ / Ar. Pressure ~ 1.5 atm.

6.6.3 Ignition Regimes

To further investigate the detailed characteristics of pre-ignition affecting the overall ignition of the mixture, the ignition delay curve is divided based on three different temperature ranges, referred to as Regimes I-III, as indicated in Figure 6-7. Selected CFD simulation results are presented in order to reveal the key differences between various regimes.

First, to assess the level of ignition advancement for different regimes, three

temperature conditions (900, 800, 600 K) are selected and comparisons of the pressure-time histories with and without energy source are plotted in Figure 6-10. It is seen that the level of ignition advancement varies significantly depending on the initial temperature of the mixture. The observed behavior is consistent with the weak versus strong ignition regimes discussed by Im et al. [126]. Qualitatively, the 900 and 800 K cases correspond to the weak ignition regime in which the flame fronts generated by the pre-ignition source consumes a significant portion of the reactant mixture until the end gas auto-ignition completes the combustion. The effect of front propagation is manifested by a more gradual pressure rise compared to the homogeneous ignition results in each case.

The 600 K case corresponds to the *mixing-dominant* strong ignition regime [126], in which the overall reactivity of the bulk mixture is extremely low, such that the pre-ignition source fails to establish significant presence of flame propagation. As such the effect of pre-ignition on the net ignition behavior is small. For the n-heptane mixture under study, an additional new feature is the presence of the NTC behavior, as manifested by the two-stage ignition in Figure 6-10 (b), which further complicates the interaction between the front propagation and bulk-gas auto-ignition. Based on this understanding, the ignition characteristics for the n-heptane mixture are categorized into the following sub-regimes. The ignition regime diagram shown in Ref. [126] may be used as a reference.

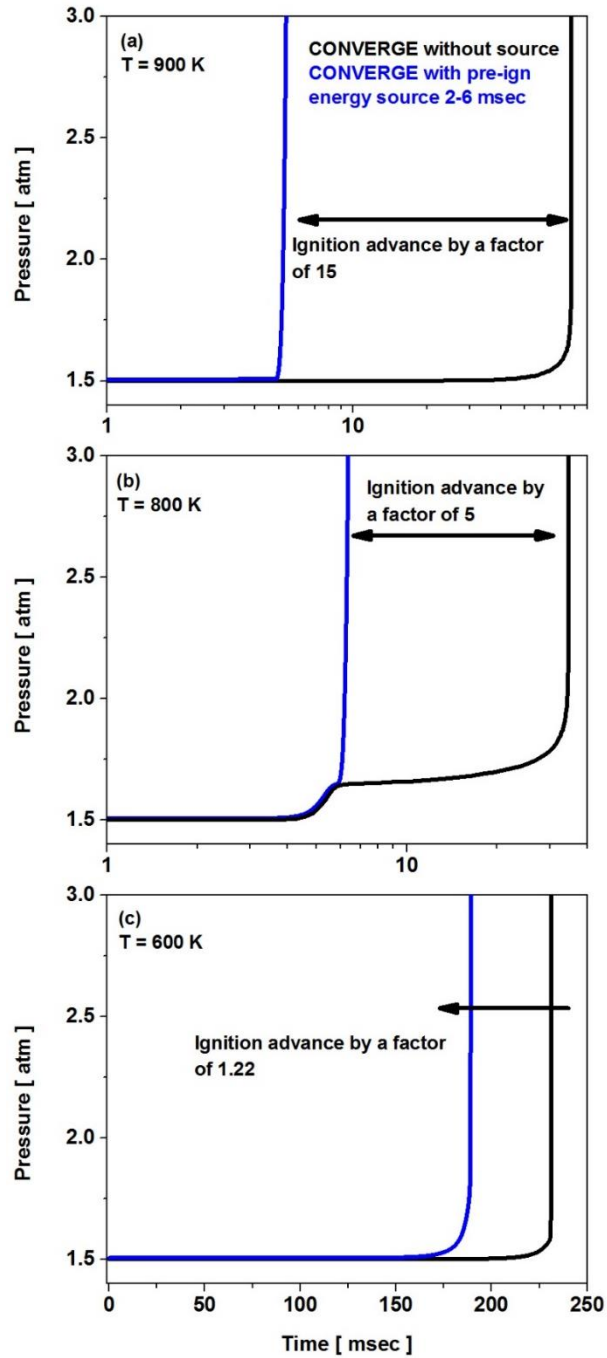


Figure 6-10: Simulated pressure-time histories at initial temperatures of (a) 900 K, (b) 800 K and (c) 600 K. Black lines: homogeneous ignition results. Blue lines: 3D pre-ignition simulation results. Mixture: 2% n-heptane/44% O₂/ Ar. P = 1.5 atm. Simulations performed using 3D 5 cm domain length.

Regime I (Reaction-dominant strong ignition):

At high temperature conditions (1100 – 1250 K), the mixture is highly reactive such that the bulk mixture auto-ignites rapidly and simultaneously regardless of the presence of the pre-ignition event. This corresponds to the *reaction-dominant* strong ignition regime [126] in which the effect of the pre-ignition is minimal, such that the net ignition delay times are hardly changed from those of homogeneous mixtures, as shown in Figure 6-7.

Regime II (Weak/mixed ignition):

This regime spans the temperature range of 700 – 1050 K. As seen from Figure 6-7 and Figure 6-10 (a) and (b), the pre-ignition advances the net ignition delay times by several factors and up to orders of magnitude. This is referred to as weak/mixed ignition regime, in which the pre-ignition induces subsequent front propagation for a significant fraction of mixture burn duration until some remaining portion of the end gas completes combustion by auto-ignition. For the n-heptane mixture, this regime is further divided into Regime IIa (positive temperature coefficient) and Regime IIb (NTC).

To further examine how the front propagation affects the pressure rise and combustion behavior, Figure 6-11 shows the temporal evolution of the maximum temperature and mean pressure inside the domain for initial temperatures of 900 K (Regime IIa) and 800 K (Regime IIb) based on the 3D simulations. The pre-ignition source was activated during 2 – 6 ms. For both cases, the rapid temperature rise indicates the front initiation and propagation, which leads to a relatively gradual pressure rise (in comparison with the homogeneous counterpart) and advanced net auto-ignition behavior. The end-gas auto-ignition is noticeable from the secondary temperature peak. The main difference between the two cases is that the front initiation for Regime IIb (800 K) occurs *after* the

bulk mixture exhibits the first stage ignition. In comparison to Regime IIa, in which the mixture reactivity increases monotonically with temperature, in Regime IIb the bulk mixture after the first stage ignition falls into the NTC condition, thus attenuating the relative enhancement in the bulk gas reactivity. This qualitatively explains why the level of ignition advancement in Regime IIa (900 K) is higher than that in Regime IIb (800 K) as shown in Figure 6-10.

For both cases in Figure 6-11 (a) and (b), the secondary rapid pressure rise after the front propagation stage is not clearly seen. This is attributed to the limited domain size, leaving only a small portion of end gas at the time of secondary homogeneous auto-ignition. This issue will be elaborated later with a larger domain size 2D simulations.

To assess the characteristic of the front, the propagation speed of the induced front was monitored and compared with the laminar flame speed at the same conditions calculated using CHEMKIN-Pro. The calculated front speed from the CONVERGE simulation is the speed with respect to the burned gas, S_b , which is subsequently converted to the front speed relative to the upstream mixture, S_u , by multiplying the density ratio as $S_u = S_b (\rho_b/\rho_u)$, where ρ_u and ρ_b are the densities of the unburned and burned mixture, respectively. Stretch effects [152] on this spherically propagating front were monitored and found to be minimal. Figure 6-12 shows the comparison of the two speeds as a function of the mixture temperature. The y-axis is plotted in logarithmic scale due to the large differences in the magnitude. It is evident that the propagation speed of the front in the CFD simulations is nearly an order of magnitude larger than the corresponding laminar flame speed. This suggests that the front induced by the pre-ignition source has the characteristics of the spontaneous ignition front rather than deflagration.

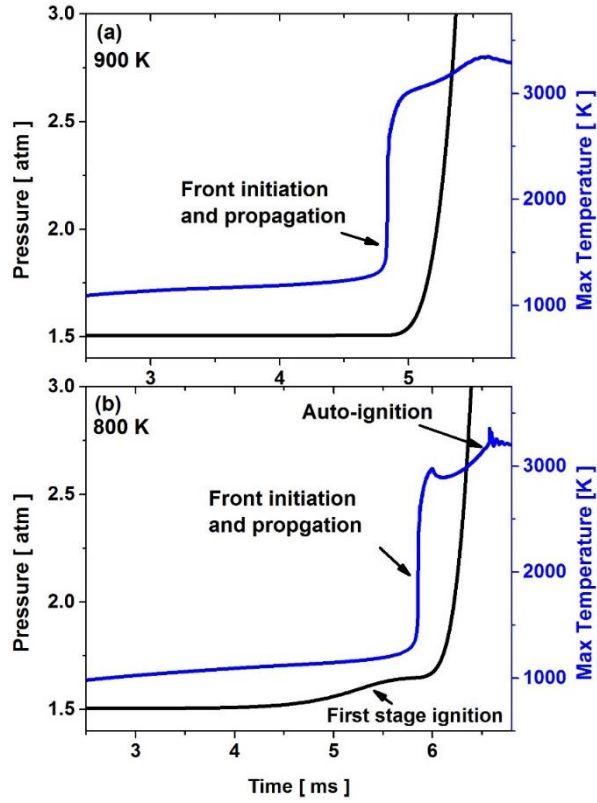


Figure 6-11: Simulated pressure and maximum temperature profiles at initial temperatures of (a) 900 K and (b) 800 K. Pre-ignition source (2 mm size and 2 – 6 ms timing). Mixture: 2% n-heptane / 44% O₂ / Ar. P = 1.5 atm. Simulations performed using 3D 5 cm domain length.

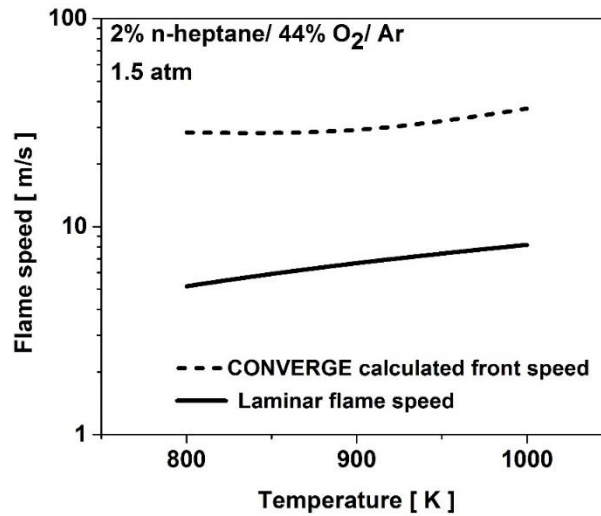


Figure 6-12: Flame speed calculated in CHEMKIN-Pro (solid line) and the front speed calculated from the CONVERGE [146] CFD simulations (dashed line).

As an attempt to reproduce the pressure rise behavior observed in the experimental measurements, simulations with a larger domain size were also conducted. Due to the excessive computational cost, however, 2D simulation results with a domain size of 50 cm x 14 cm are presented, for the 900 and 800 K conditions. Figure 6-13 shows similar qualitative behavior as in Figure 6-11; however, due to the larger mixture volume the pressure rise is seen to be more gradual during the front propagation, and the secondary auto-ignition event is more clearly observed by the sharp temperature and pressure rise toward the end of the combustion. Overall, the pressure behavior is found to be consistent with the experimental data in this study as well as the previous work by Uygun et al. [8], thus demonstrating that the validity of the pre-ignition hypothesis.

Regime III (Mixing-dominant strong ignition):

As the mixture temperature becomes lower, the overall mixture reactivity is reduced and the reference homogeneous ignition delay time becomes much longer than the characteristic time scale of the pre-ignition event. As such, the effect of pre-ignition augmenting the mixture reactivity is minimal; any initial ignition front generated by the pre-ignition source fails to sustain the front propagation and becomes dissipated by the conductive heat loss to the cold bulk mixture. Figure 6-14 shows the comparison of the pressure and maximum temperature evolution for Regime III (600 K), showing no sign of pre-ignition or gradual pressure rise. Consequently, the overall ignition delay time is found to be nearly identical to that of the homogeneous ignition calculation.

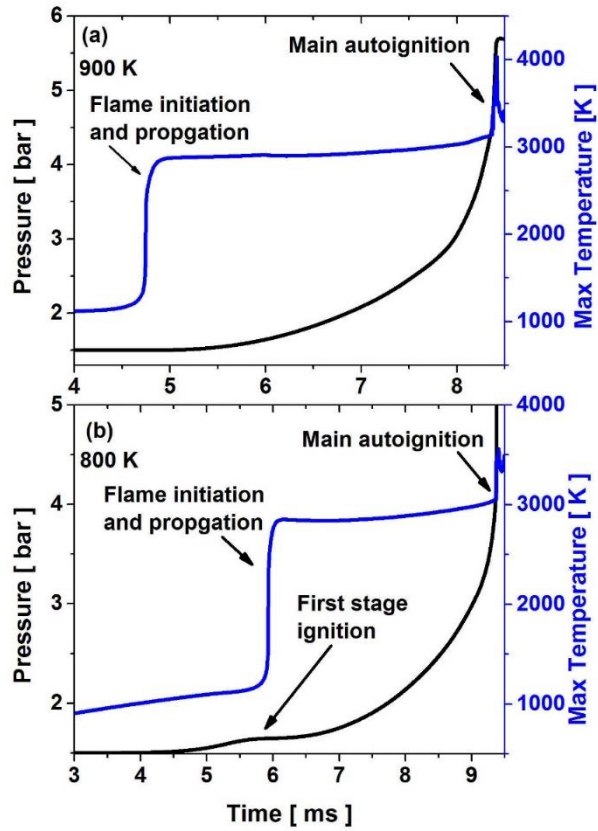


Figure 6-13: Simulated pressure and maximum temperature profiles at initial temperatures of (a) 900 K and (b) 800 K. Pre-ignition source (2 mm size and 2 – 6 ms timing). Mixture: 2% n-heptane / 44% O₂ /

Ar. P = 1.5 atm. Simulations performed using 2D 50 cm domain length.

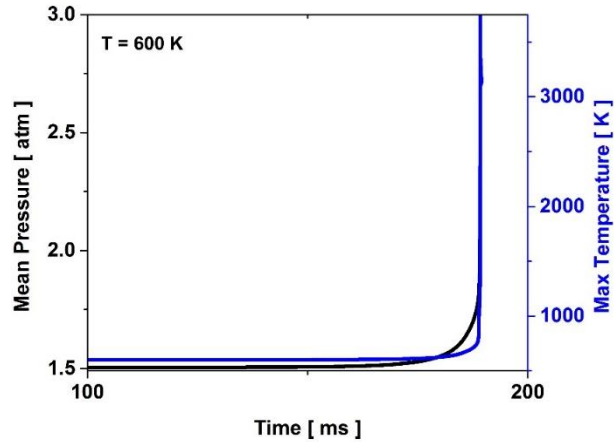


Figure 6-14: Simulated pressure and maximum temperature profiles at initial temperature of 600 K. Pre-ignition source (2 mm size and 2 – 6 ms timing). Mixture: 2% n-heptane / 44% O₂ / Ar. P = 1.5 atm. Simulations performed using 3D 5 cm domain length.

In this chapter, the non-idealities associated with low temperature long ignition delay times shock tube data are discussed in detail. The pre-ignition effected data was divided into various ignition regimes using experimental observations and CFD modeling. From a practical standpoint, the results suggest that shock tube measurements of long ignition delay times must be interpreted with caution, considering various non-idealities such as pre-ignition heat release. The present study further demonstrates the relevance and universality, albeit through different triggering mechanisms, of the pre-ignition phenomena in a variety of fundamental research techniques, for both RCM and shock tubes, as well as practical combustion applications, such as IC engines and gas turbines. Further investigations are needed for improved fundamental understanding of pre-ignition characteristics in order to predict and prevent its adverse impact.

Chapter 7: SUMMARY AND FUTURE WORK

7.1 Summary of results

7.1.1 Ignition studies of Low Octane Gasolines and Surrogates

Ignition delay times for light naphtha, a low-octane (RON = 64.5) highly paraffinic lightweight fuel, were measured in a shock tube and a rapid compression machine. Using a detailed hydrocarbon analysis of light naphtha, a five-component surrogate was formulated to reproduce the ignition delay times of the real fuel over a wide range of conditions. A simpler two-component PRF surrogate adequately reproduced the ignition behavior of light naphtha at high temperatures and in the NTC region. At low-temperature conditions, the multi-component surrogate matched the ignition delay times of light naphtha much more closely than the PRF surrogate. Kinetic analyses indicate that the higher reactivity of the PRF surrogate, compared to the real fuel and the multi-component surrogate, is attributable to its larger proportion of longer chain hydrocarbons. It can therefore be concluded that, for a highly paraffinic lightweight fuel such as light naphtha, the PRF surrogate adequately captures the ignition characteristics at high and intermediate temperatures, while a multi-component surrogate is needed to capture the reactivity of the real fuel at low temperatures.

Additionally, ignition delay times of two low octane (AKI ~ 70) full boiling range gasolines, FACE I and J, were measured using shock tube and rapid compression machine over a broad range of test conditions. It is shown that the two gasolines, with large differences in compositions but similar octane ratings, exhibit similar reactivity (ignition delay times) over the entire range of test conditions. It is further shown that a PRF

surrogate, matching the AKI of these gasolines, could be used to satisfactorily capture the ignition delay times of these gasolines. Using multi-component surrogates developed for these gasolines, it is explained that these gasolines show no differences in reactivity at low temperatures, albeit large differences in compositions, because the ignition controlling reactions are quite similar for these gasolines. This assertion is generalized using a wide range of low temperature ignition delay data from previous studies and it is shown that octane number and compositions differences are only manifested on ignition delay differences at low temperatures if the sensitivity of the fuel is high ($S > 7$). The results of this study could be used to further validate and refine the gasoline surrogate mechanisms and surrogate formulation strategies.

7.1.2 Speciation and Ignition studies of Mid Octane Gasolines and Surrogates

Oxidation characteristics of two highly paraffinic ($S \sim 0$) gasoline fuels (FACE A and C), with similar octane rating (AKI ~ 84), were measured and compared with the measured oxidation characteristics of a PRF surrogate. The PRF surrogate successfully captured the overall global reactivity of the fuel primarily due to paraffinic nature of the gasolines studied here. Multi-species time histories (CO, H₂O, OH and CO₂) measurements revealed similar trends for all three fuels. The need for refining propene/iso-butene oxidation chemistry is pointed out. Moreover, a wide range of literature ignition delay data is used to demonstrate similar reactivity trends at practical conditions. It is concluded that, for these mid octane highly paraffinic gasolines, a PRF surrogate satisfactorily matched the ignition requirements at a wide range of test conditions.

7.1.3 Ignition studies of High Octane Gasolines and Surrogates

Ignition delay times of a wider range of toluene/iso-octane/n-heptane mixtures

(TPRFs) have been measured using shock tube and rapid compression machine. The LLNL mech [79] was used to simulate and interpret these data. It is shown that the mechanism predictions are in good agreement with the shock tube data but improvements are necessary to better simulate the low-temperature RCM data. Refinements in the mechanism are particularly required to simulate the high toluene content fuels. It is shown that the TPRF fuels show a negligible octane dependence at high temperatures, a weak octane dependence at low temperatures and a strong octane dependence in the NTC region. At low temperatures, the octane dependence is more pronounced for the high-RON, high-sensitivity fuels and is attributed to the non-paraffinic (toluene) content. In the NTC region, the fuels with low RON and low sensitivity produce larger concentrations of HO_2 and H_2O_2 , and hence show the most prominent NTC behavior and ignition advancement compared to the high-RON, high-sensitivity fuels.

It is also shown that the TPRF surrogates can effectively match the ignition requirements of modestly high sensitivity gasolines (Haltermann and FACE F with Sensitivities of 7.6 and 5.6 respectively). Although the TPRF surrogate captures many trends present in the ignition delay data of high sensitivity gasolines (Coryton and FACE G with Sensitivities of 10.9 and 11 respectively), the TPRF surrogate overpredict the ignition requirements of highly sensitive ($S \sim 11$) gasolines in homogeneous shock tube/RCM environments.

7.1.4 Shock tube ignition delay data affected by localized ignition phenomena

This work, on the effect of pre-ignition on ignition delay times, was initiated by the recent KAUST shock tube measurements of n-heptane and n-hexane ignition delay times at low-pressure and low-temperature conditions showing large discrepancies against the

predictions by the latest chemical kinetic models. Experimental pressure-time histories indicated gradual pressure rise prior to the bulk auto-ignition, consistent with a recent findings by the Aachen group shock tube study [116]. This led to a hypothesis that the discrepancies are attributed to a pre-ignition event within the shock tube test section. To substantiate the hypothesis, simple CFD simulations of a model configuration of post-shock conditions were performed representing pre-ignition within a shock tube induced by a local energy source. Using the same chemical kinetic mechanism employed in the homogeneous model calculations, the CFD pre-ignition model predicted the observed ignition delay times with surprisingly good agreement, demonstrating that pre-ignition can indeed lead to the comparable level of ignition advancement observed by the shock tube measurements. From a practical standpoint, the results suggest that shock tube measurements of long ignition delay times must be interpreted with caution, considering various non-idealities such as pre-ignition heat release. The exact causes of pre-ignition in shock tubes and how to prevent its occurrence will be a subject of future studies.

It was found that the relative degree of ignition advancement by pre-ignition varies depending on the mixture temperature, in a manner consistent with the ignition regimes discussed in earlier studies [126-128, 153]. Over the range of temperatures under consideration, all three regimes identified in Ref. [126] were observed: the reaction-dominant strong ignition, weak/mixed ignition, and mixing-dominant strong ignition regimes. An additional new aspect of the present study is the presence of the NTC regime associated with complex hydrocarbon fuels. For the conditions considered in this study, the NTC conditions of the n-heptane mixture fell into the weak/mixed ignition regime, where the level of ignition advancement was attenuated due to the negative reaction

sensitivity to temperature for the mixture ahead of the propagating front.

The present study further demonstrates the relevance and universality, albeit through different triggering mechanisms, of the pre-ignition phenomena in a variety of fundamental research techniques, for both RCM and shock tubes, as well as practical combustion applications, such as IC engines and gas turbines. Further investigations are needed for improved fundamental understanding of pre-ignition characteristics in order to predict and prevent its adverse impact.

7.2 Future work

7.2.1 Surrogate complexity guidelines for homogeneous environments

At KAUST, we have significantly contributed to improving the combustion kinetics understanding of gasolines and surrogates. This was done by studying a wide range of gasolines and surrogates, of varying compositions and octane ratings, in shock tube and rapid compression machines (homogeneous environments). A major portion of our efforts towards understanding the combustion chemistry of gasolines and surrogates is presented in the current work. Using the data presented in this work, and other associated work undertaken at KAUST and at our collaborators facilities, Sarathy et al. have developed the FACE Gasoline mechanism [30], which is the most updated gasoline surrogate mechanism since the last one developed at LLNL by Mehl et al. [79]. Although some improvements are still required for improving the mechanism predictions, this mechanism includes the chemical kinetics representation of all the gasoline surrogate palette species. Also at KAUST, Ahmed et al. [77] have developed an elegant methodology to carefully design multi-component surrogates for gasolines, and other practical fuels, using a wide range of practical optimization targets and constraints.

In this work, we have presented a wealth of homogenous ignition delay times for gasolines and have formulated the surrogate complexity requirements for these gasolines. We have shown that for low sensitivity gasolines (light naphtha, FACE A, C, I and J), a PRF surrogate matching the AKI of the gasoline adequately reproduces the ignition requirements, with some discrepancies at low temperatures (especially for lightweight fuels such as light naphtha). We have also shown that TPRF surrogates not only matches the octane sensitivity requirements of high octane gasolines, but also captures, both qualitatively and quantitatively, the ignition delay times of modestly high octane gasolines (Haltermann and FACE F with Sensitivities of 7.6 and 5.6 respectively). We have also shown that, although a TPRF surrogate captures qualitatively various trends found in high sensitivity gasolines (Coryton and FACE G with Sensitivities of 10.9 and 11 respectively), the TPRF surrogate overpredict the ignition requirements of highly sensitive ($S \sim 11$) gasolines in homogeneous shock tube/ RCM environments.

What remains to be done is to summarize the findings of this work and those found in literature as a set of comprehensive guidelines for surrogate complexity requirements in homogeneous environments. We have already started putting together such guidelines, and will shortly publish them. Experimental ignition delay times of gasolines and surrogates, as well as ignition delay and HCCI (homogenous environment) simulations, are being used to come up with surrogate complexity requirements in homogenous environments.

7.2.2 Surrogate complexity requirements for various engine modes

There are various surrogate fuel formulation methodologies available in the literature proposing surrogates of increasing complexities (PRF, TPRF and multi-component) which emulate different target properties. This study aims to investigate the degree of complexity

required to describe surrogate fuels for various combustion modes of an internal combustion engine. FACE gasoline fuels are selected for appropriate engine modes based on their RON, MON and sensitivity. The surrogate formulation methodology would take into account relevant target properties for respective combustion setting.

The objectives of this proposed study are:

- (i) Evaluating surrogate formulation methodologies for various distillate fuels based on low, mid and high sensitivities and AKIs.
- (ii) Assess the fuels and corresponding surrogates in a wide range of fundamental and applied experiments, with the ultimate objective of a surrogate formulation methodology for different fuel types and engine combustion modes.
- (iii) Propose practical guidelines for surrogate complexity required to capture particular engine mode/performance target.

The gasoline fuels we propose to study are listed in Table 7-1. It can be seen that the selected fuels cover a wide range of RON, MON and sensitivity space. PRF, TPRF and multi-component surrogates will be utilized for each gasoline fuel listed in the table.

Table 7-1: Test fuels for evaluating surrogate complexity requirements for various engine modes

	FACE I	FACE C	FACE F	FACE G
RON	70.3	84.7	94.4	96.8
MON	69.6	83.6	88.8	85.8
Sensitivity	0.7	1.1	5.6	11
AKI	69.95	84.1	91.6	91.3

Engine experiments will be conducted to see how different gasolines and their

surrogates of varying complexity (bi, tri and multi-component) fare against the gasolines under particular engine operating strategy. We propose here to study different engine operating strategies based on octane ratings of selected FACE fuels. For example, low octane fuels are likely to be utilized in GCI mode[154]; whereas, high octane high sensitivity fuels are typically utilized for DISI operation [155]. Table 7-2 presents the test plan for various fuels/surrogates evaluation in different engine operating modes.

Table 7-2: Various fuels/surrogates evaluation in different engine operating modes

Engine operation		Engine operation		Engine operation	
GCI		HCCI		DISI	
FACE I and surrogates		FACE C, F and surrogates		FACE G and surrogates	
Parameters	Measurements	Parameters	Measurement	Parameters	Measurement
Injection Timing (Varied)	Emissions	Injection timing (port)(Fixed)	Emissions	Injection Timing(Fixed)	Emissions
Injection pressure (Fixed)	Soot	Inlet air temp(Varied)	Soot	Injection pressure(Fixed)	Soot
Inlet air temp (Fixed)	In-cylinder pressure	Inlet air pressure(Varied)	In-cylinder pressure	Spark timing (Varied)	In-cylinder pressure
Inlet air pressure (Fixed)					KLSA

7.2.3 Understanding the mechanisms of pre-ignition initiated super-knock using shock tubes and rapid compression machines

In Chapter 6 we have shown that, under certain conditions, shock tube ignition data is severely affected by the pre-ignition flame kernel initiation and propagation resulting in bulk ignition advance. Pre-ignition energy release in homogeneous settings have also been observed in rapid compression machines [124] [125]. Modern downsized and boosted engines encounter premature auto-ignition, or a much stronger and detrimental super-knock events, these events are the result of pre-ignition [133, 134]. As such, fundamental understanding of pre-ignition phenomena has broader impact in a wide range of practical engineering applications.

Here we propose to use shock tubes and rapid compression machines for understanding fundamentally the mechanisms leading to pre-ignition flame kernel

initiation and propagation and its transformation into a strong pressure wave which can be detrimental to engines integrity. For engines pre-ignition initiated super-knock results in much higher in-cylinder pressure rise and oscillations compared to normal (and regular knock) cycles and such energy release (pressure rise) also occur relatively early in the crank angle domain compared to normal cycles. For shock tubes, we have shown that such pre-ignition events expedites the overall homogenous ignition delay times by over a magnitude under some cases.

The prospective study will provide in-depth insights to pre-ignition and ignition advance in shock tubes and RCMs. The study will use optical imaging techniques and better analysis of pressure signals to ascertain the cause of pre-ignition and dynamics of large pressure rise and ignition advance for pre-ignition affected data. The findings of proposed fundamental work are expected to provide useful guidelines for avoiding such events in engines.

APPENDIX A

Table A1: Detailed hydrocarbon analysis of light naphtha.

Group/species	normalized % mol
Paraffin	
n-pentane	35.09
n-hexane	20.264
Isoparaffin	
i-pentane	12.542
2,2-dimethylbutane	0.282
2,3-dimethylbutane	1.741
2-methylpentane	12.419
3-methylpentane	7.933
2,4-dimethylpentane	0.221
2-methylhexane	0.351
2,3-dimethylpentane	0.137
3-methylhexane	0.225
Aromatics	
Benzene	1.315
Naphthenes	

Cyclopentane	2.289
Methylcyclopentane	3.059
Cyclohexane	1.317
Unidentified	0.815

Table A2: Composition of multi-component light naphtha surrogate (LN-KAUST).

Species	mol%
2-methylbutane	0.25
2-methylhexane	0.1
n-pentane	0.43
n-heptane	0.12
Cyclopentane	0.1

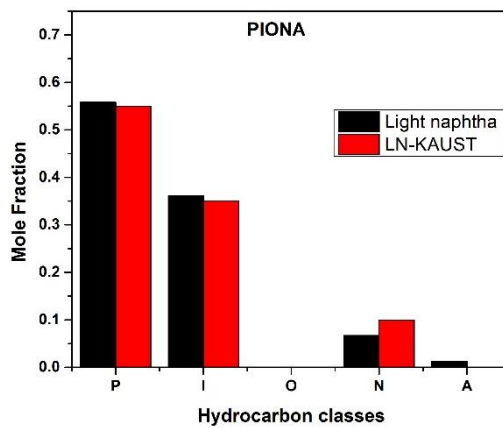


Figure A1: Mole fractions of various hydrocarbon classes for light naphtha fuel and its multi-component surrogate (P: Paraffins, I: Iso-paraffins, O: Olefins, N: Naphthenes and A: Aromatics).

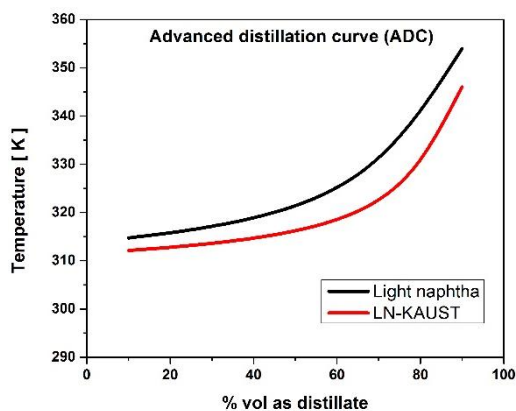


Figure A2: Simulated advanced distillation curves (ADC) for light naphtha and its multi-component surrogate.

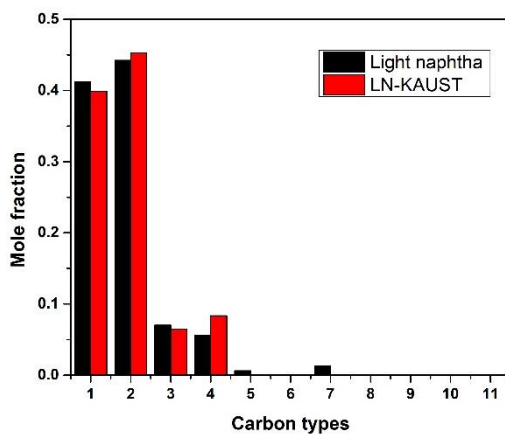


Figure A3: Carbon type mole fraction comparison between light naphtha fuel and its multi-component surrogate. For definitions of carbon types see Figure S4.

Carbon Type Classification of C to C bonds

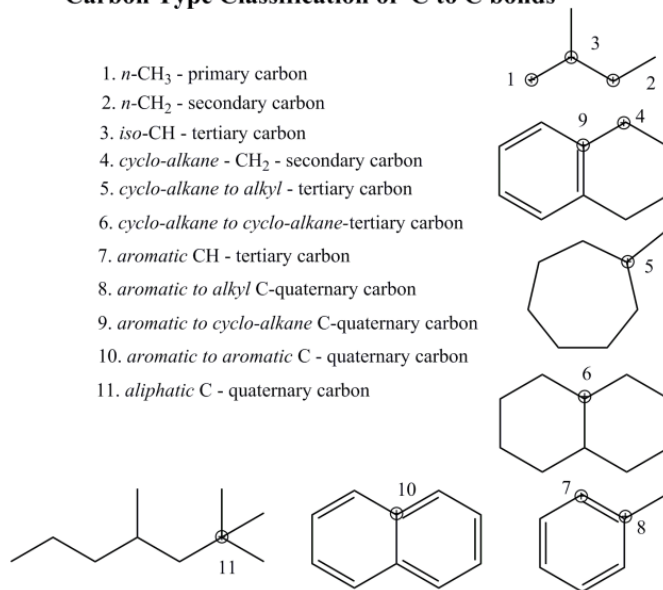


Figure A4: Carbon type classification employed in this study to capture structural attributes.

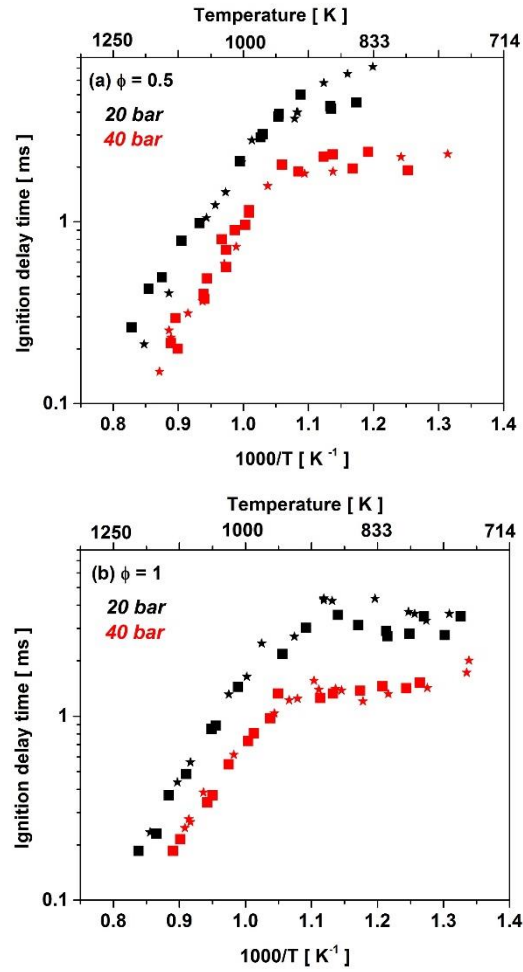


Figure A5: Comparison of light naphtha (squares) and PRF 70 (stars) ignition delay times at 20 and 40 bar at: (a) $\phi = 0.5$, (b) $\phi = 1$.

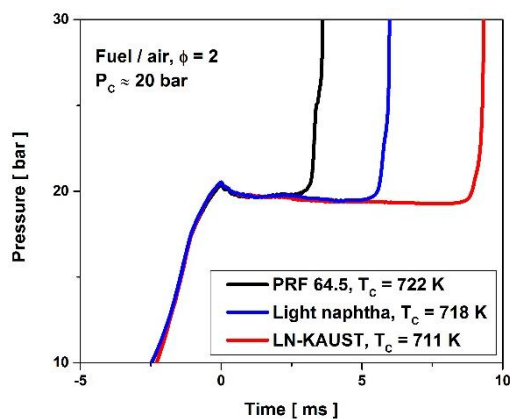
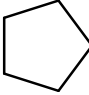
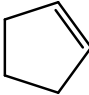
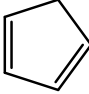
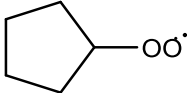
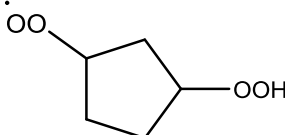
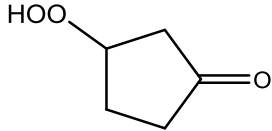
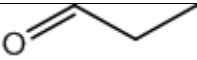
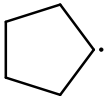
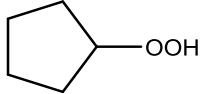
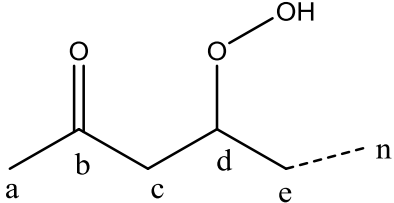
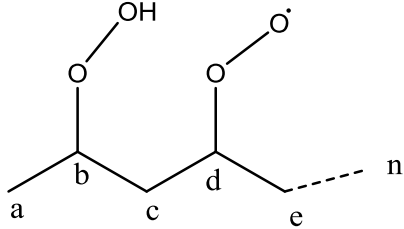
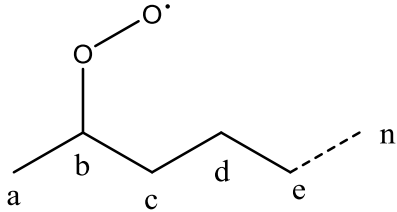
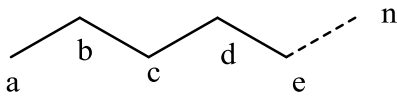


Figure A6: Pressure time histories during the oxidation of light naphtha, PRF 64.5 surrogate, and LN-KAUST surrogate. All three fuels exhibit single-stage ignition under these conditions.

Table A3: Structural formulas of species and intermediate classes appearing in rate of production analyses

Name	Structure
CPT	
CYC5H8	
C5H6	
CPTO2J	
CPTQ3QJ	

CPT1*O3Q	
CH3CH2CHO	
CYC5H9	
CPTO2H	
NC _n KET(<i>bd</i>)	
C _n H _{2n} OOH(<i>b</i>)-(<i>d</i>)O2	
C _n H _{2n+1} O2-(<i>b</i>)	
NC _n H _{2n+2}	

$C_nH_{2n+1-(b)}$	
IC8H18	

Table A4: TPRF surrogate compositions in mole fractions

Surrogate	iso-octane	<i>n</i>-heptane	Toluene
TPRF 70	0.365	0.35	0.285
TPRF 80	0.33	0.27	0.4
TPRF 91	0.29	0.17	0.54
TPRF 97.5	0.08	0.145	0.775

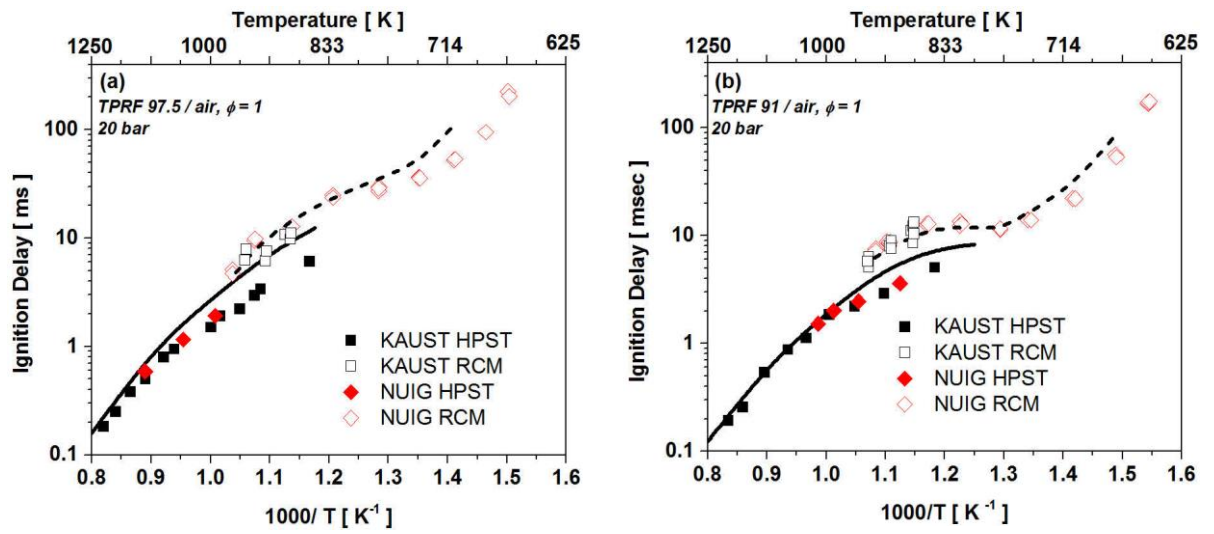


Figure A7: KAUST and NUIG cross-checked data at 20 bar $\phi = 1$ for (a) TPRF 97.5/air, (b) TPRF

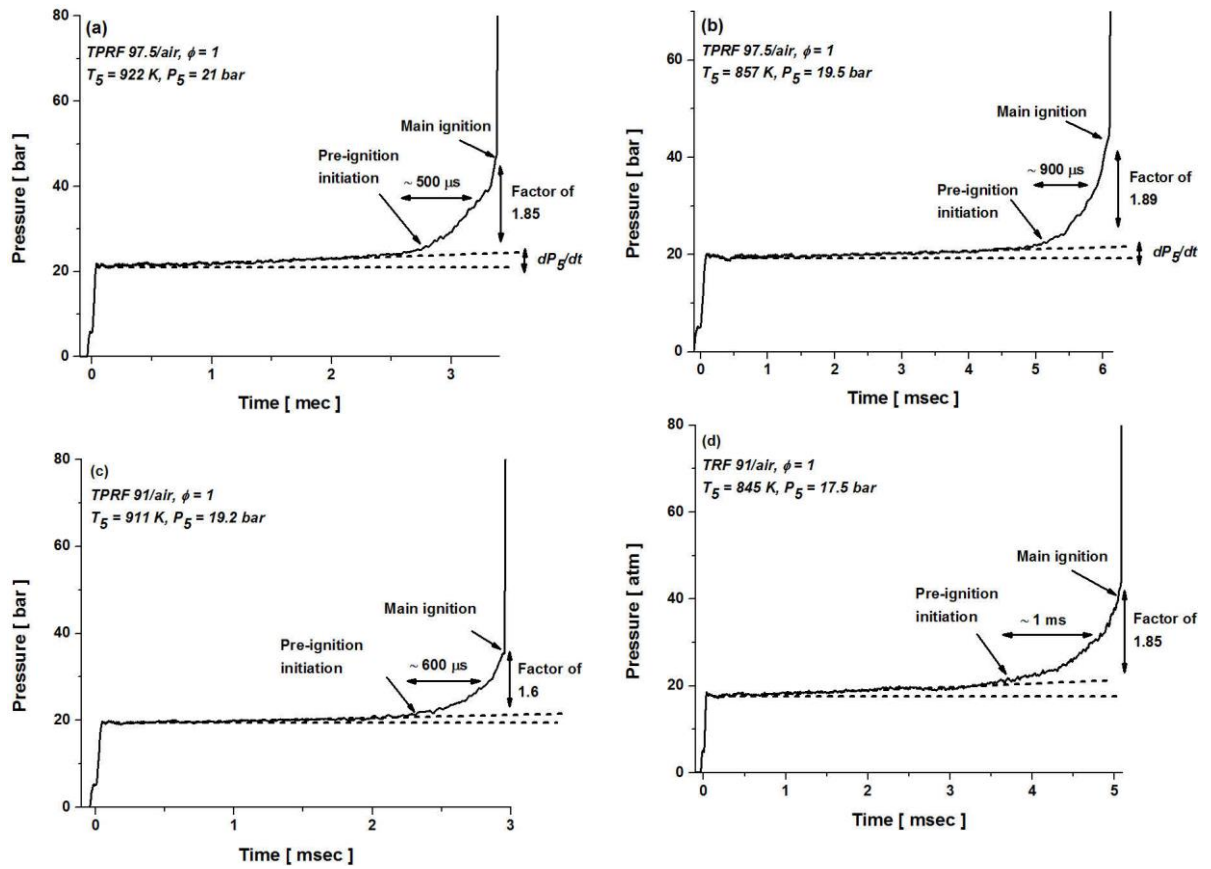


Figure A8: KAUST shock tube pressure traces at low temperatures where dp/dt and pre-ignition pressure rise are visible: (a) and (b) for TPRF 97.5 mixtures and (c) and (d) for TPRF 91 mixtures.

APPENDIX B

Example high pressure shock tube ignition measurements pressure traces

The purpose of this section is to provide example pressure traces during the high pressure shock tube (HPST) ignition delay measurements. For selected fuels, high, intermediate, and low-temperature unfiltered pressure traces are presented here.

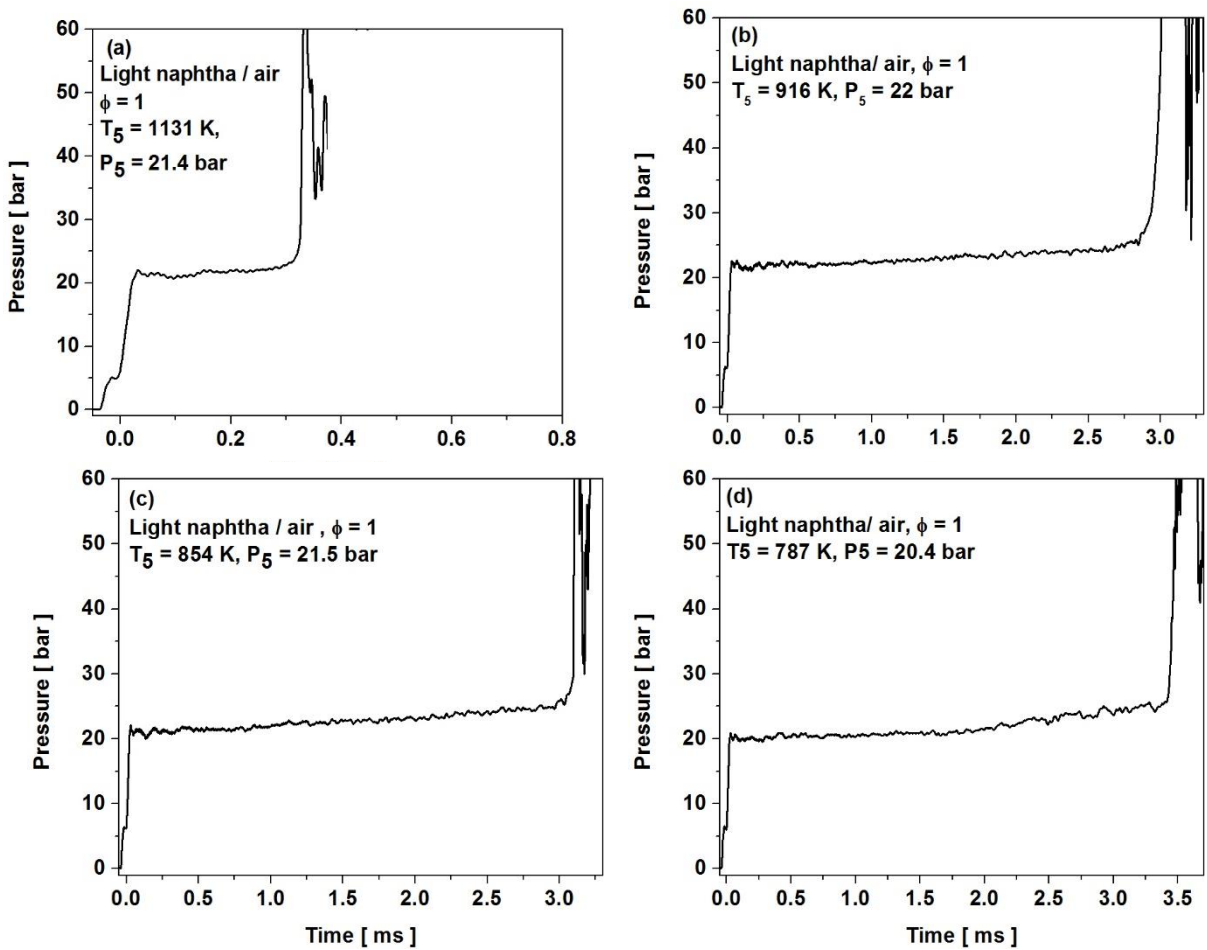


Figure B-1: Pressure traces measured during the ignition measurements of light naphtha / air mixtures at $\phi = 1$, (a) $T_5 = 1131$ K, $P_5 = 21.4$ bar, (b) $T_5 = 916$ K, $P_5 = 22$ bar, (c) $T_5 = 854$ K, $P_5 = 21.5$ bar, (d) $T_5 = 787$ K, $P_5 = 20.4$ bar

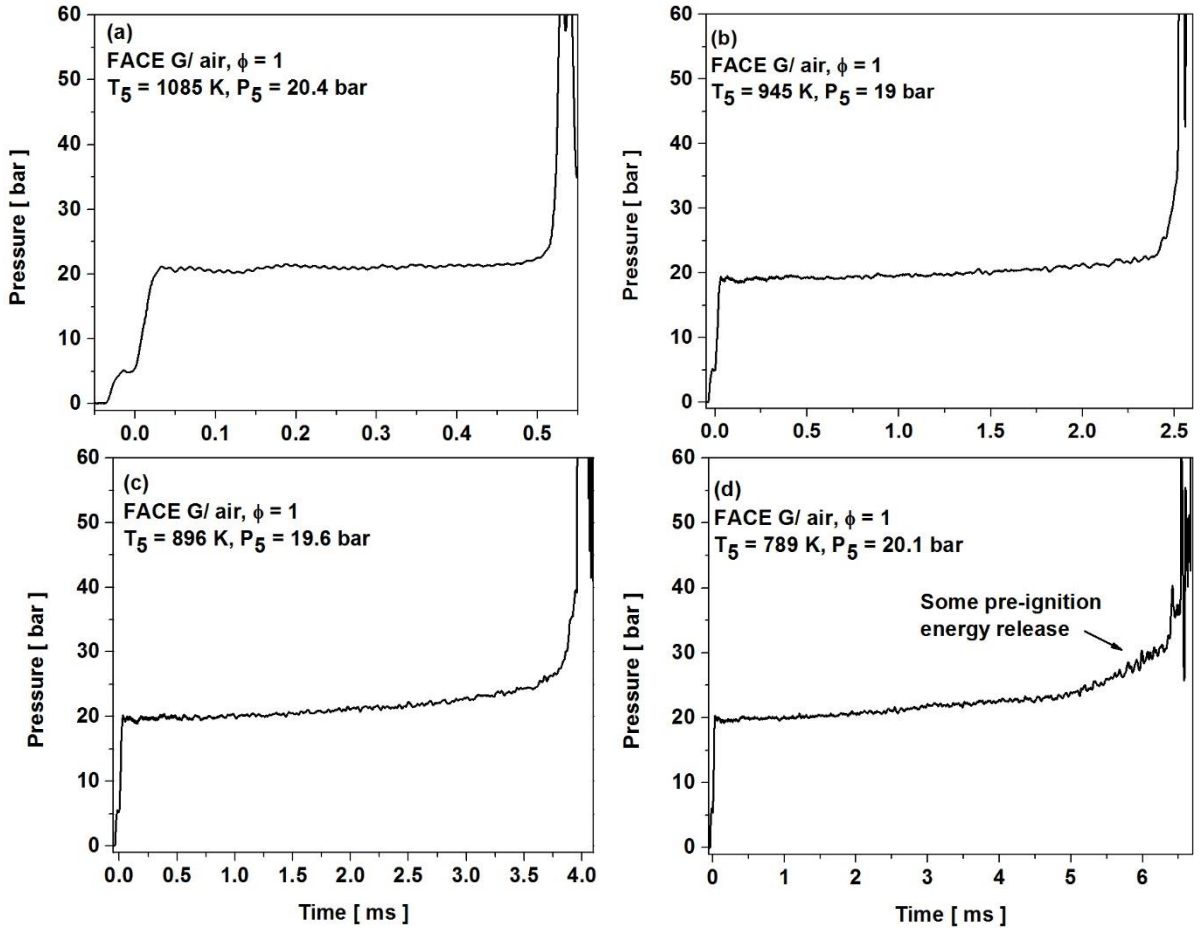


Figure B-2: Pressure traces measured during the ignition measurements of FACE G / air mixtures at $\phi = 1$, (a) $T_5 = 1085 \text{ K}$, $P_5 = 20.4 \text{ bar}$, (b) $T_5 = 945 \text{ K}$, $P_5 = 19 \text{ bar}$, (c) $T_5 = 896 \text{ K}$, $P_5 = 19.6 \text{ bar}$, (d) $T_5 = 789 \text{ K}$, $P_5 = 20.1 \text{ bar}$

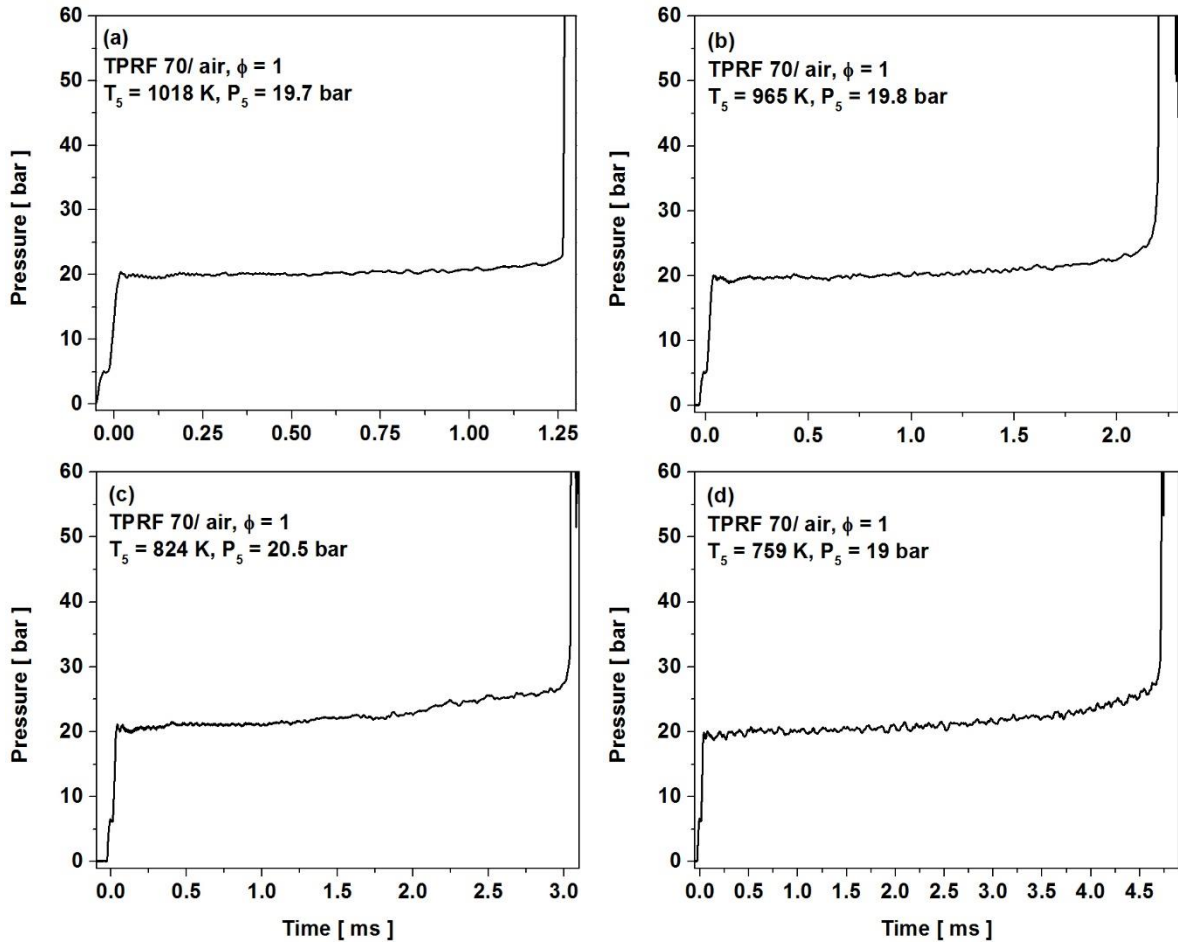


Figure B-3: Pressure traces measured during the ignition measurements of TPRF 70 / air mixtures at $\phi = 1$, (a) $T_5 = 1018$ K, $P_5 = 19.7$ bar, (b) $T_5 = 965$ K, $P_5 = 19.8$ bar, (c) $T_5 = 824$ K, $P_5 = 20.5$ bar, (d) $T_5 = 759$ K, $P_5 = 19$ bar

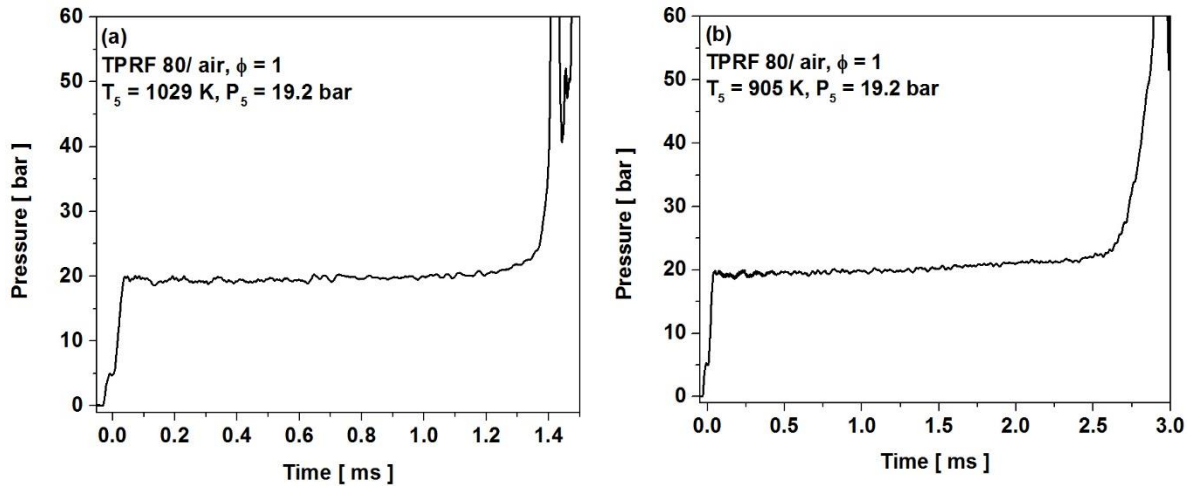


Figure B-4: Pressure traces measured during the ignition measurements of TPRF 80 / air mixtures at

$\phi = 1$, (a) $T_5 = 1029$ K, $P_5 = 19.2$ bar, (b) $T_5 = 905$ K, $P_5 = 19.2$ bar

REFERENCES

- [1] BP 2035 Energy Outlook, (2016).
- [2] H. Hao, F. Liu, Z. Liu, F. Zhao, Compression ignition of low-octane gasoline: Life cycle energy consumption and greenhouse gas emissions, *Applied Energy*, 181 (2016) 391-398.
- [3] Intergovernmental Panel on Climate Change Climate change 2014: mitigation of climate change in transport sector (chapter 8), Cambridge University Press, 2015.
- [4] W.J. Pitz, N.P. Cernansky, F.L. Dryer, F. Egolfopoulos, J. Farrell, D. Friend, H. Pitsch, SAE 2007-01-0175.
- [5] Accelerating the co-optimization of fuels and engines for sustainable transportation (OPTIMA), US Department of Energy, (2015).
- [6] K. Epping, S. Aceves, R. Bechtold, J.E. Dec, The potential of HCCI combustion for high efficiency and low emissions, in, SAE Technical Paper 2002-01-1923, 2002.
- [7] H. Curran, P. Gaffuri, W.J. Pitz, C.K. Westbrook, A comprehensive modeling study of n-heptane oxidation, *Combust Flame*, 114 (1998) 149-177.
- [8] H.J. Curran, P. Gaffuri, W. Pitz, C. Westbrook, A comprehensive modeling study of iso-octane oxidation, *Combust Flame*, 129 (2002) 253-280.
- [9] E. Ranzi, T. Faravelli, P. Gaffuri, A. Sogaro, A. D'Anna, A. Ciajolo, A wide-range modeling study of iso-octane oxidation, *Combustion and Flame*, 108 (1997) 24-42.
- [10] E. Ranzi, P. Gaffuri, T. Faravelli, P. Dagaut, A wide-range modeling study of n-heptane oxidation, *Combustion and Flame*, 103 (1995) 91-106.

- [11] E. Ranzi, A. Sogaro, P. Gaffuri, G. Pennati, C. Westbrook, W. Pitz, A new comprehensive reaction mechanism for combustion of hydrocarbon fuels, *Combustion and flame*, 99 (1994) 201-211.
- [12] C.K. Westbrook, W.J. Pitz, O. Herbinet, H.J. Curran, E.J. Silke, A comprehensive detailed chemical kinetic reaction mechanism for combustion of *n*-alkane hydrocarbons from *n*-octane to *n*-hexadecane, *Combustion and Flame*, 156 (2009) 181-199.
- [13] H. Ciezki, G. Adomeit, Shock-tube investigation of self-ignition of *n*-heptane-air mixtures under engine relevant conditions, *Combustion and Flame*, 93 (1993) 421-433.
- [14] K. Fieweger, R. Blumenthal, G. Adomeit, Shock-tube investigations on the self-ignition of hydrocarbon-air mixtures at high pressures, in: *Symposium (International) on Combustion*, Elsevier, 1994, pp. 1579-1585.
- [15] K. Fieweger, R. Blumenthal, G. Adomeit, Self-ignition of SI engine model fuels: a shock tube investigation at high pressure, *Combustion and Flame*, 109 (1997) 599-619.
- [16] R. Minetti, M. Carlier, M. Ribaucour, E. Therissen, L. Sochet, A rapid compression machine investigation of oxidation and auto-ignition of *n*-Heptane: Measurements and modeling, *Combustion and Flame*, 102 (1995) 298-309.
- [17] S. Tanaka, F. Ayala, J.C. Keck, J.B. Heywood, Two-stage ignition in HCCI combustion and HCCI control by fuels and additives, *Combust. Flame*, 132 (2003) 219-239.

- [18] M. Hartmann, M. Fikri, R. Starke, C. Schulz, Shock-tube investigation of ignition delay times of model fuels, in: Proceedings of the third European combustion meeting, Chania, 2007.
- [19] H. Curran, W. Pitz, C. Westbrook, G. Callahan, F. Dryer, Oxidation of automotive primary reference fuels at elevated pressures, in: Symposium (International) on Combustion, Elsevier, 1998, pp. 379-387.
- [20] C. Callahan, T. Held, F. Dryer, R. Minetti, M. Ribaucour, L. Sochet, T. Faravelli, P. Gaffuri, E. Rani, Experimental data and kinetic modeling of primary reference fuel mixtures, in: Symposium (International) on Combustion, Elsevier, 1996, pp. 739-746.
- [21] F. Buda, R. Bounaceur, V. Warth, P.-A. Glaude, R. Fournet, F. Battin-Leclerc, Progress toward a unified detailed kinetic model for the autoignition of alkanes from C_4 to C_{10} between 600 and 1200 K, Combustion and flame, 142 (2005) 170-186.
- [22] W. Pitz, N. Cernansky, F. Dryer, F. Egolfopoulos, J. Farrell, D. Friend, H. Pitsch, Development of an experimental database and chemical kinetic models for surrogate gasoline fuels, Society of Automotive Engineers Paper, (2007) 0175.
- [23] B. Gauthier, D. Davidson, R. Hanson, Shock tube determination of ignition delay times in full-blend and surrogate fuel mixtures, Combust. Flame, 139 (2004) 300-311.
- [24] M. Chaos, Z. Zhao, A. Kazakov, P. Gokulakrishnan, M. Angioletti, F. Dryer, A PRF+ toluene surrogate fuel model for simulating gasoline kinetics, in: Fifth US Combustion Meeting, 2007.

- [25] G. Vanhove, G. Petit, R. Minetti, Experimental study of the kinetic interactions in the low-temperature autoignition of hydrocarbon binary mixtures and a surrogate fuel, *Combust. Flame*, 145 (2006) 521-532.
- [26] C.V. Naik, W.J. Pitz, M. Sjöberg, J.E. Dec, J. Orme, H.J. Curran, J.M. Simmie, C.K. Westbrook, Detailed chemical kinetic modeling of surrogate fuels for gasoline and application to an HCCI engine, SAE paper, (2005) 3741.
- [27] G. Kukkadapu, K. Kumar, C.-J. Sung, M. Mehl, W.J. Pitz, Experimental and surrogate modeling study of gasoline ignition in a rapid compression machine, *Combust. Flame*, 159 (2012) 3066-3078.
- [28] G. Kukkadapu, K. Kumar, C.-J. Sung, M. Mehl, W.J. Pitz, Autoignition of gasoline and its surrogates in a rapid compression machine, *Proci. Combust. Inst.*, 34 (2013) 345-352.
- [29] S.M. Sarathy, G. Kukkadapu, M. Mehl, W. Wang, T. Javed, S. Park, M.A. Oehlschlaeger, A. Farooq, W.J. Pitz, C.-J. Sung, Ignition of alkane-rich FACE gasoline fuels and their surrogate mixtures, *Proci. Combust. Inst.*, 35 (2015) 249-257.
- [30] S.M. Sarathy, G. Kukkadapu, M. Mehl, T. Javed, A. Ahmed, N. Naser, A. Tekawade, G. Kosiba, M. AlAbbad, E. Singh, Compositional effects on the ignition of FACE gasolines, *Combust. Flame*, 169 (2016) 171-193.
- [31] T. Javed, E.F. Nasir, A. Ahmed, J. Badra, K. Djebbi, M. Beshir, W. Ji, S.M. Sarathy, A. Farooq, Ignition delay measurements of light naphtha: A fully blended low octane fuel, *Proci. Combust. Inst.*, (2016 Available online).
- [32] N. Fomin, 110 years of experiments on shock tubes, *Journal of Engineering Physics and Thermophysics*, 83 (2010) 1118-1135.

- [33] P. Vieille, Sur les discontinuités produites par la détente brusque de gaz comprimés, *Comptes Rendus des Séances de l'Académie des Sciences*, 129 (1899) 1228-1230.
- [34] W. Gardiner, Shock tube studies of combustion chemistry, in: *Shock Waves*, Springer, 1992, pp. 49-60.
- [35] R.L. Belford, R.A. Strehlow, Shock tube technique in chemical kinetics, *Annual Review of Physical Chemistry*, 20 (1969) 247-272.
- [36] D.F. Davidson, R. Hanson, Recent advances in shock tube/laser diagnostic methods for improved chemical kinetics measurements, *Shock Waves*, 19 (2009) 271-283.
- [37] J. Michael, K. Lim, Shock tube techniques in chemical kinetics, *Annual Review of Physical Chemistry*, 44 (1993) 429-458.
- [38] W. Tsang, A. Lifshitz, Shock tube techniques in chemical kinetics, *Annual Review of Physical Chemistry*, 41 (1990) 559-599.
- [39] M. Chaos, F.L. Dryer, Chemical-kinetic modeling of ignition delay: Considerations in interpreting shock tube data, *Intl. Journ. Chem. Kinetics*, 42 (2010) 143-150.
- [40] D. Davidson, R. Hanson, Interpreting shock tube ignition data, *International Journal of Chemical Kinetics*, 36 (2004) 510-523.
- [41] E.L. Petersen, R.K. Hanson, Nonideal effects behind reflected shock waves in a high-pressure shock tube, *Shock Waves*, 10 (2001) 405-420.
- [42] G. Pang, D. Davidson, R. Hanson, Experimental study and modeling of shock tube ignition delay times for hydrogen–oxygen–argon mixtures at low temperatures, *Proci. Combust. Inst.*, 32 (2009) 181-188.

- [43] S.M. Sarathy, T. Javed, F. Karsenty, A. Heufer, W. Wang, S. Park, A. Elwardany, A. Farooq, C.K. Westbrook, W.J. Pitz, A comprehensive combustion chemistry study of 2, 5-dimethylhexane, *Combust. Flame*, 161 (2014) 1444-1459.
- [44] A.R. Amadio, M.W. Crofton, E.L. Petersen, Test-time extension behind reflected shock waves using CO₂-He and C₃H₈-He driver mixtures, *Shock Waves*, 16 (2006) 157-165.
- [45] Z. Hong, D.F. Davidson, R.K. Hanson, Contact surface tailoring condition for shock tubes with different driver and driven section diameters, *Shock Waves*, 19 (2009) 331-336.
- [46] B. Esser, State variables of a shock tube as result from an exact Riemann solver, Ph.D. thesis, RWTH Aachen University, Aachen, Germany, (1991).
- [47] E. Petersen, R. Hanson, Measurement of reflected-shock bifurcation over a wide range of gas composition and pressure, *Shock Waves*, 15 (2006) 333-340.
- [48] S.M. Burke, U. Burke, R. Mc Donagh, O. Mathieu, I. Osorio, C. Keesee, A. Morones, E.L. Petersen, W. Wang, T.A. DeVerter, An experimental and modeling study of propene oxidation. Part 2: Ignition delay time and flame speed measurements, *Combust. Flame*, 162 (2015) 296-314.
- [49] J. Wurmel, J. Simmie, H. Curran, Studying the chemistry of HCCI in rapid compression machines, *Intl. Journ. Vehicle Design*, 44 (2007) 84-106.
- [50] G. Mittal, C.-J. Sung, A rapid compression machine for chemical kinetics studies at elevated pressures and temperatures, *Combust. Sci. Tech.*, 179 (2007) 497-530.

- [51] W. Ren, A. Farooq, D. Davidson, R. Hanson, CO concentration and temperature sensor for combustion gases using quantum-cascade laser absorption near 4.7 μm , *Appl Phys B*, 107 (2012) 849-860.
- [52] L.S. Rothman, I.E. Gordon, A. Barbe, D.C. Benner, P.F. Bernath, M. Birk, V. Boudon, L.R. Brown, A. Campargue, J.-P. Champion, The HITRAN 2008 molecular spectroscopic database, *J Quant Spectrosc Radiat Transfer*, 110 (2009) 533-572.
- [53] W. Ren, R.M. Spearrin, D.F. Davidson, R.K. Hanson, Experimental and Modeling Study of the Thermal Decomposition of C3-C5 Ethyl Esters Behind Reflected Shock Waves, *The Journal of Physical Chemistry A*, (2014).
- [54] R. Spearrin, W. Ren, J. Jeffries, R. Hanson, Multi-band infrared CO₂ absorption sensor for sensitive temperature and species measurements in high-temperature gases, *Appl Phys B*, (2014) 1-11.
- [55] A. Farooq, J.B. Jeffries, R.K. Hanson, In situ combustion measurements of H₂O and temperature near 2.5 μm using tunable diode laser absorption, *Meas Sci Technol*, 19 (2008) 075604.
- [56] Z. Hong, A. Farooq, E.A. Barbour, D.F. Davidson, R.K. Hanson, Hydrogen peroxide decomposition rate: a shock tube study using tunable laser absorption of H₂O near 2.5 μm , *The Journal of Physical Chemistry A*, 113 (2009) 12919-12925.
- [57] J.T. Herbon, R.K. Hanson, D.M. Golden, C.T. Bowman, A shock tube study of the enthalpy of formation of OH, *Proceedings of the Combustion Institute*, 29 (2002) 1201-1208.

- [58] G.T. Kalghatgi, The outlook for fuels for internal combustion engines, Intl. Journ. Engine Research, (2014) 1468087414526189.
- [59] J. Chang, G. Kalghatgi, A. Amer, Y. Viollet, Enabling high efficiency direct injection engine with naphtha fuel through Partially Premixed Charge Compression Ignition Combustion, in, SAE Technical Paper 2012-01-0677, 2012.
- [60] J. Chang, Y. Viollet, A. Amer, G. Kalghatgi, Fuel economy potential of partially premixed compression ignition (PPCI) combustion with naphtha fuel, in, SAE Technical Paper 2013-01-2701, 2013.
- [61] B. Wang, S.-J. Shuai, H.-Q. Yang, Z. Wang, J.-X. Wang, H. Xu, Experimental Study of Multiple Premixed Compression Ignition Engine Fueled with Heavy Naphtha for High Efficiency and Low Emissions, in, SAE Technical Paper 2014-01-2678, 2014.
- [62] A.B. Dempsey, N.R. Walker, E. Gingrich, R.D. Reitz, Comparison of low temperature combustion strategies for advanced compression ignition engines with a focus on controllability, Combust. Sci. Technol., 186 (2014) 210-241.
- [63] J. Chang, G. Kalghatgi, A. Amer, Y. Viollet, Enabling high efficiency direct injection engine with naphtha fuel through partially premixed charge compression ignition combustion, (SAE Technical Paper 2012-01-0677).
- [64] J. Chang, Y. Viollet, A. Amer, G. Kalghatgi, Fuel economy potential of partially premixed compression ignition (PPCI) combustion with naphtha fuel, (SAE Technical Paper 2013-01-2701).
- [65] H. Yang, S. Shuai, Z. Wang, J. Wang, H. Xu, New premixed compression ignition concept for direct injection IC engines fueled with straight-run naphtha, Energy Conversion and Management, 68 (2013) 161-168.

- [66] H. Yang, S. Shuai, Z. Wang, J. Wang, H. Xu, Performance of straight-run naphtha single-and two-stage combustion modes from low to high load, Intl. Journ. Engine. Research, 14 (2013) 469-478.
- [67] Y. Yang, J.E. Dec, N. Dronniou, M. Sjöberg, W. Cannella, Partial fuel stratification to control HCCI heat release rates: fuel composition and other factors affecting pre-ignition reactions of two-stage ignition fuels, SAE Intl. Journ. Engines, 4 (2011) 1903-1920.
- [68] A. Ahmed, M. Khurshid, N. Naser, J. Badra, P. Gaillard, S. Chung, W.L. Roberts, S.M. Sarathy, *Surrogate fuel formulation for light naphtha combustion in advanced combustion engines*, Proceedings of the European Combustion Meeting, Budapest, Hungary 2015.
- [69] T. Javed, C. Lee, M. AlAbbad, K. Djebbi, M. Beshir, J. Badra, H. Curran, A. Farooq, Ignition studies of n-heptane/iso-octane/toluene blends, Combust. Flame, 171 (2016) 223-233.
- [70] M. AlAbbad, T. Javed, F. Khaled, J. Badra, A. Farooq, Ignition Delay Time Measurements of Primary Reference Fuel Blends, (submitted Combustion and Flame 2016).
- [71] W.J. Pitz, N.P. Cernansky, F.L. Dryer, F. Egolfopoulos, J. Farrell, D. Friend, H. Pitsch, Development of an experimental database and chemical kinetic models for surrogate gasoline fuels, (SAE Technical Paper 2007-01-0175).
- [72] M. Chaos, Z. Zhao, A. Kazakov, P. Gokulakrishnan, M. Angioletti, F. Dryer, A PRF+ toluene surrogate fuel model for simulating gasoline kinetics, in: 5th US Combustion Meeting, 2007, pp. 25-28.

- [73] G. Kukkadapu, K. Kumar, C.-J. Sung, M. Mehl, W.J. Pitz, Autoignition of gasoline surrogates at low temperature combustion conditions, *Combust. Flame*, 162 (2015) 2272-2285.
- [74] S. Dooley, S.H. Won, J. Heyne, T.I. Farouk, Y. Ju, F.L. Dryer, K. Kumar, X. Hui, C.-J. Sung, H. Wang, The experimental evaluation of a methodology for surrogate fuel formulation to emulate gas phase combustion kinetic phenomena, *Combust. Flame*, 159 (2012) 1444-1466.
- [75] S. Dooley, S.H. Won, S. Jahangirian, Y. Ju, F.L. Dryer, H. Wang, M.A. Oehlschlaeger, The combustion kinetics of a synthetic paraffinic jet aviation fuel and a fundamentally formulated, experimentally validated surrogate fuel, *Combust. Flame*, 159 (2012) 3014-3020.
- [76] C.J. Mueller, W.J. Cannella, T.J. Bruno, B. Bunting, H.D. Dettman, J.A. Franz, M.L. Huber, M. Natarajan, W.J. Pitz, M.A. Ratcliff, Methodology for formulating diesel surrogate fuels with accurate compositional, ignition-quality, and volatility characteristics, *Energy Fuels*, 26 (2012) 3284-3303.
- [77] A. Ahmed, G. Goteng, V.S. Shankar, K. Al-Qurashi, W.L. Roberts, S.M. Sarathy, A computational methodology for formulating gasoline surrogate fuels with accurate physical and chemical kinetic properties, *Fuel*, 143 (2015) 290-300.
- [78] D. Kim, J. Martz, A. Violi, A surrogate for emulating the physical and chemical properties of conventional jet fuel, *Combust. Flame*, 161 (2014) 1489-1498.
- [79] M. Mehl, W.J. Pitz, C.K. Westbrook, H.J. Curran, Kinetic modeling of gasoline surrogate components and mixtures under engine conditions, *Proci. Combust. Inst.*, 33 (2011) 193-200.

- [80] B. Smith, T. Bruno, Advanced distillation curve measurement with a model predictive temperature controller, *Intl. Journ. Thermophysics*, 27 (2006) 1419-1434.
- [81] S. Japanwala, K.H. Chung, H.D. Dettman, M.R. Gray, Quality of distillates from repeated recycle of residue, *Energy Fuels*, 16 (2002) 477-484.
- [82] M. Mehl, J.-Y. Chen, W.J. Pitz, S. Sarathy, C.K. Westbrook, An approach for formulating surrogates for gasoline with application toward a reduced surrogate mechanism for CFD engine modeling, *Energy Fuels*, 25 (2011) 5215-5223.
- [83] M. Mehl, J.-Y. Chen, W.J. Pitz, S.M. Sarathy, C.K. Westbrook, An approach for formulating surrogates for gasoline with application toward a reduced surrogate mechanism for CFD engine modeling, *Energy Fuels*, 25 (2011) 5215-5223.
- [84] M. Mehl, T. Faravelli, F. Giavazzi, E. Ranzi, P. Scorletti, A. Tardani, D. Terna, Detailed chemistry promotes understanding of octane numbers and gasoline sensitivity, *Energy Fuels*, 20 (2006) 2391-2398.
- [85] S.S. Merchant, C.F. Goldsmith, A.G. Vandeputte, M.P. Burke, S.J. Klippenstein, W.H. Green, Understanding low-temperature first-stage ignition delay: Propane, *Combust. Flame*, 162 (2015) 3658-3673.
- [86] J. Zádor, C.A. Taatjes, R.X. Fernandes, Kinetics of elementary reactions in low-temperature autoignition chemistry, *Prog. Energy. Combust. Sci.*, 37 (2011) 371-421.
- [87] R. Sivaramakrishnan, J. Michael, Rate constants for OH with selected large alkanes: shock-tube measurements and an improved group scheme, *Journ. Phys. Chem. A*, 113 (2009) 5047-5060.

- [88] J. Badra, A. Farooq, Site-specific reaction rate constant measurements for various secondary and tertiary H-abstraction by OH radicals, *Combust. Flame*, 162 (2015) 2034-2044.
- [89] J. Griffiths, P. Halford-Maw, C. Mohamed, Spontaneous ignition delays as a diagnostic of the propensity of alkanes to cause engine knock, *Combust Flame*, 111 (1997) 327-337.
- [90] X. He, M. Donovan, B. Zigler, T. Palmer, S. Walton, M. Wooldridge, A. Atreya, An experimental and modeling study of iso-octane ignition delay times under homogeneous charge compression ignition conditions, *Combust Flame*, 142 (2005) 266-275.
- [91] K. Anand, Y. Ra, R. Reitz, B. Bunting, Surrogate model development for fuels for advanced combustion engines, *Energy & Fuels*, 25 (2011) 1474-1484.
- [92] D. Davidson, Z. Hong, G. Pilla, A. Farooq, R. Cook, R. Hanson, Multi-species time-history measurements during *n*-heptane oxidation behind reflected shock waves, *Combust Flame*, 157 (2010) 1899-1905.
- [93] D. Davidson, Z. Hong, G. Pilla, A. Farooq, R. Cook, R. Hanson, Multi-species time-history measurements during *n*-dodecane oxidation behind reflected shock waves, *Proceedings of the Combustion Institute*, 33 (2011) 151-157.
- [94] D. Haylett, D. Davidson, R. Cook, Z. Hong, W. Ren, S. Pyun, R. Hanson, Multi-species time-history measurements during *n*-hexadecane oxidation behind reflected shock waves, *Proceedings of the Combustion Institute*, 34 (2013) 369-376.
- [95] M.E. MacDonald, D.F. Davidson, R.K. Hanson, W.J. Pitz, M. Mehl, C.K. Westbrook, Formulation of an RP-1 pyrolysis surrogate from shock tube measurements of fuel and ethylene time histories, *Fuel*, 103 (2013) 1051-1059.

- [96] M.E. MacDonald, W. Ren, Y. Zhu, D.F. Davidson, R.K. Hanson, Fuel and Ethylene Measurements during n-dodecane, methylcyclohexane, and iso-cetane pyrolysis in shock tubes, *Fuel*, 103 (2013) 1060-1068.
- [97] I. CHEMKIN-PRO release 15101. Reaction Design, San Diego, CA; 2010.
- [98] H. Li, Z. Owens, D. Davidson, R. Hanson, A simple reactive gasdynamic model for the computation of gas temperature and species concentrations behind reflected shock waves, *Int J Chem Kinet*, 40 (2008) 189-198.
- [99] C. Ji, S.M. Sarathy, P.S. Veloo, C.K. Westbrook, F.N. Egolfopoulos, Effects of fuel branching on the propagation of octane isomers flames, *Combust Flame*, 159 (2012) 1426-1436.
- [100] N. Liu, S. Mani Sarathy, C.K. Westbrook, F.N. Egolfopoulos, Ignition of non-premixed counterflow flames of octane and decane isomers, *Proceedings of the Combustion Institute*, 34 (2013) 903-910.
- [101] E.J. Silke, H.J. Curran, J.M. Simmie, The influence of fuel structure on combustion as demonstrated by the isomers of heptane: a rapid compression machine study, *Proceedings of the Combustion Institute*, 30 (2005) 2639-2647.
- [102] T. Bieleveld, A. Frassoldati, A. Cuoci, T. Faravelli, E. Ranzi, U. Niemann, K. Seshadri, Experimental and kinetic modeling study of combustion of gasoline, its surrogates and components in laminar non-premixed flows, *Proceedings of the Combustion Institute*, 32 (2009) 493-500.
- [103] E. Ranzi, A. Frassoldati, R. Grana, A. Cuoci, T. Faravelli, A. Kelley, C. Law, Hierarchical and comparative kinetic modeling of laminar flame speeds of hydrocarbon and oxygenated fuels, *Prog Energy Combust Sci*, 38 (2012) 468-501.

- [104] H. Ciezki, G. Adomeit, Shock-tube investigation of self-ignition of n-heptane-air mixtures under engine relevant conditions, *Combust. Flame*, 93 (1993) 421-433.
- [105] R. Minetti, M. Carlier, M. Ribaucour, E. Therssen, L. Sochet, A rapid compression machine investigation of oxidation and auto-ignition of n-heptane: measurements and modeling, *Combust. Flame*, 102 (1995) 298-309.
- [106] H. Curran, P. Gaffuri, W.J. Pitz, C.K. Westbrook, A comprehensive modeling study of n-heptane oxidation, *Combust. Flame*, 114 (1998) 149-177.
- [107] E. Ranzi, P. Gaffuri, T. Faravelli, P. Dagaut, A wide-range modeling study of n-heptane oxidation, *Combust. Flame*, 103 (1995) 91-106.
- [108] H.J. Curran, W. Pitz, C. Westbrook, G. Callahan, F. Dryer, Oxidation of automotive primary reference fuels at elevated pressures, *Intl. Sympo. Combust.*, 27 (1998) 379-387.
- [109] F. Buda, R. Bounaceur, V. Warth, P.-A. Glaude, R. Fournet, F. Battin-Leclerc, Progress toward a unified detailed kinetic model for the autoignition of alkanes from C 4 to C 10 between 600 and 1200 K, *Combust. Flame*, 142 (2005) 170-186.
- [110] L. Cai, H. Pitsch, Optimized chemical mechanism for combustion of gasoline surrogate fuels, *Combust. Flame*, 162 (2015) 1623-1637.
- [111] G. Kalghatgi, R. Head, J. Chang, Y. Viollet, H. Babiker, A. Amer, An alternative method based on toluene/n-heptane surrogate fuels for rating the anti-knock quality of practical gasolines, *SAE Int. Journ. Fuels Lubricants*, 7 (2014) 663-672.
- [112] G. Kalghatgi, H. Babiker, J. Badra, A Simple Method to Predict Knock Using Toluene, N-Heptane and Iso-Octane Blends (TPRF) as Gasoline Surrogates, *SAE Int. Journ. Engines*, 8 (2015) 505-519.

- [113] N. Morgan, A. Smallbone, A. Bhave, M. Kraft, R. Cracknell, G. Kalghatgi, Mapping surrogate gasoline compositions into RON/MON space, *Combust. Flame*, 157 (2010) 1122-1131.
- [114] C. Pera, V. Knop, Methodology to define gasoline surrogates dedicated to auto-ignition in engines, *Fuel*, 96 (2012) 59-69.
- [115] Z. Wang, S.M. Sarathy, Third O₂ addition reactions promote the low-temperature auto-ignition of n-alkanes, *Combust. Flame*, (2016).
- [116] Y. Uygun, S. Ishihara, H. Olivier, A high pressure ignition delay time study of 2-methylfuran and tetrahydrofuran in shock tubes, *Combust. Flame*, 161 (2014) 2519-2530.
- [117] J.A. Badra, N. Bokhumseen, N. Mulla, S.M. Sarathy, A. Farooq, G. Kalghatgi, P. Gaillard, A methodology to relate octane numbers of binary and ternary n-heptane, iso-octane and toluene mixtures with simulated ignition delay times, *Fuel*, 160 (2015) 458-469.
- [118] C. Lee, A. farooq, M. Sarathy, H. Curran, Experimental and Modelling Study of Autoignition of Oxygenated Gasoline at elevated pressure and low-to-high temperature, *Combustion and Flame*, (2016, to be submitted).
- [119] R.K. Hanson, D.F. Davidson, Recent advances in laser absorption and shock tube methods for studies of combustion chemistry, *Prog. Energy Combust. Sci.*, 44 (2014) 103-114.
- [120] C. Frazier, M. Lamnaouer, E. Divo, A. Kassab, E. Petersen, Effect of wall heat transfer on shock-tube test temperature at long times, *Shock Waves*, 21 (2011) 1-17.

- [121] R.K. Hanson, G.A. Pang, S. Chakraborty, W. Ren, S. Wang, D.F. Davidson, Constrained reaction volume approach for studying chemical kinetics behind reflected shock waves, *Combust. Flame*, 160 (2013) 1550-1558.
- [122] Y. Zhu, D.F. Davidson, R.K. Hanson, 1-Butanol ignition delay times at low temperatures: An application of the constrained-reaction-volume strategy, *Combust. Flame*, 161 (2014) 634-643.
- [123] M.F. Campbell, S. Wang, C.S. Goldenstein, R.M. Sparrin, A.M. Tulgestke, L.T. Zaczek, D.F. Davidson, R.K. Hanson, Constrained reaction volume shock tube study of n-heptane oxidation: Ignition delay times and time-histories of multiple species and temperature, *Proci. Combust. Inst.*, 35 (2015) 231-239.
- [124] A.B. Mansfield, M.S. Wooldridge, High-pressure low-temperature ignition behavior of syngas mixtures, *Combust. Flame*, 161 (2014) 2242-2251.
- [125] Z. Wang, Y. Qi, X. He, J. Wang, S. Shuai, C.K. Law, Analysis of pre-ignition to super-knock: Hotspot-induced deflagration to detonation, *Fuel*, 144 (2015) 222-227.
- [126] H.G. Im, P. Pal, M.S. Wooldridge, A.B. Mansfield, A Regime Diagram for Autoignition of Homogeneous Reactant Mixtures with Turbulent Velocity and Temperature Fluctuations, *Combust. Sci. Tech.*, 187 (2015) 1263-1275.
- [127] P. Pal, A.B. Mansfield, P.G. Arias, M.S. Wooldridge, H.G. Im, A computational study of syngas auto-ignition characteristics at high-pressure and low-temperature conditions with thermal inhomogeneities, *Combustion Theory and Modelling*, (2015) 1-15.
- [128] K.P. Grogan, S.S. Goldsborough, M. Ihme, Ignition regimes in rapid compression machines, *Combust. Flame*, (2015).

- [129] B. Choi, K. Kim, S. Chung, Autoignited laminar lifted flames of propane in coflow jets with tribrachial edge and mild combustion, *Combust. Flame*, 156 (2009) 396-404.
- [130] B. Choi, S.-H. Chung, Autoignited laminar lifted flames of methane, ethylene, ethane, and n-butane jets in coflow air with elevated temperature, *Combust. Flame*, 157 (2010) 2348-2356.
- [131] S.K. Choi, S.H. Chung, Autoignited and non-autoignited lifted flames of pre-vaporized n-heptane in coflow jets at elevated temperatures, *Combust. Flame*, 160 (2013) 1717-1724.
- [132] S.M. Al-Noman, S.K. Choi, S.H. Chung, Autoignition characteristics of laminar lifted jet flames of pre-vaporized iso-octane in heated coflow air, *Fuel*, 162 (2015) 171-178.
- [133] G.T. Kalghatgi, D. Bradley, Pre-ignition and 'super-knock' in turbo-charged spark-ignition engines, *Int. Journ. Engine Research*, 13 (2012) 399-414.
- [134] N. Peters, B. Kerschgens, G. Paczko, SAE Technical Paper, 2013-01-1109, in, 2013.
- [135] H.J. Curran, P. Gaffuri, W.J. Pitz, C.K. Westbrook, A comprehensive modeling study of n-heptane oxidation, *Combust. Flame*, 114 (1998) 149-177.
- [136] J. Badra, A. Elwardany, A. Farooq, Shock tube measurements of the rate constants for seven large alkanes+ OH, *Proci. Combust. Inst.*, 35 (2015) 189-196.
- [137] T. Javed, E.F. Nasir, E.-t. Es-sebbar, A. Farooq, A comparative study of the oxidation characteristics of two gasoline fuels and an n-heptane/iso-octane surrogate mixture, *Fuel*, 140 (2015) 201-208.

- [138] H.-P.S. Shen, J. Steinberg, J. Vanderover, M.A. Oehlschlaeger, A shock tube study of the ignition of n-heptane, n-decane, n-dodecane, and n-tetradecane at elevated pressures, *Energy & Fuels*, 23 (2009) 2482-2489.
- [139] E. Ranzi, A. Frassoldati, A. Stagni, M. Pelucchi, A. Cuoci, T. Faravelli, Reduced Kinetic Schemes of Complex Reaction Systems: Fossil and Biomass-Derived Transportation Fuels, *Int. Journ. Chem. Kinetics*, 46 (2014) 512-542.
- [140] P. Dagaut, M. Reuillon, M. Cathonnet, Experimental study of the oxidation of n-heptane in a jet stirred reactor from low to high temperature and pressures up to 40 atm, *Combust. Flame*, 101 (1995) 132-140.
- [141] S.M. Villano, H.-H. Carstensen, A.M. Dean, Rate Rules, Branching Ratios, and Pressure Dependence of the HO₂+ Olefin Addition Channels, *Journ. Phys. Chem. A*, 117 (2013) 6458-6473.
- [142] S.M. Villano, L.K. Huynh, H.-H. Carstensen, A.M. Dean, High-pressure rate rules for alkyl+ O₂ reactions. 1. The dissociation, concerted elimination, and isomerization channels of the alkyl peroxy radical, *Journ. Phys. Chem. A*, 115 (2011) 13425-13442.
- [143] H. Yamashita, J. Kasahara, Y. Sugiyama, A. Matsuo, Visualization study of ignition modes behind bifurcated-reflected shock waves, *Combust. Flame*, 159 (2012) 2954-2966.
- [144] U. Pfahl, K. Fieweger, G. Adomeit, Self-ignition of diesel-relevant hydrocarbon-air mixtures under engine conditions, in: *Symposium (International) on Combustion*, Elsevier, 1996, pp. 781-789.

- [145] P. Dai, Z. Chen, S. Chen, Y. Ju, Numerical experiments on reaction front propagation in n-heptane/air mixture with temperature gradient, *Proci. Combust. Inst.*, 35 (2015) 3045-3052.
- [146] P. Senecal, K. Richards, E. Pomraning, *CONVERGE (Version 2.2.0) Manual*, Convergent Science Inc., Madison, WI (2014) (2014).
- [147] P.K. Senecal, E. Pomraning, K.J. Richards, T.E. Briggs, C.Y. Choi, R.M. McDavid, M.A. Patterson, Multi-Dimensional Modeling of Direct-Injection Diesel Spray Liquid Length and Flame Lift-off Length using CFD and Parallel Detailed Chemistry, *SAE Technical Paper*, 2003-01-1043 (2003).
- [148] J.C. Andrae, T. Brinck, G. Kalghatgi, HCCI experiments with toluene reference fuels modeled by a semidetailed chemical kinetic model, *Combust. Flame*, 155 (2008) 696-712.
- [149] M. Blanc, P. Guest, G. von Elbe, B. Lewis, Ignition of explosive gas mixtures by electric sparks. I. Minimum ignition energies and quenching distances of mixtures of methane, oxygen, and inert gases, *Journ. Chem. Phys.*, 15 (1947) 798-802.
- [150] B. Lewis, G. Von Elbe, *Combustion, flames and explosions of gases*, Academic Press, London (1987).
- [151] P. Dai, Z. Chen, Supersonic reaction front propagation initiated by a hot spot in n-heptane/air mixture with multistage ignition, *Combust. Flame*, 162 (2015) 4183-4193.
- [152] S.G. Davis, C.K. Law, Determination of and fuel structure effects on laminar flame speeds of C1 to C8 hydrocarbons, *Combust. Sci. Tech.*, 140 (1998) 427-449.
- [153] Y.B. Zeldovich, Regime classification of an exothermic reaction with nonuniform initial conditions, *Combust. Flame*, 39 (1980) 211-214.

[154] J. Badra, A. Elwardany, J. Sim, Y. Viollet, H. Im, J. Chang, Effects of In-Cylinder Mixing on Low Octane Gasoline Compression Ignition Combustion, in, SAE International, 2016.

[155] T. Davies, R. Cracknell, G. Lovett, L. Cruff, J. Fowler, Fuel effects in a boosted DISI engine, in, SAE Technical Paper, 2011.